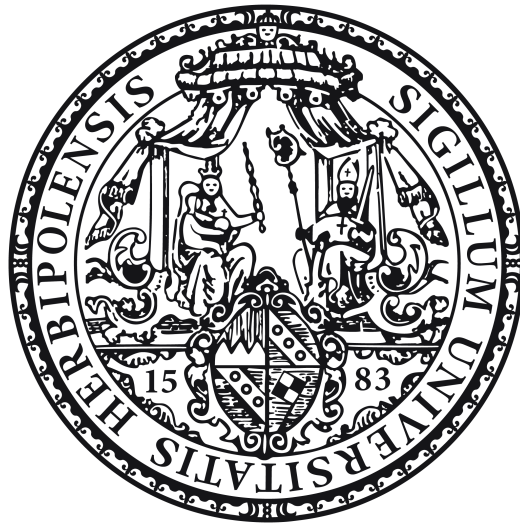**Studies on the role of the cytoskeleton in platelet production**

Studien über die Rolle des Zytoskeletts in der Produktion von Thrombozyten

Doctoral thesis for a doctoral degree
at the Graduate School of Life Sciences
Julius-Maximilian-Universität Würzburg
Section Biomedicine

submitted by

Katja Aurbach
from Mühlhausen/Sulz

Würzburg, January 2021

Submitted on:

Members of the Promotionskomitee:

Chairperson: Prof. Dr. Markus Sauer

Primary Supervisor: Dr. Irina Pleines

Supervisor (Second):   Prof. Dr. Bernhard Nieswandt

Supervisor (Third):   Prof. Dr. Antje Gohla

Supervisor (Fourth):   Dr. Steve G Thomas

Date of Public Defense: _____

Date of Receipt of Certificates: _____

Let us fight to free the world - to do away with national barriers - to do away with greed, with hate and intolerance. Let us fight for a world of reason, a world where science and progress will lead to all people´s happiness.
after Charlie Chaplin

Summary

Platelets are small anucleated cell fragments that originate from *megakaryocytes* (MKs), which are large cells located in the *bone marrow* (BM). MKs extend long cytoplasmic protrusions, a process which is called proplatelet formation, into the lumen of the sinusoidal vessels where platelets are sized by the bloodstream. During the process of platelet biogenesis, segments of the MK penetrate the endothelium and, through cytoskeletal remodeling inside the MK, proplatelet fragments are released. Rho GTPases, such as RhoA and RhoB, are critically involved in cytoskeletal rearrangements of both the actin and the tubulin cytoskeleton.

The first part of this thesis concentrated on the protein RhoB and its involvement in cytoskeletal organization in MKs and platelets. Single *knockout* (KO) mice lacking RhoB had a minor microthrombocytopenia, which means a smaller platelet size and reduced platelet number, accompanied by defects in the microtubule cytoskeleton in both MKs and platelets. In particular, tubulin organization and stability, which is regulated by posttranslational modifications of α-tubulin, were disturbed in $RhoB^{-/-}$ platelets. In contrast, $RhoB^{-/-}$ MKs produced abnormally shaped proplatelets but had unaltered posttranslational modifications of α-tubulin.

The second part focused on the influence of RhoA and RhoB on MK localization and platelet biogenesis in murine BM. Many intact $RhoA^{-/-}$ MKs are able to transmigrate through the endothelial layer and stay attached to the vessel wall, whereas only 1% of *wildtype* (*wt*) MKs are detectable in the intrasinusoidal space. Concomitant deficiency of RhoA and RhoB reverts this transmigration and results in macrothrombocytopenia, MK clusters around the vessel in the BM and defective MK development. The underlying mechanism that governs MKs to distinct localizations in the BM is poorly understood, thus this thesis suggests that this process may be dependent on RhoB protein levels, as RhoA deficiency is coincided with increased RhoB levels in MKs and platelets.

The third part of this thesis targeted the protein PDK1, a downstream effector of Rho GTPases, in regard to MK maturation and polarization throughout thrombopoiesis. MK- and platelet-specific KO in mice led to a significant macrothrombocytopenia, impaired actin cytoskeletal reorganization during MK spreading and proplatelet formation, with defective MK maturation. This was associated with decreased PAK activity and, subsequently, phosphorylation of its substrates LIMK and Cofilin. Together, the observations of this thesis highlight the importance of Rho GTPases and their downstream effectors on the regulation of the MK and platelet cytoskeleton.

Zusammenfassung

Thrombozyten sind kleine Zellfragmente ohne Zellkern, die von *Megakaryozyten* (MKs) produziert werden. MKs sind riesige Zellen im Knochenmark, welche lange zytoplasmatische Ausläufer in die sinusoidalen Blutgefäße strecken, woraus durch den Blutstrom Thrombozyten abgeschnürt werden. Während der Thrombozyten-Biogenese penetrieren Teile des MKs das Endothel und durch zytoskeletales Umorganisieren innerhalb des MKs werden Proplättchen-Fragmente gebildet. Rho GTPasen wie die Proteine RhoA und RhoB sind maßgebliche Regulatoren des Zytoskeletts, sowohl des Aktins als auch des Tubulin Zytoskeletts.

Der erste Teil dieser Thesis konzentrierte sich auf das Protein RhoB und dessen Einfluss auf die Organisation des Zytoskeletts. Mäuse mit einer Defizienz für das Protein RhoB zeigen eine Microthrombozytopenie und eine Reduktion der Thrombozytenzahl und -größe. Dies ist begleitet von Defekten des Mikrotubuli Zytoskeletts sowohl in MKs als auch in Blutplättchen. In Thrombozyten waren insbesondere Tubulin Organisation und Stabilisation betroffen, welche durch posttranslationale Modifizierungen von α-Tubulin bestimmt wurde. RhoB-negative MKs hingegen produzierten abnormal geformte Proplättchen, hatten jedoch unveränderte posttranslationale Modifizierungen von α-Tubulin.

Der zweite Teil dieser Thesis fokussierte sich auf den Einfluss von RhoA und RhoB auf die Lokalisation von MKs im Knochenmarkt von Mäusen. Eine große Anzahl von RhoA-negativen MKs können durch das Endothel in die Blutgefäße wandern und bleiben dort adhärent, während nur etwa 1% wildtypischer MKs am Blutgefäß detektierbar sind. Gleichzeitige Defizienz von RhoA und RhoB revertiert die Translokation von RhoA-negativen MKs und führt in Mäusen zu Makrothrombozytopenie, die Formierung von MK Clustern um die Gefäßwand im Knochenmark und eine fehlerhafte MK Entwicklung. Der Mechanismus, der MKs zu bestimmten Positionen im Knochenmarkt führt, ist bisher kaum verstanden. In dieser Thesis konnte gezeigt werden, dass dieser Prozess von dem Level an RhoB Protein abhängig sein könnte, da eine Defizienz von RhoA zu einer Hochregulierung von RhoB in MKs und Thrombozyten führte.

Der dritte Teil dieser Thesis zielte auf ein Signalprotein der Rho GTPasen ab, dem Protein PDK1. Es wurde die Rolle von PDK1 in der Regulation von MK Reifung und Polarisation während der Bildung von Thrombozyten untersucht. Ein MK und Thrombozyten spezifischer KO von PDK1 führte zu einer signifikanten Makrothrombozytopenie, einem gestörten Aktin Zytoskelett, während des MK Spreadings und der Proplättchen Bildung, begleitet von einer fehlerhaften MK Reifung. Dies war mit einer Reduktion in der Aktivität von PAK und folglich dem Phosphorylierungsstatus seiner Substrate LIMK und Cofilin assoziiert.

Die Beobachtungen dieser Doktorarbeit arbeiteten die Relevanz von Rho GTPasen und ihren Signalproteinen für die Regulation des MK und Thrombozyten Zytoskelettes im Maus-Modell hervor.

Table of content

1. Introduction

1.1. Megakaryocytes

The name *megakaryocyte* (MK) originates from the greek words mega (μέγας, big), karyon (káryon, core) and kytos (κύτος, cell) and translates into the definition of 'cell with a big nucleus'. Besides their polyploid nucleus, MKs are with an average size of 50 – 100 μm the largest cells in the BM, but account for less than 0.1% of nucleated cells (Italiano et al., 1999). During embryonic development of mice, MKs were shown to be present in fetal liver, yolk sac and spleen (Figure 1), while platelet production shifts to the BM in adult mice. The presence of MKs has also been reported in the lung (Howell and Donahue, 1937), but their contribution to thrombopoiesis remains controversial (Kaufman et al., 1965; Lefrançais et al., 2017).

1.1.1. Megakaryopoiesis

At present, various models of megakaryopoiesis are discussed in the literature. According to one model, MK progenitors leave the endosteal/osteoblastic niche and migrate towards the BM sinusoidal vascular niche during maturation, where, eventually, platelets are produced by mature MKs (Calvi et al., 2003; Kiel and Morrison, 2006). However, a revised model implicates that MKs mature at the sinusoidal niche, since the fully vascularized BM leaves no space for a distant periostic niche (Stegner et al., 2017).

Nevertheless, the maturation of *hematopoietic stem cells* (HSCs) to MKs is tightly regulated by diverse cytokines at multiple stages and involves various signaling pathways (such as *Phosphoinositide 3-kinase* [PI3K], *protein kinase B* [Akt], *Mitogen-activated protein kinase* [MAPK], Src/Syk/*Phosphoinositide-phospholipase C* isoform γ [PLCy]), transcription factors (*GATA-1/friend of GATA 1* [FOG1], GATA-2, *Runt-related transcription factor 1* [RUNX1]) and cytokines (S*tromal cell-derived factor* [SDF]-1, *Interleukin* [IL]-1β, IL-3, IL-6, IL-1α, *C-C motif chemokine ligand 5* [CCL5]) (Noetzli et al., 2019). The most prominent cytokine for HSC to MK maturation is *thrombopoietin* (TPO), which was discovered and cloned with its respective receptor *myeloproliferative leukemia protein* (c-mpl) in 1994 (Bartley et al., 1994; De Sauvage et al., 1994; Sohma et al., 1994). The importance of TPO and c-mpl were highlighted by the generation of c-mpl-deficient mice, which displayed a pronounced macrothrombocytopenia and decreased MK number in the BM (Gurney et al., 1994). Moreover, mutations in the *MPL* gene, encoding for c-mpl, were shown to be associated with *congenital amegakaryocytic thrombocytopenia* (CAMT) in humans (Ballmaier et al., 2001; Ihara et al., 1999). The discovery of TPO enabled the in vitro cultivation of human CD34^{+} cells as well as the maturation of *lineage-negative* (Lin^{-}) progenitors from murine fetal livers or BM into MKs (Choi et al., 1995). This in vitro cell culture system facilitated the analysis of MK differentiation, maturation,

proplatelet formation and the final platelet production in more detail and helped to identify pivotal regulators of these processes (Figure 1).
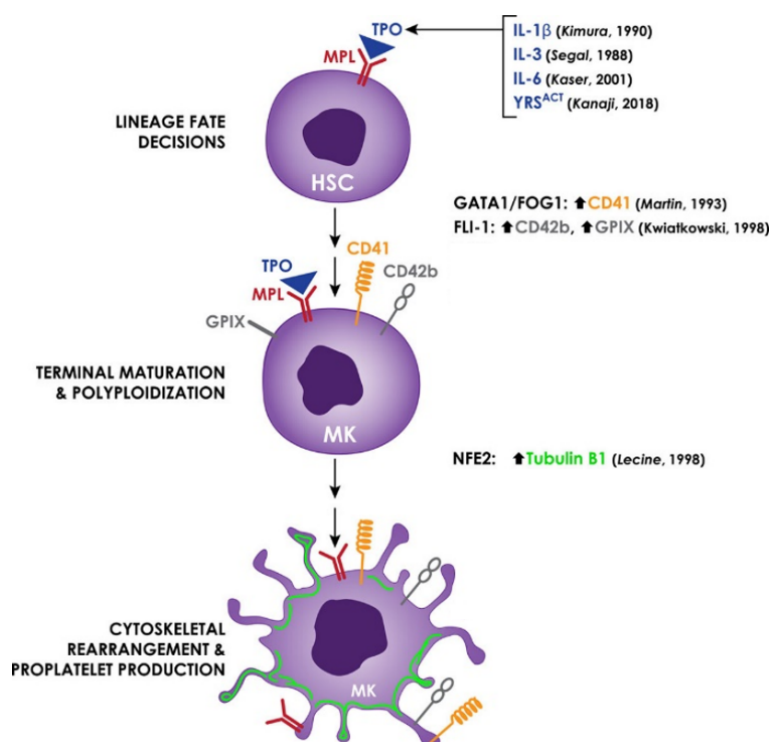
Figure 1 Regulation of MK maturation by cytokines and transcription factors. During MK maturation from HSC to mature MK to proplatelet forming MK, various cytokines (blue) and transcription factors determine their fate. The most important cytokine is TPO (blue) interacting with its receptor c-mpl (red), which is expressed throughout the differentiation stages and guides MK maturation. Besides TPO, cytokines such as IL-1β, IL-3, and IL-6 are involved in HSC differentiation. Transcription factors like GATA1/FOG1 and *Friend leukemia integration* 1 (FLI-1) induce the expression of C*luster of differentiation* 41 (CD41, orange), CD42b and *Glycoprotein IX* (GPIX, both grey), whereas NFE1 is crucial for the terminal maturation stages by regulating cytoskeletal components (tubulin β1, green). Modified from Noetzli, French and Machlus, 2019.

TPO triggers the polyploidization of MKs, a process called endomitosis, in which MKs undergo multiple cycles of DNA replication without cell division (Machlus and Italiano, 2013; Zimmet and Ravid, 2000). In the course of maturation, MKs reach DNA contents of 4N, 8N, 16N or 64N and can contain up to 128 sets of chromosomes (128N) in their polylobulated nucleus. In addition to endomitosis, MKs expand their membrane surface area and develop a highly *invaginated membrane system* (IMS or *demarcation system* [DMS]) during maturation). This DMS consists of numerous cytoplasmic membranes, the formation of which are highly dependent of cytoskeletal rearrangements and later serve as a membrane reservoir for platelet formation (Schulze et al., 2006).

1.1.2. Thrombopoiesis

The process of thrombopoiesis is characterized by the extension of long cytoplasmic protrusions (proplatelets) by mature MKs through the endothelium into the vessel lumen where platelets are sized by the bloodstream. It is highly discussed, how MKs are able to extend proplatelets into sinusoids in vivo and the mechanism behind this process is still barely understood. In vitro studies suggest that mature MKs disintegrate into thin long cytoplasmic extensions with platelet-sized swellings at their ends (´beads on a string´-theory, Italiano et al.,

1999), in which *microtubules* (MTs) are arranged into a sub-membranous scaffold (´marginal band´) that encircles the edges of the proplatelets (Figure 2). This elongation of proplatelets is driven by a Dynein/Dynactin-dependent sliding of MTs and is highly dependent on the MT network (Bender et al., 2015; Patel-Hett et al., 2008). Finally, the whole MK is surrounded by a large network of proplatelet extensions with only the nucleus remaining in the centre (Figure 2). Nevertheless, a big discrepancy between platelet production in vivo and in vitro hinders studies, since in vitro *proplatelet formation* (PPF) of BM derived MKs is far less efficient. Only murine *fetal liver cell*-derived (FLC) MKs can produce proplatelets under TPO stimulation, whereas murine BM derived MKs do not produce proplatelets in the presence of TPO only. Recently, it has been shown that the addition of heparin or hirudin stimulated PPF in BM derived MKs, to a similar extent to what has been observed using FLC derived MKs in vitro (Strassel et al., 2012). Additionally, the culture of BM derived MKs in methylcellulose with 30 - 60 Pa stiffness, which mimics the BM stiffness, led to a twofold increase in PPF in comparison to MKs grown in liquid culture (Aguilar et al., 2016). Furthermore, in vivo PPF has been described as a polarized process culminating in a directed release of platelets into the vessels, which contrasts with the multidirectional ´beads on a string´ PPF observed in vitro (Eckly et al., 2020; Bornert et al., 2020).
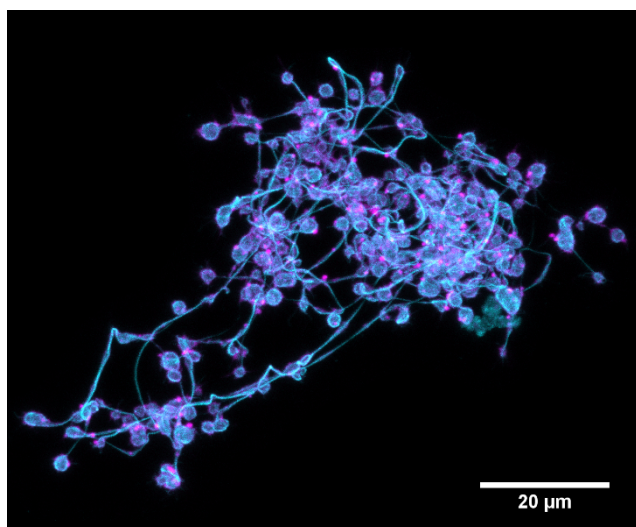
Figure 2 Mature proplatelet forming BM derived MK. Under static conditions, mature BM derived MKs produce long thin protrusions in an undirected manner. The long protrusions end in platelet-sized swellings containing MT bundles, whereas *filamentous actin* (F-actin) is distributed within the whole MK. A-tubulin is visualized using Alexa488 (cyan) and phalloidin-A647 labels F-actin (magenta). Images were obtained at a Leica TCS SP8 confocal microscope with a 40x magnification.

20 µm

Recent studies using advanced imaging methods suggest that the theory of long thin protrusions that are released into the bloodstream does not fully apply to in vivo PPF. Big fragments that reach into the vessel lumen were observed, that potentially generate circulating platelets (Brown et al., 2018; Kowata et al., 2014). By taking advantage of a combination of high-resolution microscopy approaches, Eckly and colleagues observed similar results by showing that MKs form actin/myosin-dependent transendothelial pores that allow them to extend large fragments in the bloodstream, which could be remodeled into proplatelets (Figure 3) (Eckly et al., 2020). These in vivo results together with in vitro data clearly show that the

mechanism of platelet generation by MKs is highly dependent on cytoskeletal rearrangements, of both the MT and the actin network.
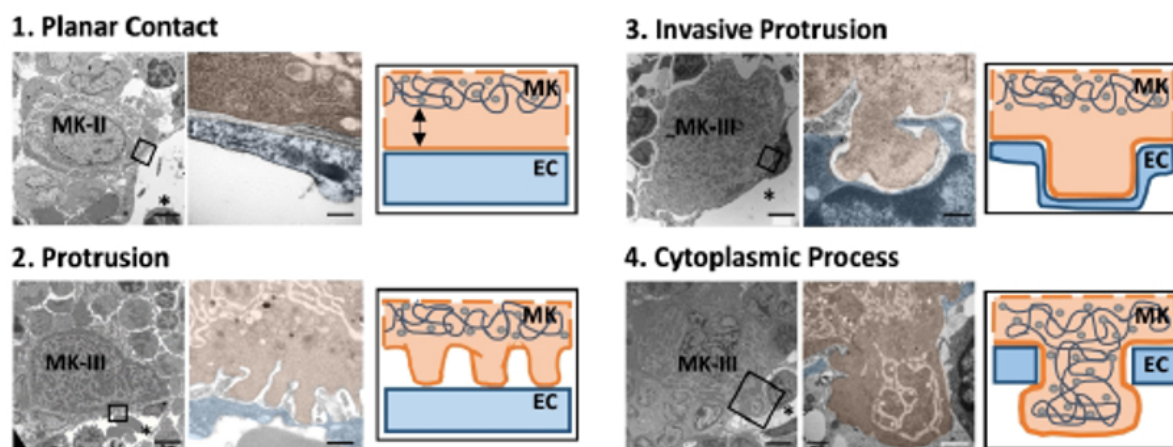
Figure 3 Model of transendothelial pore formation proposed by Eckly et al., 2020. Four types of contact between MKs and sinusoidal *endothelial cells* (ECs). (1) planar contact, (2) protrusion formation of MKs towards ECs, (3) MKs form an invasive protrusion into the EC, (4) MKs extends cytoplasm through the EC into the BM sinusoids. Respective left panel: Overview of MK-EC interaction by electron microscopy; Middle panel: MKs with a 75% transparency orange overlay and EC with a 75% transparency blue overlay. Right panel: schematic model of MK-EC interaction. MK-II and MK-III stand for the stage of maturation. Scale bars represent 5 µm in the left panels and 1 µm in the middle panels. Adapted from Eckly et al., 2020.

Moreover, Potts, Farley, Dawson, Rimes and colleagues recently showed that MK membrane budding also results in platelet release directly into the circulation in multiple BM sites and the spleen (Potts et al., 2020). This process occurs without signs of ´classical´ PPF, highlighting alternative options in addition to the classical proplatelet formation theory.

1.2. Platelets

Primary hemostasis is dependent on the adhesion, activation and aggregation of platelets, but these processes are also key factors during acute arterial thrombotic occlusion causing fatal disease states such as myocardial infarction or ischemic stroke (Jackson, 2011). Furthermore, platelets have been described as mediators of thrombo-inflammation, atherogenesis and tumor vascular integrity (Mezger et al., 2019; Volz et al., 2019). In humans, platelet size ranges from 1 - 2 µm and around 150-400 x 10^3 platelets/µl circulate in the bloodstream with a life span of around 7 -10 days (Baker et al., 1997; Schmitt et al., 2001). Murine platelets have an average diameter of 0.5 µm and around 1 x 10^6 platelets/µl circulate in the blood for 5 days (Aurbach and Spindler et al., 2019). Final clearance of aged (human and murine) platelets takes place in the reticulo-endothelial system of the spleen and liver by macrophages.

The platelet surface contains integrins (e.g., β1, β3, α2, αIIb), *glycoproteins* (GPs), such as the GPIb-V-IX complex, G-protein coupled receptors (e.g., G_i, G_q, $G_{12/13}$) and the (hem) *immunoreceptor tyrosine-based activation motif* (ITAM) receptors GPVI and *C-type lectin-like receptor 2* (CLEC-2), among others. Beneath and parallel to the plasma membrane marginal MTs coil around the platelet cell periphery, which, together with the actin cytoskeleton, maintain the platelet shape during resting conditions. In their cytoplasm, platelets possess a mixture of intracellular granules, with three major subtypes: α-granules, dense granules, and lysosomes. While lysosomes are less well-described, α-granules, among a plethora of other molecules, cargo *von Willebrand Factor* (vWF) and fibrinogen, which can be secreted upon platelet activation sites of injury. Furthermore, α-granules contain around third to half of integrin αIIbβ3 and one-third of GPVI receptors, which are transported to the platelet surface upon activation (Blair and Flaumenhaft, 2009). Dense granules incorporate a variety of molecules such as *adenosine diphosphate* (ADP), *adenosine triphosphate* (ATP), *5-hydroxytryptamin* (5-HT), magnesium and calcium (Golebiewska and Poole, 2015).

Under physiological conditions, platelets circulate in a discoid shape in close proximity to the vessel wall and are not activated until the endothelial layer covering the vascular wall is disrupted and the subendothelial matrix is exposed (Golebiewska and Poole, 2015). Once the vessel wall is compromised, the platelet GPIb-V-IX complex transiently interacts with immobilized vWF (tethering) and subsequently a firm platelet adhesion to the *extracellular matrix* (ECM) is mediated through an interaction of GPVI with collagen (Figure 4). This interaction induces intracellular signaling, which leads to platelet activation and thereby the generation of secondary platelet agonists (e.g., *Thromboxane* A_2 [TxA_2] and ADP). These agonists contribute to a progressing platelet activation through the mobilization of G-protein coupled receptors together with locally produced thrombin (Nieswandt et al., 2011).
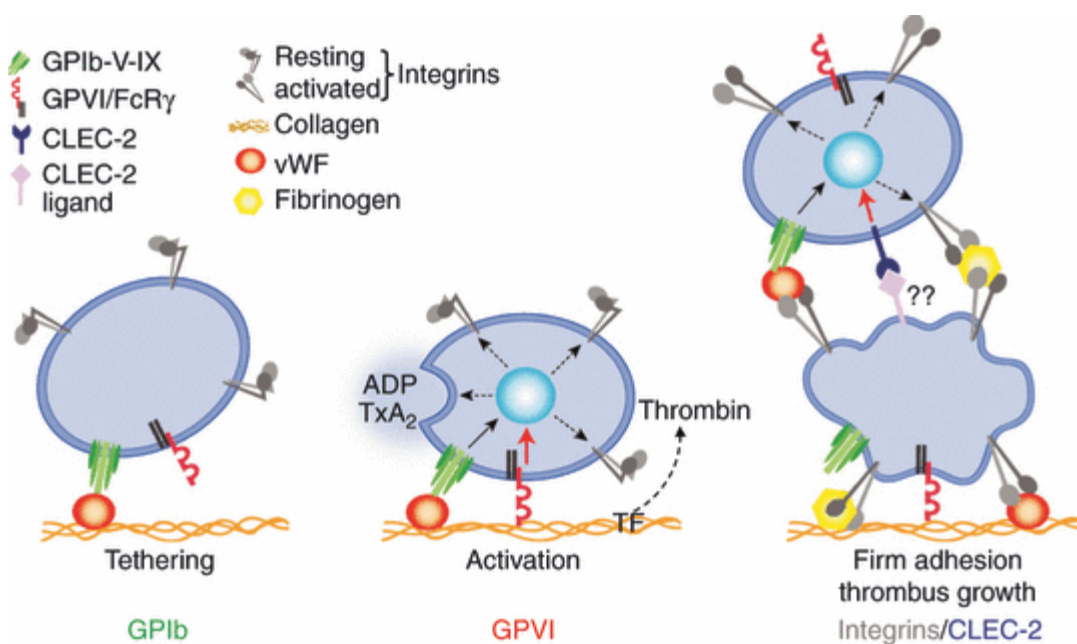
Figure 4 Three steps of thrombus formation. Upon vessel wall injury ECM proteins (vWF, collagen) are exposed leading to initial platelet tethering mediated by GPIb-vWF interactions. Subsequently, platelets get activated and adhere to collagen through GPVI. The secretion of soluble factors such as thrombin, ADP and TxA$_2$ leads to further platelet activation, firm adhesion by integrins and thrombus growth. Adapted from Nieswandt, Pleines and Bender, 2011 (Nieswandt et al., 2011).

During platelet activation in mice, which is mainly mediated through the receptor GPVI, CLEC-2 and integrins α2β1 and αIIbβ3, the *PLC isoform γ2* (PLCγ2) is phosphorylated and thus activated, which induces the release of Ca^{2+} from intracellular stores (Mammadova-Bach et al., 2019). The increase of Ca^{2+} in the cytoplasm then contributes to further steps of cellular activation, such as degranulation and inside-out activation of integrin αIIbβ3 and cytoskeletal rearrangements pivotal for platelet shape change (Varga-Szabo et al., 2009).

1.3. The megakaryocyte and platelet cytoskeleton

The cytoskeleton is crucial for many cellular mechanisms in platelets and MKs. It retains the discoid shape of resting platelets in the circulation, but also mediates platelet shape change during thrombosis. In MKs, cytoskeletal arrangements are required for PPF and platelet generation. So far, predominantly the actin and MT network have been investigated regarding the MK and platelet cytoskeleton (Antkowiak et al., 2016; Bender et al., 2015; Geue and Aurbach et al., 2019; Italiano et al., 1999; Schachtner et al., 2013; Stritt et al., 2018). However, MKs express both Spectrin isoforms, erythroid (α1 and β1) and non-erythroid (α2 and β2) isoforms, which are distinctly located within MKs. Erythroid isoforms are equally distributed in the cell as punctuate structures, whereas the non-erythroid isoforms are located near the plasma membrane in association with F-actin. In proplatelet forming MKs, the non-erythroid isoforms cover the whole proplatelet protrusion from shaft to tip and the erythroid isoforms are found as punctuate patterns. The tetramerization of those Spectrin isoforms is required for PPF

and MK maintenance, since the expression of a tetramer disrupting-construct in FLC derived MKs results in a failure of proplatelet production and DMS maturation (Patel-Hett et al., 2011).

Intermediate filaments are another component of the cytoskeleton with more flexible and elastic properties than MTs and actin and regulate actin branching, focal adhesion and stress fiber stability during cell migration (Lowery et al., 2015). The most prominent members are Vimentin, Desmin and Nestin, with only Vimentin described in platelets so far. Vimentin interacts with vWF on the platelet surface hereby contributing to platelet adhesion at high shear stress (Cerecedo et al., 2013; Da et al., 2014).

1.3.1. The actin cytoskeleton

Actin filaments are highly dynamic structures, which are constantly remodeled to allow flexible cellular dynamics for migration, polymerization, or differentiation. Depending on cellular needs, F-actin can be severed and capped (e.g., by *Actin depolymerizing* factor [ADF]/Cofilin]), stabilized (e.g., by *Tropomyosin* [Tpm]), crosslinked (e.g., by Filamin A or Actinin) or recycled into new structures (Rohn and Baum, 2010). Mutations in actin-regulatory genes (either due to a loss-of-function mutation in the gene or a complete KO) lead to various alterations in cells and are usually associated with the deregulation of other actin regulatory proteins leading to a disturbance of the protein equilibrium. For example, mutations in *TPM4,* the gene encoding for *Tropomyosin 4* (Tpm4) were associated with macrothrombocytopenia in humans and mice due to failures in the terminal stages of PPF. Mutant platelets and MKs displayed a higher level of active Cofilin (assessed by phosphorylation at Ser_3), which indicates an increased F-actin severing, and reduced protein levels of Actinin and Filamin A (Pleines et al., 2017).

The actin cytoskeleton is a constant transition between monomeric *globular* (G-) actin and polymeric F-actin. In vertebrates, three different actin isoforms have been described: the α, β and γ-isoforms. Skeletal, cardiac, and smooth muscles express α-isoforms, whereas the β and γ-isoform are expressed in non-muscle and muscle cells. These actin isoforms are solely distinguished by few amino acids and can be modified by *posttranslational modifications* (PTMs) (Herman, 1993). In vitro analysis revealed that actin monomers exist in three energetic states: ATP-G-actin, ADP-Pi-G-actin, and ADP-G-actin. ADP-G-actin monomers are bound by the nucleotide exchange factors Profilin and Thymosin-β4 and charged to ATP-G-actin. As these factors have a low affinity for ATP-G-actin, they directly dissociate after charging and the monomers join the fast-growing barbed (+) end of F-actin (Figure 5A) (De La Cruz et al., 2000; Pollard, 2016).

Deficiency in Profilin1 in platelets and MKs results in microthrombocytopenia, premature platelet release into the BM (´ectopic platelet release´) and defective β1 and β3 integrin function (Bender et al., 2014; Stritt et al., 2018). Filament elongation is accelerated by formins (in mammalians: *Dishvelled-associated activator 1-2* [DAAM1-2], *Protein diaphanous homolog 1-3*

[DIAPH1-3], *FH1/FH2 domain-containing protein 1,3* [FOD1,3], *Formin 1,2* [FMN1,2] and *Formin like protein 1,2* [FMNL1,2] (Zuidscherwoude et al., 2019)), which bind to ATP-G-actin and the barbed end of F-actin bringing them into close proximity. While deficiency of the formin DIAPH1 has no impact on platelet count and function in mice (Zuidscherwoude et al., 2019), a gain-of function mutation in DIAPH1 in humans results in macrothrombocytopenia, decreased PPF and an augmentation of F-actin polymerization in human platelets (Stritt et al., 2016).
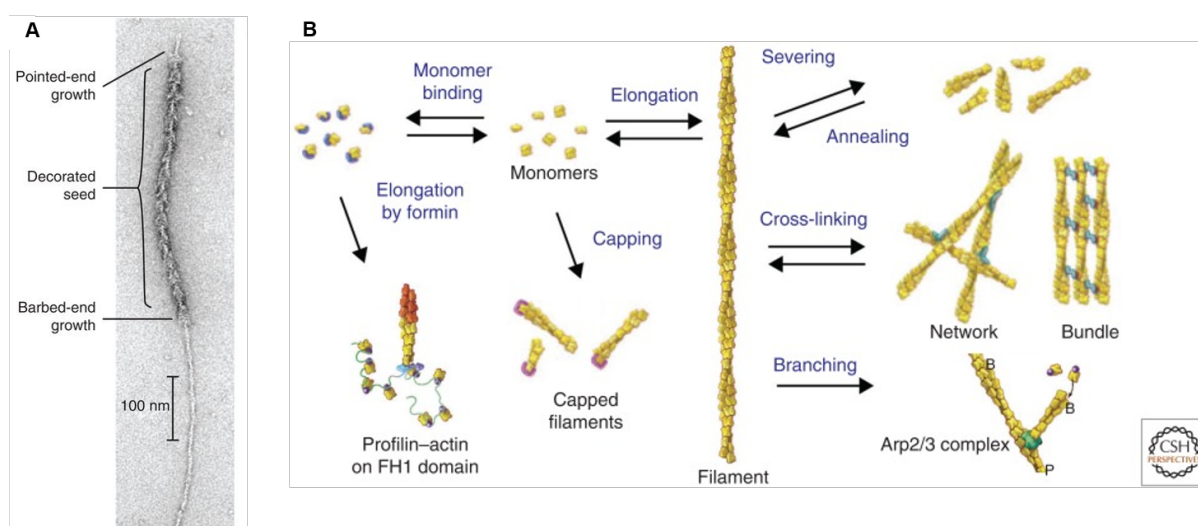
Figure 5 Actin polymerization by actin binding proteins. (A) Electron microscopic picture of a negatively stained actin filament depicting the pointed and barbed-end of F-actin. (B) Overview of interactions between actin and actin-binding proteins such as Profilin, Arp2/3, and formins. Modified after Pollard et al., 2016.

During F-actin aging, ATP-actin is depolymerized to ADP-Pi-actin and then uncharged to ADP-actin. The newly formed ADP-G-actin disassociates from the slower growing pointed (-) end of F-actin and joins the pool of uncharged ADP-G-actin. This process of depolymerization and severing is guided by ADF and Cofilin. Double deficiency of the two proteins in mice results in macrothrombocytopenia, reduced PPF and the absence of F-actin in platelets (Bender et al., 2010).

Besides the constant conversion of G-actin to F-actin and vice-versa, F-actin is branched and cross-linked depending on the cellular need. F-actin branching is mainly mediated by the Arp2/3 complex consisting of the two subunits Arp2 and Arp3, which organize into a dimer. The complex binds to actin filaments and Arp2 and Arp3 together form the base for F-actin branch formation (Figure 5B) (Rouiller et al., 2008). Loss of Arp2/3 leads to microthrombocytopenia in human and mice, premature platelet release into the BM and a disorganized actin and tubulin cytoskeleton in platelets in mice (Kahr et al., 2017; Paul et al., 2017). Furthermore, the Arp2/3 complex (together with integrins, *src family kinases* [SFK] and *Wiskott-Aldrich Syndrome protein* [WASP]) is located in podosomes, which are short lived F-actin-rich nodules in MKs mediating the adhesion to ECM proteins in vitro (Poulter et al., 2015). It was recently shown, that MK

podosomes are pivotal mediators of transcellular intravasation in vivo by generation of pores through *endothelial cells* (ECs) hereby facilitating PPF in the BM (Eckly et al., 2020).

Furthermore, the accession of actin-binding proteins such as Tropomodulin, ADF/Cofilin, Arp2/3, Caldesmon and Myosin motors to F-actin can be mediated by Tpms in an isoform dependent manner (Gunning et al., 2008). Tpms are divided into non-muscle and muscle-specific isoforms, with the muscle-specific Tpm as the best-characterized type. Tpms form dimers and the affinity for a single Tpm to bind actin is very low (Lorenz et al., 1995), in fact Tpms form polymers along the major groove of F-actin providing a high affinity and stability of the interaction (Perry, 2001). Besides, Tpms can contribute to inhibition of both, actin polymerization and depolymerization (Lai and Korn, 1986). Polymerization is inhibited by mechanical stabilization of the filament by inhibition of F-actin branching, which results in less F-actin ends accessible for polymerization (Hitchcock-DeGregori et al., 1988). F-actin depolymerization is driven by ADF/Cofilin, which is in an antagonistic relationship with Tpm and competes with Tpm for actin filament binding (Bernstein and Bamburg, 1982). A loss-of function mutation within *TPM4* leads to macrothrombocytopenia accompanied by bleeding episodes (Pleines et al., 2017).

1.3.2. The microtubule cytoskeleton

MTs are polar structures that together with actin and intermediate filaments represent the three main classes of cytoskeletal filaments in eukaryotic cells. MTs are heterodimers, which consist of GTP-bound α- and β-tubulin. The heterodimers assemble in a head-to-tail arrangement and form linear protofilaments. Thirteen of these linear protofilaments can be assembled into hollow polymer tubes of about 25 nm width and a length range from 1 µm to 100 µm, which have exposed β-tubulin at the fast-growing plus end and exposed α-tubulin at the slow-growing minus end. This polarity of the MTs plays a pivotal role for the function of Kinesin (Vale and Fletterick, 1997) and Dynein (Gelfand, 1995) families that move along the MT by utilizing the energy of ATP hydrolysis.

Furthermore, MTs constantly shift between polymerization and depolymerization by a perpetual switch between ADP- and ATP-bound heterodimers hereby providing the capacity for many properties of the MT cytoskeleton. The term ´catastrophe´ describes the transition from growth to shrinkage, while the term ´rescue´ is used for the transition from shrinkage to growth (Figure 6).
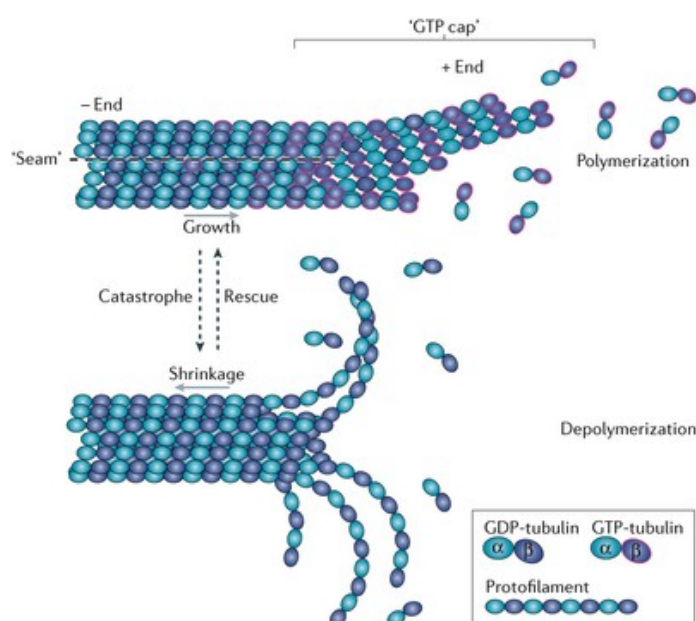
Nature Reviews | Molecular Cell Biology

Figure 6 MT dynamics. GTP-loaded αβ-tubulin heterodimers arrange into polar MT consisting of 13 protofilaments. The interaction between the α-tubulin of the incoming dimer and the β-tubulin incorporated at the + end leads to GTP hydrolysis and release of phosphate resulting in a GTP-tubulin-rich region, the so termed GTP gap. MTs cycle between growth and shrinkage and indicators for the dynamic shrinkage of MTs. Adapted from Roostalu and Surrey, 2017.

Five different α- and eight different β-tubulin isoforms exist in eukaryotic cells with the tubulin isoform β1 being solely expressed in MKs and platelets. Homozygous loss of the isoform in mice results in defective platelet biogenesis, thrombocytopenia and increased bleeding tendency (Schwer et al., 2001). Another crucial tubulin isoform predominantly expressed in platelets and MKs is α4A-tubulin. A missense mutation in the *Tuba4a* gene in mice and a monoallelic double missense mutation in TUBA4A gene in one patient resulted in macrothrombocytopenia and a reduced number of misarranged MT coils in the platelet marginal band. Additionally, defective MK maturation, PPF and altered PTMs were observed in the mutant mice compared to *wt* controls (Strassel et al., 2019).

The properties of MT polymers can be regulated by PTMs such as polyglutamylation, acetylation, detyrosination/tyrosination and phosphorylation. These PTMs affect MT dynamics and stability, but also influence binding/interactions of MTs with *microtubule interacting partners* (MIP). Acetylation of the α-tubulin subunit lysine 40 (Lys_{40}) and the exposure of the C-terminal glutamate by detyrosination (falsely often termed glutamylation) of the α-tubulin subunit are indicators for long-lived, ´stable´ MTs (Song and Brady, 2015; Wloga et al., 2017). While tubulin detyrosination is regulated by *Vasohibins 1 and 2* (VASH1 and 2) (Nieuwenhuis et al., 2017), the main mediator of K40 acetylation is the enzyme *α-tubulin N-acetyltransferase 1* (α-TAT1) (Kalebic et al., 2013). Deacetylation is performed by *Histone-deacetylase 6* (HDAC6), which has been described as a positive regulator of MK differentiation and PPF in humans, but not in mice (Messaoudi et al., 2017).

1.4. Rho GTPases

1.4.1. Structure and function of Rho GTPases

Rho guanosine triphosphatases (GTPases) are small GTP/GDP-binding proteins about 20 - 25 kDa in size that are associated with the regulation of both actin and MT cytoskeletal dynamics in virtually all cell types (Etienne-Manneville and Hall, 2002; Jaffe and Hall, 2005). They are key players in cell migration, polarization, differentiation and cell-cell contacts (Arnold et al., 2017; Karlsson et al., 2009; Sahai and Marshall, 2002; Vega and Ridley, 2008; Wheeler and Ridley, 2004). Most Rho GTPases cycle between an active GTP-bound and an inactive GDP-bound form, as the GTPase activity needs to be finely tuned to enable distinct cellular reactions. While the displacement of GDP and binding to GTP is mediated by *guanine exchange factors* (GEFs), GTP hydrolysis is regulated by *GTPase-activating proteins* (GAPs) (Cherfils and Zeghouf, 2013).

GTPases can be divided into several subfamilies in which the Rho-like subfamily (RhoA, RhoB, RhoC), the *ras related C3 botulinum toxin substrate* (Rac)-like subfamily and the *cell division control protein 42* (Cdc42)-like subfamily are the most prominent (Figure 7). The function of the Rho GTPases RhoA, Cdc42, Rac1 and RhoG has been well characterized in platelets and MKs (Pleines et al., 2019), whereas the role of the GTPases RhoB or RhoC is still largely unknown in these cell types.
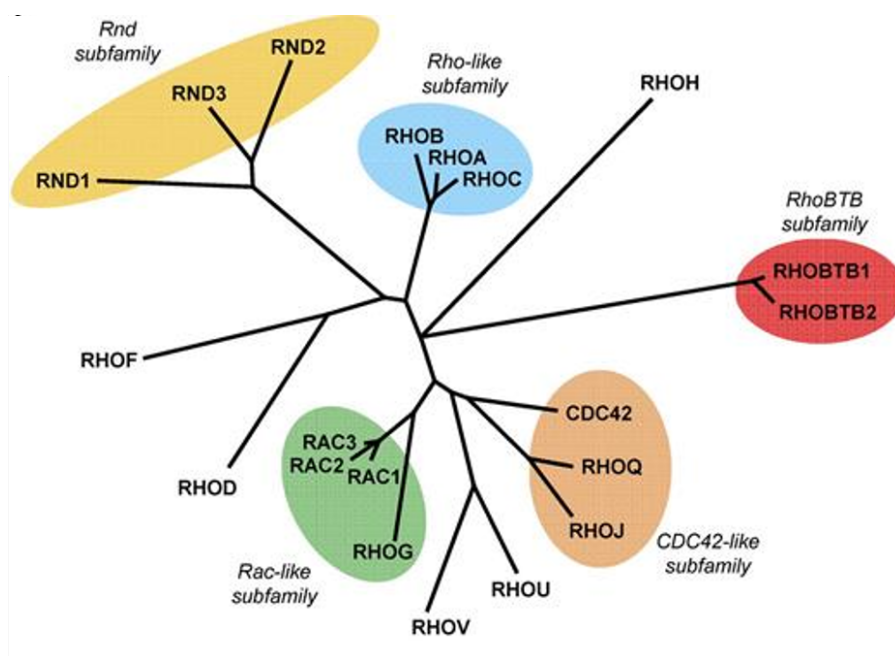
Figure 7 The Rho GTPase phylogenetic tree. Unrooted phylogenetic tree of the 20 human Rho GTPase family members divided in subfamilies by their sequence identity. Modified after Lawson and Ridley, 2018.

1.4.2. Role of Rho GTPases in platelet function

Most studies related to the function of Rho GTPases in platelet biology focused on RhoA, Rac1 and Cdc42 (Pleines et al., 2009, 2010, 2012). The Rho/Rho-kinase (*Rho-associated protein kinase,* ROCK) pathway is activated upon platelet stimulation with soluble agonists such as thrombin, ADP and TxA$_2$, which bind to heterodimeric G protein-coupled receptors such as G$_i$, G$_q$ and G$_{12/13}$, (Moers et al., 2003). Thrombin and TxA$_2$ activation lead to RhoA-GTP formation consecutively resulting in ROCK activation that induces ROCK phosphorylation and inactivation of *Myosin light chain* (MLC) phosphatases, which in turn results in an increased MLC phosphorylation and platelet shape change (Essler et al., 1998; Klages et al., 1999). MK- and platelet-specific deletion of RhoA revealed that RhoA is essential for platelet shape change, activation of integrin α$_{IIb}$β$_3$, granule secretion, clot retraction and thrombus formation (Pleines et al., 2012). Additionally, *RhoA$^{-/-}$* platelets displayed mild aggregation defects downstream of Gα$_{13}$ and Gα$_q$, while platelet spreading on fibrinogen was unaffected.

Cdc42 was described as a regulator of platelet filopodia formation and granule secretion (Pula and Poole, 2008), however, the specific role of Cdc42 in platelets is still controversially discussed (Akbar et al., 2011; Pleines et al., 2010). Studies of Pleines and colleagues suggested that Cdc42 has a unique role downstream of GPIb, since Cdc42 deficiency impaired filopodia formation on vWF. Furthermore, MK- and platelet-specific deletion of Cdc42 resulted in increased granule secretion accompanied by accelerated thrombus formation ex vivo under flow on collagen and in a model of arterial thrombosis in vivo (Pleines et al., 2010).

Rac1 is the only of three Rac isoforms being expressed in platelets and plays a major role in platelet lamellipodium formation (McCarty et al., 2005). It was suggested that Rac1 regulates lamellipodium formation and thrombus formation in vivo through GPVI-dependent PLCγ2 activation (Pleines et al., 2009). Interestingly, a recent study by Schurr and colleagues highlighted that lamellipodia formation is not necessary for thrombus growth and stability in vivo (Schurr et al., 2019).

1.4.3. Role of Rho GTPases in platelet biogenesis

Studies on the function of Rho GTPases in MK biology emerged within the last 10 years, but still little is known about the exact mechanisms regarding their role in platelet biogenesis. Inhibition of RhoA was shown to rescue severely diminished platelet counts in mice lacking *26S protease regulatory subunit 4* (PSMC1) in platelets through an enhanced PPF indicating that RhoA is a negative regulator of PPF (Shi et al., 2014a). In contrast, MK-specific deletion of RhoA (further referred as *RhoA$^{-/-}$*) in mice led to moderate thrombocytopenia partly caused by a decreased platelet life span in vivo (Pleines et al., 2012). Recently, it was reported that Cdc42 and RhoA are critical regulators of directed transendothelial platelet biogenesis in the BM in a GPIb-dependent manner (Antkowiak et al., 2016; Dütting et al., 2017). Duetting and colleagues

showed that *RhoA^-/-* MKs were able to transmigrate through ECs into the BM sinusoids and around 30% of those MKs stayed visibly attached to the vessel sinusoids (Dütting et al., 2017). Interestingly, this transmigration was reverted by double deficiency of RhoA and Cdc42 in MKs, which additionally resulted in a severe macrothrombocytopenia. These findings implied that RhoA and Cdc42 are key regulators of MK localization in BM sinusoids in vivo, with RhoA providing a ´stop signal´, and Cdc42 a ´go signal´ for MKs. Additionally, double deficiency of Rac1 and Cdc42 specifically in MKs led to macrothrombocytopenia, abnormal BM derived MK morphology and an abrogated PPF due to a heavily disturbed α-tubulin organization (Pleines et al., 2013).

Of note, although Rho GTPases share a plethora of common interaction partners and signaling pathways, little is known about redundancies and non-redundancies of the Rho GTPase family member in regard to platelet production and function. Therefore, compensatory mechanisms must be carefully examined to rule out the concrete pathways that are involved. Data such as unpublished data by Heib et al. (Dr. Tobias Heib, doctoral thesis), who show that the GTPases RhoA and Cdc42 are involved in compensatory mechanisms, but also take over different functions in platelets and MKs, are pivotal for our understanding of cellular processes (Gerald et al., 2013).

1.4.4. Role of RhoB in eukaryotic cells

In most eukaryotic cells three Rho isoforms namely RhoA, RhoB and RhoC can be found. The small Rho GTPases RhoA and RhoB share an amino acid sequence identity of about 87%, nevertheless they reportedly display distinct functions in eukaryotic cells (Vega and Ridley, 2018; Wheeler and Ridley, 2004).

To date, a role of RhoB has not been described in the literature in platelet biology. In other cell types, RhoB is involved in cytokine trafficking and cell survival (Vega et al., 2012), affects cell adhesion and migration through β2 and β3 integrin (Königs et al., 2014), but is not required for podosome assembly in macrophages (Wheeler and Ridley, 2007). A variety of lipid modifications within RhoB promotes its localization to the plasma membrane, endosomes and *multivesicular bodies* (MVB) (Fernandez-Borja et al., 2005; Wherlock et al., 2004). RhoB was also found in the nucleus (Gerald et al., 2013). Small Rho GTPases are target for ubiquitin-mediated proteasomal degradation, and with a short half-life of about 30 min, RhoB is more rapidly degraded than RhoA or RhoC (Zalcman et al., 1995). The low steady-state levels of RhoB can be upregulated promptly by stimuli as UV irradiation, growth factors or cytokines. Additionally, RhoB expression is amplified by downregulation of RhoA or RhoC, even though it is unclear whether this effect is caused by changes in protein stability or by miRNAs (Ho et al., 2008; Marcos-Ramiro et al., 2016; Vega et al., 2011).

1.4.5. Role of PDK1 in platelets

The AGC serine/threonine kinase *Phosphoinositide-dependent kinase 1* (PDK1) is a membrane associated and a downstream effector of *Phosphoinositide 3-kinase* (PI3K). PDK1 activates other AGC kinases by phosphorylation, which in turn mediate cellular responses including metabolism, development, proliferation and survival (Gagliardi et al., 2014; Weber et al., 2004). Moreover, PDK1 was described as a regulator of the actin cytoskeleton in migrating cancer cells, dendritic cells and ECs (Gagliardi et al., 2014; Primo et al., 2007; Zaru et al., 2008). The role of PDK1 in platelets was investigated by taking advantage of MK- and platelet-specific KO mice, as genetic deletion of *PDK1* resulted in embryonic lethality (Lawlor et al., 2002). Chen and colleagues demonstrated that platelet PDK1 activates Akt and inhibits by thrombin stimulation of *Glycogen synthase kinase 3 beta* (GSK3β), which is a major substrate of PDK1. Hereby, PDK1 promotes thrombin-induced platelet aggregation, spreading on fibrinogen and thrombus formation in vivo (Chen et al., 2013). Manne and colleagues demonstrated that PDK1 is crucial for the crosstalk of *mitogen-activated protein kinase* (MAPK) and PI3K in platelets, thus altering TxA_2 generation, thrombosis and *2-Methylthio-adenosine-5'-diphosphate* (2MeSADP)-induced platelet activation (Manne et al., 2018). However, the role of PDK1 in platelet biogenesis was just recently investigated by Geue, Aurbach and colleagues (see Results 3.3, Geue and Aurbach et al., 2019).

1.5. Aim of this study

The platelet and MK cytoskeleton is constantly rebuilt by various key players, which is crucial for proper megakaryopoiesis, MK function, platelet biogenesis and platelet function. In the last decade, various proteins were identified that influence these processes in human and mice. Scientists used the murine system to generate KO or mutant mice for a basic understanding of the underlying mechanisms behind the before mentioned processes. The aim of this study was to understand the role of small Rho GTPases, most notably RhoB and RhoA, and their possible downstream effector the AGC serine/threonine kinase PDK1 in platelet biogenesis and function by the use of conditional and constitutive genetic KO systems in mice (Figure 8). Hereby, a specific focus was set on the platelet and MK cytoskeleton, which is tightly regulated by Rho GTPase signaling. Hereby both, the actin and tubulin cytoskeleton were investigated.
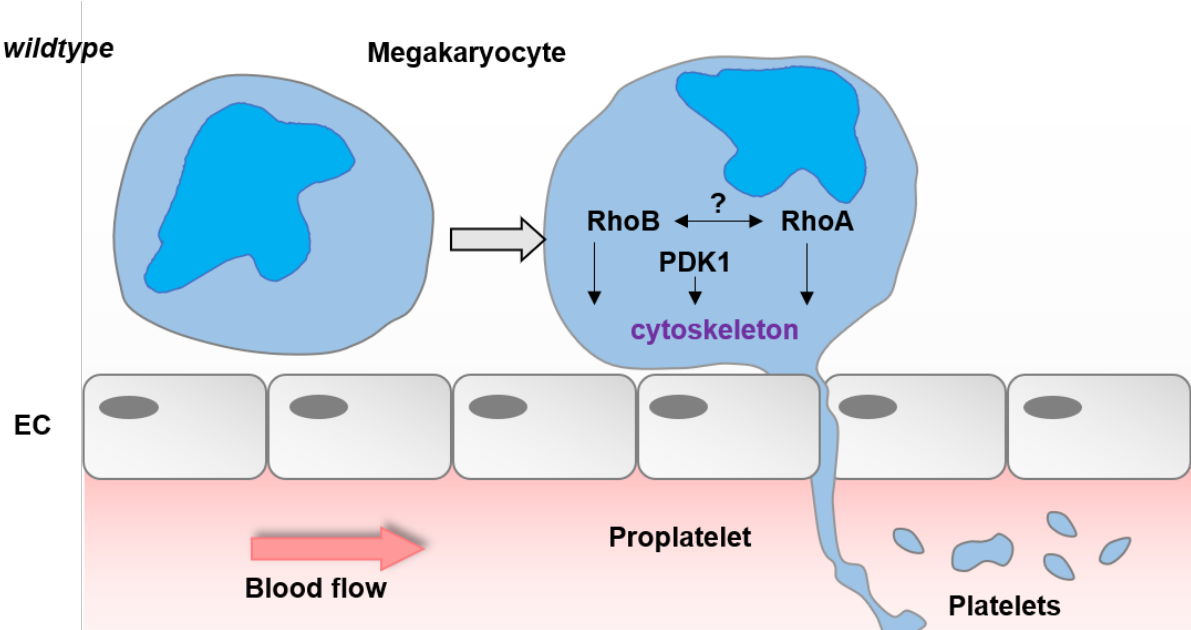
Figure 8 Overview of the investigated proteins. Under *wt* conditions, MKs maturate in the BM and migrate towards the BM sinusoids. MKs extend long protrusions through the endothelial layer and produce platelets. The Rho GTPases RhoB and RhoA are localized in the MK cytoplasm, and their interaction is not clear to date. RhoB, RhoA and their possible downstream effector PDK1 are involved in the regulation of the actin and MT cytoskeleton. EC = endothelial cell. Modified after a graphic kindly provided by Dr. Irina Pleines-Meinhold.

2. Materials and Methods

2.1. Materials

2.1.1. Chemicals and reagents

Product	Company
Adenosine diphosphate (ADP)	Sigma-Aldrich (Steinheim, Germany)
Agarose	Roth (Karlsruhe, Germany)
Ammonium persulfate (APS)	Roth (Karlsruhe, Germany)
Apyrase (grade III)	Sigma-Aldrich (Steinheim, Germany)
Adenosine triphosphate (ATP)	Fermentas (St. Leon-Rot, Germany)
β-mercaptoethanol	Roth (Karlsruhe, Germany)
Bovine serum albumin (BSA)	Sigma-Aldrich (Steinheim, Germany)
Cacodylate	AppliChem (Darmstadt, Germany)
Calcium chloride	Roth (Karlsruhe, Germany)
Collagen Horm® suspension + SKF sol.	Takeda (Linz, Austria)
Complete protease inhibitors (+EDTA)	Roche Diagnostics (Mannheim, Germany)
Convulxin (CVX)	Enzo Life Sciences (New York, USA)
4',6-diamidino-2-phenylindole (DAPI)	ThermoFisher Scientific (Waltham, USA)
Deoxynucleotide triphosphates (dNTP) mix	Fermentas (St. Leon-Rot, Germany)
Dimethyl sulfoxide (DMSO)	Sigma-Aldrich (Steinheim, Germany)
DyLight-488	Pierce (Rockford, USA)
Ethylenediaminetetraacetic acid (EDTA)	AppliChem (Darmstadt, Germany)
Eukitt® quick-hardening mounting medium	Sigma-Aldrich (Steinheim, Germany)
Enhanced chemiluminescence (ECL) detection substrate	MoBiTec (Göttingen, Germany)
Eosin	Roth (Karlsruhe, Germany)
Ethanol	Roth (Karlsruhe, Germany)
Fentanyl	Janssen-Cilag GmbH (Neuss, Germany)
Fibrinogen from human plasma (F3879)	Sigma-Aldrich (Steinheim, Germany)
Fluorescein-isothiocyanate (FITC)	Molecular Probes (Oregon, USA)
Fluoroshield™	Sigma-Aldrich (Steinheim, Germany
Fluorshield™ with DAPI	Sigma-Aldrich (Steinheim, Germany)
GeneRuler DNA Ladder Mix	Fermentas (St. Leon-Rot, Germany)
Halt protease & phosphatase inhibitor cocktail	ThermoFisher Scientific (Waltham, USA)
High molecular weight heparin	Ratiopharm (Ulm, Germany)
Igepal®CA-630	Sigma-Aldrich (Steinheim, Germany)

Immobilon-P transfer membrane, PVDF	Merck Millipore (Darmstadt, Germany)
Integrilin® (Eptifibatide)	Millennium Pharmaceuticals Inc. (Cambridge, USA)
Isofluran CP®	cp-pharma (Burgdorf, Germany)
Isopropanol	Roth (Karlsruhe, Germany)
iTaq Universal SYBR Green Supermix	Bio-Rad (Hercules, USA)
Loading Dye solution, 6x	Fermentas (St. Leon-Rot, Germany)
Magnesium chloride	Roth (Karlsruhe, Germany)
Magnesium sulfate	Roth (Karlsruhe, Germany)
Manganase chloride	Roth (Karlsruhe, Germany)
Medetomidine (Dormitor)	Pfizer (Karlsruhe, Germany)
Methanol	Roth (Karlsruhe, Germany)
Midazolam (Dormicum)	Roche (Grenzach-Wyhlen, Germany)
Midori Green™	Biozym Scientific (Oldenburg, Germany)
Neuraminidase (Sialidase)	Roche Diagnostics (Mannheim, Germany)
Nonidet P-40 (NP-40)	Roche Diagnostics (Mannheim, Germany)
Osmium tetroxide	Merck Millipore (Darmstadt, Germany)
PageRuler® Prestained Protein Ladder	Fermentas (St. Leon-Rot, Germany)
Paraformaldehyde (PFA)	Roth (Karlsruhe, Germany)
Phalloidin-Atto647N	Sigma-Aldrich (Steinheim, Germany)
Phalloidin-FITC	Enzo Life Sciences (New York, USA)
Poly-L-lysine	Sigma-Aldrich (Steinheim, Germany)
Propidium iodide (PI)	ThermoFisher Scientific (Waltham, USA)
Prostacyclin (PGI$_2$)	Calbiochem (Bad Soden, Germany)
Protease Inhibitor Cocktail	Sigma-Aldrich (Steinheim, Germany)
Proteinase K	Fermentas (St. Leon-Rot, Germany)
Recombinant hirudin	Hyphen Biomed (Neuville-sur-Oise, France)
R-phycoerythrin (PE)	EUROPA (Cambridge, UK)
Rotiphorese Gel 30% (PAA)	Roth (Karlsruhe, Germany)
Sodium azide	Sigma-Aldrich (Steinheim, Germany)
Sodium chloride	AppliChem (Darmstadt, Germany)
Sodium citrate	AppliChem (Darmstadt, Germany)
Sodium dodecyl sulfate (SDS)	Sigma-Aldrich (Steinheim, Germany)
Sodium hydroxide	AppliChem (Darmstadt, Germany)
Sodium orthovanadate	Sigma-Aldrich (Steinheim, Germany)
Sucrose	Sigma-Aldrich (Steinheim, Germany)
Tail lysis buffer	Viagen Biotech (Los Angeles, USA)
Tetramethylethylenediamine (TEMED)	Roth (Karlsruhe, Germany)
TissueTek O.C.T Compound	Sakura Finetec (Staufen, Germany)

Tris(hydroxymethyl)aminomethane (TRIS)	Roth (Karlsruhe, Germany)
Triton X-100	Sigma-Aldrich (Steinheim, Germany)
TRIzol®	ThermoFisher Scientific (Waltham, USA)
Trypan Blue	Sigma-Aldrich (Steinheim, Germany)
Tween 20®	Roth (Karlsruhe, Germany)
U46619	Alexis Biochemicals (San Diego, USA)
Uranyl acetate	EMS (Hatfield, USA)
Vectashield hardset mounting medium	Vector Labs, Inc. (Burlingame, USA)
Water, nuclease-free	Roth (Karlsruhe, Germany)

2.1.2. Consumables, kits, and cell culture material

Product	Company
Cell Strainer, 70 µm	PluriSelect (Leipzig, Germany)
CellTiter-Glo® Luminescent Cell Viability Assay	Promega (Madison, USA)
Cryo-tubes	Roth (Karlsruhe, Germany)
Cryofilm type 3C (16UF)	Section Lab Co Ltd. (Hiroshima, Japan)
Cryofilm type 2C (10)	Section Lab Co Ltd. (Hiroshima, Japan)
Dulbecco's phosphate-buffered saline (DPBS)	Gibco (Karlsruhe, Germany)
Dulbecco's Modified Eagle Media (DMEM)	Gibco (Karlsruhe, Germany)
Essential amino acids	Gibco (Karlsruhe, Germany)
Fetal calf serum (FCS)	Perbio (Bonn, Germany)
Glass slide superfrost	Roth (Karlsruhe, Germany)
Heparinized capillaries	Hartenstein (Würzburg, Germany
Microcapillaries (100 µl)	Hartenstein (Würzburg, Germany
Microcapillaries (50 µl)	Hartenstein (Würzburg, Germany
Non-essential amino acids	Gibco (Karlsruhe, Germany)
Penicillin/streptomycin	Gibco (Karlsruhe, Germany)
Recombinant mouse stem cell factor (SCF)	BioLegend (San Diego, USA)
StemPro®-34	Gibco (Karlsruhe, Germany)
TPO	Biosource (Solingen, Germany)
Tissue culture dishes (100/20 mm)	Greiner (Frickenhausen, Germany)
Tissue culture flasks (T25/75/175)	Greiner (Frickenhausen, Germany)
6/12/24/48/96-well plates	Greiner (Frickenhausen, Germany)
Mouse Thrombopoietin DuoSet	R&D Systems (Wiesbaden, Germany)
Dynal® Mouse CD4 Negative Isolation Kit	ThermoFisher Scientific (Waltham, USA)
Pierce™ BCA Protein Assay Kit	ThermoFisher Scientific (Waltham, USA)

All other reagents and materials were purchased from Sigma-Aldrich (Steinheim, Germany) or Roth (Karlsruhe, Germany). *Rhodocytin* (Rhc) was kindly provided by Johannes Eble (University Hospital Frankfurt, Germany). CRP was gifted by Paul Bray (Baylor College, USA).

2.1.3. Antibodies

2.1.3.1. Purchased primary antibodies

Antibody	Host organism	Manufacturer
anti-acetylated tubulin	mouse	Santa Cruz (Dallas, USA)
anti-α-tubulin (B-5-1-2)	mouse	Sigma-Aldrich (Steinheim, Germany)
polyclonal anti-beta1 tubulin	rabbit	GeneTex (Irvine, USA)
anti-APC	rabbit	Abcam (Cambridge, UK)
anti-Arp2	rabbit	Abcam (Cambridge, UK)
anti-β-actin	rabbit	Sigma-Aldrich (Steinheim, Germany)
anti-β-tubulin	mouse	Sigma-Aldrich (Steinheim, Germany)
anti-Cdc42	mouse	Cytoskeleton (Denver, USA)
anti-CD105	rat	BioLegend (San Diego, USA)
anti-CD31	rabbit	BioLegend (San Diego, USA)
anti-Cofilin	rabbit	Cell Signaling (Denver, USA)
anti-P-Cofilin	rabbit	Cell Signaling (Denver, USA)
anti-GAPDH	rabbit	Sigma-Aldrich (Steinheim, Germany)
anti-detyrosinated tubulin	rabbit	Merck Millipore (Darmstadt, Germany)
anti-LIM-Kinase1	rabbit	Cell Signaling (Denver, USA)
anti-P-LIM-Kinase1	rabbit	Cell Signaling (Denver, USA)
anti-NMIIa	rabbit	Abcam (Cambridge, UK)
anti-NMIIb	rabbit	Abcam (Cambridge, UK)
anti-P-PAK1/2	rabbit	Cell Signaling (Denver, USA)
anti-PAK1/2	rabbit	Cell Signaling (Denver, USA)
anti-PDK1	rabbit	Cell Signaling (Denver, USA)
anti-P-PKCζ/λ	rabbit	Cell Signaling (Denver, USA)
anti-PKCζ/λ	rabbit	Cell Signaling (Denver, USA)
anti-Rac1	mouse	Cytoskeleton (Denver, USA)
anti-RhoA	mouse	Cytoskeleton (Denver, USA)
anti-RhoB	rabbit	Abcam (Cambridge, UK)

| anti-TER-119 | rat | BioLegend (San Diego, USA) |
| anti-Vinculin | rabbit | Santa Cruz (Dallas, USA) |

2.1.3.2. In-house generated antibodies

Antibody	Clone	Isotype	Antigen	Reference
p0p4	15E2	IgG2b	GPIbα	(Nieswandt et al., 2000a)
p0p/B	57E12	IgG2b	GPIbα	(Massberg et al., 2003)
DOM2	89H11	IgG2a	GPV	(Nieswandt et al., 2000a)
p0p6	56F8	IgG2b	GPIX	(Nieswandt et al., 2000a)
JAQ1	98A3	IgG2a	GPVI	(Nieswandt et al., 2001)
INU1	11E9	IgG1	CLEC-2	(May et al., 2009)
ULF1	97H1	IgG2a	CD9	Unpublished
LEN1	12C6	IgG2b	α2	(Nieswandt et al., 2000b)
EDL-1	57B10	IgG2a	β3	(Bergmeier et al., 2000)
JON/A	4H5	IgG2b	αIIbβ3	(Bergmeier et al., 2002)
JON6	14A3	IgG2b	αIIbβ3	Unpublished
WUG 1.9	5C8	IgG1	P-Selectin	(Schulte et al., 2003)

2.1.4. Buffers, Media, and Solutions

All stock solutions and buffers were prepared in deionized water (MilliQ Water Purification System, Millipore, Schwabach, Germany) and the pH was adjusted with HCL or NaOH.

Acid-Citrate-Dextrose (ACD) Buffer, pH 4.5

Trisodium citrate dehydrate	85 mM
Anhydrous citric acid	65 mM
Anhydrous glucose	110 mM

Decalcification buffer, pH 7.4

| PBS | |
| EDTA | 10% |

Fixation buffer with ions (TEM)

Cacodylate	50 mM
KCl	50 mM
$MgCl_2$	2.5 mM

Glutardialdehyde	2.5%

Fixation buffer (Kawamoto/MK staining)

PHEM	
PFA	4%
TritonX100	0.1%

Freezing medium

DMEM	
FCS	50%
DMSO	10%

Karnovsky fixation buffer, pH 7.2

Paraformaldehyde	2%
Glutardialdehyde	2.5%
Cacodylate	0.1 M

Laemmli buffer (for SDS-PAGE)

TRIS	40 mM
Glycine	0.95 M
SDS	0.5%

MK medium

DMEM	
FCS	10%
L-Glutamine	2 mM
Penicillin/streptomycin	1%

PHEM buffer, pH 6.8

PIPES	100 mM
HEPES	5.25 mM
EGTA	10 mM
$MgCl_2$	20 mM

***Phosphate-buffered saline* (PBS), pH 7.14**

NaCl	137 mM
KCl	2.7 mM
KH_2PO_4	1.5 mM
Na_2HPO_4 x $2H_2O$	8 mM

10x platelet buffer, pH 7.4

HEPES	10 mM
NaCl	140 mM
KCl	3 mM
$MgCl_2$	0.5 mM
$NaHCO_3$	5 mM
Glucose	10 mM

Protein lysis buffer, 2x, pH 7.4

HEPES	15 mM
NaCl	150 mM
EGTA	10 mM
Triton X-100	2%

SDS sample buffer, 2x

β-mercaptoethanol (for red. conditions)	10%
TRIS buffer (1.25 M), pH 6.8	10%
Glycerin	20%
SDS	4%
Bromophenol blue	0.02%

Separating gel buffer (Western Blot), pH 8.8

TRIS/HCl	1.5 M

Stacking gel buffer (Western Blot), pH 6.8

TRIS/HCl	0.5 M

StemPro MK medium

StemPro®-34	
L-Glutamine	2 mM
Nutrient	2.6%
Penicillin/streptomycin	1%

Stripping buffer (Western Blot), pH 6.8

TRIS/HCl	62.5 mM
SDS	2%
β-mercaptoethanol	100 mM

50x TAE

TRIS base	0.2 M
Acetic acid	5.7%
EDTA (0.5 M)	10%

Transfer buffer (semi-dry blot)

TRIS ultra	48 mM
Glycine	39 mM
Methanol	20%

***TRIS-buffered saline* (TBS), pH 7.3**

NaCl	137 mM
TRIS/HCl	20 mM

Tyrode's buffer, pH 7.3

NaCl	137 mM
KCl	2.7 mM
$NaHCO_3$	12 mM
NaH_2PO_4	0.43 mM
Glucose	0.1%
Hepes	5 mM
BSA	0.35%
$CaCl_2$	2 mM
$MgCl_2$	1 mM

Washing buffer (Kawamoto staining)

PHEM	
TritonX100	0.1%

Washing buffer (Western Blot)

TBS	
Tween 20®	0.1%

2.1.5. Mouse strains

C57BL/6J and NMRI mice were purchased from Charles River (Sulzfeld, Germany) or Janvier (Le Grenest-Saint-Isle, France). The list of the KO and transgenic mice used in this work is placed below. All transgenic and KO mice are on the genetic background of C57BL/6J or a mixed SV129/ C57BL/6J background. Mice were used at an age of 8-15 weeks. All animal

studies were approved by the District Government of Lower Franconia (Bezirksregierung Unterfranken, Würzburg, Germany).

Mouse strain	Publication	Description
129B6.RhoA/B-PF4	unpublished	*RhoB$^{-/-}$* mice were kindly provided by Ulla Knauß, Trinity University, Dublin
PDK1	Geue and Aurbach et al., 2019	Mice were kindly provided by Oliver Borst, University Clinics, Tübingen

2.2. Methods

2.2.1. Genotyping of mice

2.2.1.1. Isolation of genomic mouse DNA from ear punches
Genomic DNA (gDNA) was isolated by two methods equally suited for subsequent PCR analysis.

2.2.1.1.1 gDNA isolation with Phenyl/Chloroform
Ear punches from transgenic mice were lysed in 500 µl DNA-lysis buffer supplemented with Proteinase K (final concentration 0.1 mg/ml) for at least 3 h at 56 °C and 1400 rpm on a thermocycler. Next, the samples were mixed with 500 µl Phenol/Chloroform and centrifuged at 4°C, 14000 rpm for 10 min. The upper phase was transferred into new reaction tubes and mixed with 500 µl isopropanol. After centrifugation at 4°C, 14000 rpm for 10 min, the supernatant was discarded and pelletized DNA was washed with 70% ethanol and centrifuged at 4°C, 14000 rpm for 10 min. DNA was dried by leaving reaction tubes on 40°C on a thermocycler for 30 - 60 min and solved in TE-buffer for at least 30 min and then stored at -20°C.

2.2.1.1.2 gDNA isolation with Tail Lysis Buffer
Mouse DNA was obtained by incubation of a 5 mm^2 piece of the ear in 100 µL tail lysis buffer containing 5 µl proteinase K for 2 h at 56°C and 1200 rpm. The reaction was stopped by incubating lysed DNA at 85°C for 30 min.

2.2.1.2. Polymerase chain reaction
Polymerase chain reaction (PCR) analysis were performed to confirm the presence of the Cre recombinase cassette on chromosome 9 (*Pf4-Cre$^{tg/+}$*), as well as to verify the targeting strategy of the *RhoB* loci.

<u>PCR-mix for *Pf4*-Cre samples</u>

1 µl	DNA sample
2.5 µl	DreamTaqTM green buffer (10x)
1 µl	dNTPs (10 mM)
1 µl	forward Primer (1:10 in H2O)
1 µl	reverse Primer (1:10 in H2O)
0.5 µl	MgCl$_2$
0.25 µl	DreamTaq DNA Polymerase
17.75 µl	H$_2$O

_Pf4_-Cre PCR program

Temperature [°C]	Time [s]	Repeats
96	180	1
94	30	35
55.5-69.0	30	35
72	60	35
72	300	1
22	∞	1

Expected band sizes: 450 bp for positive samples

PCR-mix for _RhoA_-floxed samples

2 µl	DNA sample
2 µl	DreamTaqTM green buffer (10x)
0.4 µl	dNTPs (10 mM)
0.2 µl	forward Primer
0.2 µl	reverse Primer
0.125 µl	DreamTaq DNA Polymerase
15.075 µl	H_2O

RhoA-floxed PCR program

Temperature [°C]	Time [s]	Repeats
94	120	1
94	30	35
55	30	35
72	30	35
72	600	1
22	∞	1

Expected band sizes: _wt_ locus: 297 bp; Floxed locus: 393 bp

Primer sequences RhoB-PCR

RF4   5´ ggcagaatggtattgtttagtggtg 3´

NF2   5´ gccttctatcgccttcttgacg 3´

RR1   5´ ggcacaaagttcgcttatggc 3´

PCR-mix for *RhoB-wt* samples

1 µl	DNA sample
2.5 µl	DreamTaqTM green buffer (10x)
1 µl	dNTPs (10 mM)
0.1 µl	RR1
0.1 µl	NF2
0.5 µl	DreamTaq DNA Polymerase
17.1 µl	H_2O

PCR-mix for *RhoB-KO* samples

1 µl	DNA sample
2.5 µl	DreamTaqTM green buffer (10x)
1 µl	dNTPs (10 mM)
0.1 µl	RR1
0.1 µl	RF4
0.5 µl	DreamTaq DNA Polymerase
17.1 µl	H_2O

RhoB PCR program

Temperature [°C]	Time [s]	Repeats
94	300	1
94	60	35
55	30	35
72	30	35
72	600	1
4	∞	1

Expected band sizes: *wt* locus: 100 bp; *KO* locus: 150 bp

2.2.1.3. Agarose gel electrophoresis

The PCR products were analyzed by size separation on 1% agarose/TEA gels, which were prepared by dilution of agarose in TAE buffer. The cooled agarose (60°C) was supplemented with Midori Green™ (50 µl/l) to allow visualization of DNA. The respective samples were loaded together with a specific marker to determine the DNA sample size and the gels run for 30 – 45 min at 130 V. DNA was visualized using UV light and imaged with a camera (Herolab GmbH, Wiesloch, Germany).

2.2.2. In vitro analysis of platelet function

2.2.2.1. Platelet isolation from whole blood

For the isolation of murine platelets from whole blood, mice were anesthetized in isoflurane and 1 ml blood was taken retro-orbitally into 300 µl heparin (20 U/ml in TBS). Subsequently, the platelets were prepared at previously described Aurbach and Spindler et al., 2019.

2.2.2.2. Measurement of peripheral blood parameters

Peripheral blood parameters and platelet count and size were determined in approximately 50 µl undiluted whole blood in EDTA coated tubes. The tubes were gently inverted and immediately measured with an automated blood cell analyzer (scil Vet, scil animal care company GmbH) as described in Aurbach and Spindler et al., 2019.

2.2.2.3. Determination of platelet count and size by flow cytometry

Platelet count and size are also determined using a flow cytometric approach with help of size-determined beads by a FACSCalibur (BD BioSciences, Heidelberg, Germany).as described previously Aurbach and Spindler et al., 2019.

2.2.2.4. Platelet glycoprotein expression by flow cytometry

Diluted blood for flow cytometry was prepared as described in Aurbach and Spindler et al., 2019. The glycoprotein surface expression was determined on resting platelets by the *mean fluorescence intensity* (MFI) of fluorophore-conjugated antibodies.

2.2.2.5. Platelet integrin activation and granule release by flow cytometry

Anesthetized mice in isoflurane were bled to 50 µl in 300 µl heparin (20 U/ml in TBS), washed twice in Tyrode´s buffer without Ca^{2+} and centrifuged at 2800 rpm for 5 min at RT. After the washing steps, washed blood was carefully resuspended in 1 ml Tyrode´s buffer supplemented with 2 mM Ca^{2+} for platelet activation. The 1:1 mixture of antibodies directed against αIIbβ3 integrins (JON/A-PE) and the α-granule specific protein P-selectin (WUG 1.9-FITC) was added into the bottom of the tubes and incubated with 50 µl of washed blood. The platelets were activated by addition of agonists against GPCRs (thrombin, the TxA_2 analogue U46619 and

ADP) and against the (hem)ITAM receptors CLEC-2 (Rhc) and GPVI (CRP and CVX) for 6 min at 37°C and then for 6 min at RT. By the addition of 500 µl PBS the reaction was stopped, and the MFI of the respective fluorophore-coupled antibodies was assessed by flow cytometry at a FACS Calibur (BD Biosciences).

2.2.2.6. Platelet aggregation

Platelets were isolated as described in 2.2.2.1, adjusted to a count of 500,000 platelets per µl and allowed to rest for 30 min at 37°C. For platelet aggregation 1.5×10^6 platelets were suspended in Tyrode´s buffer supplemented with Ca^{2+} and 100 µg/ml fibrinogen and activated in cuvettes by 100-fold concentrated agonists against GPCRs (thrombin, the TxA_2 and ADP), the (hem)ITAM receptors CLEC-2 (Rhc) and GPVI (CRP and CVX). Importantly, thrombin stimulation was performed without fibrinogen and ADP stimulation was conducted in platelet rich plasma (PRP). Light transmission was assessed over time (600 s) using a four-channel aggregometer (APACT, Laborgeräte und Analysensysteme).

2.2.2.7. Platelet adhesion under flow conditions ex vivo

To mimic in vivo thrombotic events ex vivo with whole blood, coverslips (24 x 50 mm) were coated with 70 µg/ml HORM collagen at 37°C overnight or at least for 3 h and unspecific bindings were blocked with 1% BSA in PBS on the previous day. Anesthetized mice were bled to 1 ml into 300 µl heparin [20 U/ml in TBS], the whole blood was diluted 1:2 in Tyrode´s buffer supplemented with Ca^{2+} and the platelets were incubated with a Dylight-488-coupled anti-GPIX antibody derivate [0.2 µg/ml] for 5 min at 37°C. Subsequently, the coated and blocked coverslips were placed into a metal holder and covered with a transparent flow chamber with a slit depth of 50 µm. After the incubation, the blood was perfused over the coverslip for 4 min using a pulse free pump, followed by a washing step with Tyrode's buffer containing 2 mM Ca^{2+} for 4 min at the same shear rate. During this step, around 10 *brightfield* (BF) and fluorescent images were taken by a Zeiss HBO 100 (Axiovert, 200M, Zeiss) and thrombus volume and surface coverage were analyzed using ImageJ Software.

2.2.2.8. Platelet spreading on fibrinogen

For platelet spreading in vitro, coverslips (24 x 60 mm) were coated with 10 µg/ml human fibrinogen in a humid chamber overnight at 4°C or for at least 3 h, blocked with 1% BS in PBS for 1 h at RT and washed with Tyrode´s buffer with Ca^{2+} on the following day. The respective mice were anesthetized, platelets were washed as described in 2.2.2.1 and adjusted to a count of 300,000 platelets per µl. 30 µl of the platelet suspension was gently resuspended in 70 µl Ca^{2+} Tyrode´s buffer, stimulated with 0.01 U/ml thrombin and directly added onto the fibrinogen-coated coverslips. The platelets were let to adhere for 5, 15 and 30 mins and fixed at the respective time points with 4% PFA in PHEM containing 0.1% TritonX100 (for following confocal microscopy) or 4% PFA in PBS (for differential interference contrast [DIC] microscopy only) for 5

min. Platelet spreading capacity was observed by DIC microscopy and imaged using a Zeiss HBO 100 (Axiovert, 200M, Zeiss). For analysis, ImageJ Software (NIH, USA) was used. The inspected platelets were differentiated in 4 phases: 1 resting, 2 filopodia only, 3 filo- and lamellipodia, 4 fully spread and counted manually.

For in-depth analysis of the platelet cytoskeleton, confocal microscopy was performed. The platelet spreading was stopped at the 30 min time point, fixed and permeabilized as described above and the slides were blocked with 1% BSA in PBS. The actin cytoskeleton was visualized by incubation with Phalloidin-Atto647N and the tubulin cytoskeleton was visualized incubation with an anti-α-tubulin-Alexa488 antibody for 1 h at RT. After washing with PHEM, the slides were mounted with Fluoroshield. Platelet morphology was analyzed by confocal microscopy at a Leica TCS SP5 or SP8 using a 100x objective.

2.2.2.9. Determination of F-actin content and assembly by flow cytometry

Platelets were prepared as described in 2.2.2.1, adjusted to 500,000 platelets per µl and diluted 1:2 with Tyrode´s supplemented with Ca^{2+} in a final volume of 50µl per sample or condition. Subsequently, the platelet suspension was incubated with an anti-GPXI antibody derivate (20 µg/ml, clone 56F8) for 3 min at 37°C and 400 rpm. The samples were either let to rest or stimulated with different concentrations of thrombin for 2 min at 37°C and 400 rpm and then fixed with 10% PFA in PHEM buffer for 5 min at 37°C and 400 rpm. After fixation, the suspension was washed at 2800 rpm for 5 min at RT and resuspended in 55 µl Tyrode´s buffer containing Ca^{2+} and 0.1% TritonX100. The samples were immediately transferred into FACS tubes containing 10 µM phalloidin-FITC and incubated for 30 min RT in the dark. The binding reaction was stopped by the addition of 500 µl PBS and the tubes were centrifuged at 2800 rpm for 5 min at RT. The remaining pellet was then resuspended in 500 µl PBS, the tubes were stored on ice and immediately measured by flow cytometry at a FACS Calibur (BD Biosciences).

2.2.2.10. Cold-induced microtubule disassembly

Platelets were prepared as described in 2.2.2.1, adjusted to 500,000 platelets per µl and diluted 1:2 with Tyrode´s buffer without Ca^{2+} in a final volume of 50µl per sample or condition. The samples were treated in three different conditions. Either the platelet suspension was incubated at 4°C for 2 h for MT depolymerization and subsequent reassembly was allowed at 37°C for 30 min, or the platelets were kept at 37°C or at 4°C for 30 min. After the respective incubation time, the samples were fixed and permeabilized in PHEM buffer supplemented with 1.5% PFA and 0.075% IGEPAL CA-630 and allowed to adhere to a poly-L-lysine-coated coverslip. For visualization of the platelet cytoskeleton, the samples were stained using Phalloidin-Atto647N and anti-α-tubulin-Alexa488 antibody for 1 h at RT and analyzed by confocal microscopy at a Leica TCS SP5 or SP8 using a 100x objective.

2.2.2.11. *Direct Stochastic Optical Reconstruction Microscopy (dSTORM)*

Platelets were prepared as described in 2.2.2.1, adjusted to 300,000 platelets per µl Tyrode´s buffer without Ca^{2+}. For platelet spreading, an 8-well chamber (Cellvis, Mountain View, USA) was coated with 200 µl of human fibrinogen (10 µg/ml) for 2 h at 37°C and for resting platelets, the wells were coated with 200 µL glycine (2 M) for 10 min at RT. 60 µl for the respective samples were then either added into the fibrinogen-coated wells, covered with 200 µl Tyrode´s buffer with Ca^{2+} and stimulated with 0.01 U/ml thrombin or added into glycine coated wells and covered with 200 µl of Tyrode´s buffer without Ca^{2+}. Both conditions were incubated for 30 min at 37°C. Afterwards, the supernatant was removed, and the spread or resting platelets were fixed with 200 µL prewarmed cytoskeleton buffer I for 2 min at 37°C, succeeded by incubation with 200 µl cytoskeleton buffer II for 18 min at RT. The samples were quenched with 0.1% $NaBH_4$ for 15 min and blocked with 5% BSA for 1 h. For visualization of the platelet cytoskeleton, the samples were stained with either 5 µl AF647conjugated Phalloidin (#A22287) or a total of 1 µg AF647-conjugated anti-α-tubulin antibody at 4°C overnight.

One color *d*STORM samples were imaged on a widefield setup based on an inverted microscope (Olympus IX-71) equipped with an oil immersion objective (Olympus APON 60xO TIRF, NA 1.49, Olympus, Hamburg, Germany). The dye was excited with a semiconductor laser at 639 nm at an irradiation intensity of ~ 7 kW/cm^2 (Genesis MX639-1000, Coherent). The excitation light was spectrally filtered from the emitted fluorescence using an emission filter Brightline HC 679/41 (Semrock, Rochester, USA). Imaging was performed with an EMCCD camera (iXon Ultra 897, Andor, Belfast, UK) with an exposure time of 10 min for at least 30000 frames in photo switching buffer containing 100 mM ß-mercaptoethylamin pH 7.4. Spread platelets were imaged by *total internal reflection fluorescence* (TIRF) illumination, resting platelets were measured by *epifluorescence* (EPI). *d*STORM images were reconstructed using the open source software rapidSTORM 3.3 (Wolter et al., 2012). *d*STORM was performed by Charly Kusch and the protocol was previously described in Schurr at al., 2020 and in the doctoral thesis of Dr. Julia Volz and the doctoral thesis of Dr. Tobias Heib.

2.2.2.12. Transelectron Microscopy

Platelets were prepared as described in 2.2.2.1 and the platelet pellet was resuspended in *Transelectron Microscopy* (TEM) fixation buffer with ions. After fixation overnight at 4°C, the platelets were washed for three times in cacodylate buffer and centrifuged at 1500 rpm for 5 min. Subsequently, the sampled were treated with 1% OsO_4 for 1 h at RT, washed again with cacodylate buffer, followed by addition of H_2O_{bidest} and 2% uranyl acetate (in H_2O) for 1 h at 4°C. The dehydration was achieved by an ethanol series, incubation twice for 10 min in propylenoxide and a rotation in a 1:1 mixture of propylenoxide and epon for 1 h. Eventually, the propylenoxide was discarded and the sampled incubated overnight at RT in epon, which was then hardened for 48 h. Ultra-thin sections were generated and stained using 2% uranyl acetate

and lead citrate. Images were acquired at a JEM-2100 (JEOL). Granule and MT coil abundance was determined manually using ImageJ Software.

2.2.2.13. Preparation of platelet lysates

After platelet isolation as previously described, the last washing was performed in PBS containing 2 mM EDTA, the platelet pellet was immediately lysed in IP-buffer supplemented with 2% NP-40 as well as 1x protease inhibitors on ice for 20 min. Afterwards, sampled were mixed with 4x reducing or non-reducing Laemmli buffer and boiled at 95°C for 5 min. For lysates of activated platelets, the respective platelet suspension in Tyrode´s buffer without BSA or Ca^{2+} with the agonist of choice and lysed on ice using 2x protein lysis buffer supplemented with 2% NP-40, 1x protease inhibitor, and 1x Na_3VO_4 after different agonist incubation time points. After addition of 4x reducing Laemmli buffer, lysates were heated at 70°C for 5 min.

2.2.2.14. Immunoblotting of platelet lysates

The respective lysates of resting or activated platelets were loaded onto a *sodium dodecyl sulfate-* (SDS) *polyacrylamide gel electrophoresis* (PAGE) and denatured proteins were separated by size. The proteins were then blotted onto *polyvinylidene difluoride* (PVDF) membranes, which were blocked in Blue-Block for 1 h at RT and probed with antibodies listed in 2.1.3.1. Images were recorded using an Amersham Image 680 (GE Healthcare). As loading control, GAPDH levels were determined.

2.2.3. In vivo analysis of platelet function

2.2.3.1. Tail bleeding time on filter paper

Hemostasis of anesthetized mice with triple narcotics (Midazolam [5 µg/g], Medetomidine [0.5 µg/g], Fentanyl [0.05 µg/g]) was analyzed by removal of 2 mm of the tail tip with a scalpel and every 20 s a small drop of blood was absorbed on the filter paper until tail bleeding stopped.

2.2.3.2. $FeCl_3$-induced injury of mesenteric arterioles

3 – 4 weeks old mice were anesthetized by ketamine/xylazine (100/5 mg /kg) and the mesentery was exposed by an abdominal midline. Using a 3 mm filter paper soaked with 20/13% $FeCl_3$, endothelial damage was induced in mesenteric arterioles. Arterioles were visualized using a Zeiss Axiovert 200 inverted microscope equipped with a 100-W HBO fluorescent lamp source and a CoolSNAP-EZ camera (Visitron). Digital images were recorded and analyzed using the Metavue software. Adhesion and aggregation of fluorescently labeled platelets with Dylight-488–conjugated anti-GPIX derivative, was monitored until complete occlusion occurred. Experiments were performed by Dr. Ayesha A. Baig.

2.2.3.3. Determination of platelet life span by flow cytometry

Anesthetized mice in isoflurane were retro-orbitally injected with 5 µg of a Dylight488-coupled anti-GPIX antibody derivative. Labeled platelets were measured over five days in diluted whole blood by flow cytometry using a FACS Calibur (BD Biosciences).

2.2.3.4. Determination of platelet recovery upon depletion

Depletion of platelets in mice was conducted using 50 µg of an anti-GPIbα antibody derivative (R300), which was injected *intra-peritoneal* (i.p.). Platelet counts were assessed prior and 1 h after depletion by subsequent flow-cytometric analysis. Recovery of platelet counts was then observed by flow cytometry over 10 consecutive days beginning on day 4. Experiments were performed by Dr. Irina Pleines-Meinhold.

2.2.4. In vitro analysis of Megakaryocytes

2.2.4.1. Isolation and culture of BM derived MKs

Depending on the experiment, two different isolation and culture methods were chosen.

2.2.4.1.1. MK isolation after the Boston Protocol

Anesthetized mice were killed by cervical dislocation and femora were dissected and kept on ice in DMEM (supplemented with 100 U/ml penicillin and 50 mg/ml streptomycin). Bones were flushed by a 21 G needle into DMEM (supplemented with 100 U/ml penicillin and 50 mg/ml streptomycin), resuspended three times with a 21 G needle and a 23 G needle and stored on ice. Cells were filtered by 70 µm cell strainers (pluriStrainer Mini) and centrifuged for 5 min at 30 G. The obtained cells were used for MK lysates and spreading experiments.

2.2.4.1.2. MK isolation with lineage depletion

Cells were obtained as described in 2.2.4.2.1.1 and incubated with an antibody mixture (Biolegend) in combination with magnetic beads for lineage depletion. The remaining antibody negative fraction was then cultured in MK medium containing 50 ng/ml TPO and 100 U/ml recombinant hirudin for 72 h. The obtained cells were used for PPF experiments.

2.2.4.2. Spreading of BM derived MKs on matrices

To analyze spreading behavior of BM derived MKs on different matrices, glass cover slips were coated with fibrinogen (100 µg/ml) or Horm collagen (50 µg/ml) for 3 h at 37°C in 24 well plates. Slides were blocked in 1% BSA for 1 h, washed with PBS and 500 µl of the cell suspension in StemPro medium (0.5% recombinant TPO) were pipetted onto the slides. MKs adhered onto the ECM proteins for 3 h at 37°C and 5% CO_2, were fixed and permeabilized in PHEM fixations buffer for 20 min. To avoid unspecific antibody binding, the wells were blocked with 1% BSA/

PBS for 30 min and afterwards stained at 4°C overnight with antibodies listed in 2.1.3.1. If necessary, coverslips were washed three times with PBS and incubated with 300 µl of the respective AF-conjugated secondary antibody for 1 h at RT (1:400). Afterwards, MKs were washed twice with PBS and once with H_2O and were mounted using Fluoroshield. Visualization was performed with a Leica TCS SP8 confocal microscope and a 40x oil immersion objective (Leica Microsystems, Wetzlar, Germany).

2.2.4.3. Proplatelet formation of BM derived MKs

MK PPF was analyzed 72 h after MK isolation following the lineage depletion protocol. The MKs were seeded into 96-well-plates and diluted in a dilution series to obtain optimal cell density for manual MK counting. The cells were incubated for 48 h and counted at different time points manually at a Zeiss PrimoVert brightfield microscope. Brightfield images were acquired at an Evos Microscope (ThermoFisher Scientific). The MKs were divided in round and PPF MKs. For visualization of the cytoskeleton, coverslips were coated with 0.1% Poly-L-Lysine for 20 min at RT and subsequently washed with H_2O, 500 µl of 1x platelet buffer were added and 300 µl of the cell suspension were gently added to the wells. This was followed by centrifugation for 4 min at 900 rpm. Fixation of cells was done by addition of 800 µl 4% PFA in PHEM containing 0.1% TritonX100 and then blocked in 3% BSA for 1 h. MKs were stained with anti-α-tubulin Alexa488 (3.33 mg/ml) and phalloidin-Atto647N (170 nM), and analyzed by confocal microscopy at a Leica TCS SP8.

2.2.4.4. Immunoblotting of BM derived MKs

Resting MKs enriched according to the Boston-Protocol or PPF MKs enriched according to the lineage depletion protocol were washed using 5 mM EDTA in PBS and immediately lysed using 1x RIPA buffer supplemented with 1x Halt protease and phosphatase inhibitors, stored on ice for 30 minutes and centrifuged at 14.000 rpm for 10 min at 4°C. The supernatant was collected and by a *Bicinchoninic acid assay* (BCA) protein assay, the protein content was determined followed by analysis of absorbance at 562 nm at a Tecan Spark microplate reader. Samples were added with 4x reducing sample buffer, boiled at 95°C for 5 min and proteins were separated by SDS-PAGE. Proteins were blotted onto PVDF membranes and membranes were probed with antibodies listed in 2.1.3.1.

2.2.4.5. TEM of femora

Anesthetized mice were sacrificed, femora were dissected and cut into approximately 4 mm pieces and fixed in Karnovsky fixation buffer overnight at 4°C under rotation. Bones were either decalcified in decalcification buffer over 4 days or directly subjected with 2% osmium tetroxide in 50 mM cacodylate buffer (pH 7.2). Finally, bones were stained with 0.5% aqueous uranyl acetate, dehydrated in a graded ethanol series, and embedded in epon. Ultra-thin sections were obtained and imaged at a JEOL JEM-2100.

2.2.4.6. Hematoxylin-Eosin staining on paraffin sections

Femora, spleens, and livers of anesthetized and sacrificed mice were dissected and fixed in 4% PFA at 4°C overnight. Femora were decalcified in 10% EDTA in PBS for 4 days and eventually all organs were dehydrated, and paraffin embedded. Sections of the organs were cut at a Leica microtome, rehydrated with an ethanol gradient, and stained with *Hematoxylin-Eosin* (HE). The number of MKs as well as the general appearance of the organs were determined at a Leica DMI 4000B microscope.

2.2.5. In vivo analysis of megakaryocytes

2.2.5.1. Two-Photon microscopy of the mouse scull

Mice were anesthetized using triple narcotics and intravenously injected with 100 µg BSA-FITC, 20 µg anti-CD105-Alexa Fluor 488 and an Alexa F546-coupled anti-GPIX antibody-derivative (clone 56F8, [0.6 mg/g]). A small incision along the midline was made to expose the frontoparietal skull and mice were immobilized on a customized metal stage equipped with a stereotactic holder. Time-lapse acquisition was performed at a fluorescence microscope equipped with a TriM Scope II multiphoton system (20x objective, LaVision BioTec), and ImSpector Pro-V380 software. Emission was captured using a tunable broad-band Ti: Sa laser (780 nm) and detected with HQ535/50-nm and ET605/70-nm filters. ImageJ software was used to process and generate time-lapse videos. Two-Photon microscopy experiments were performed by Dr. Isabelle Becker.

2.2.5.2. Cryosections of murine femora

Anesthetized mice in isoflurane were sacrificed, femora were dissected and fixed in 4% PFA in PBS supplemented with 5 mM sucrose for 1 h at RT and rotated in 10% sucrose/PBS overnight. On the consecutive two days, a sucrose gradient was performed and eventually, femora were embedded in SCEM medium, frozen at -20°C and cut into 10 µm sections at a Cryostat (Leica) using the Kawamoto-tape system (Morodomi et al., 2020). The sections were kept at -20°C and for staining thawed and rehydrated in PHEM for 15 min. Afterwards, sections were fixed in 4% PFA in PHEM, blocked in 3% goat serum and stained using antibodies against CD105 (5 µg/ml), MKs were visualized by staining with a directly labeled antibody derivative against GPIX (10 µg/ml). Nuclei were counterstained using 1x DAPI. Slides were afterwards washed and mounted using Fluoroshield. Tile scan images were acquired at a confocal microscope using a 25x objective (Leica TCS SP8), while single MKs were imaged using a 40x objective. Sections were analyzed manually using ImageJ Software.

2.2.6. Statistical Analysis

Student t test (two-tailed) and Wilcoxon-Mann-Whitney test were used for the statistical analysis of differences between two groups with normal and non-normal distribution. For multiple comparisons, a two-way ANOVA with Bonferroni correction was applied. Stars indicate significances with * $p \leq 0.05$, ** $p \leq 0.01$ and *** $p \leq 0.001$.

3. Results

3.1. RhoB is critically involved in microtubule organization in platelets and MKs

3.1.1. RhoB-deficient mice are microthrombocytopenic

To study the role of the Rho GTPase RhoB in platelets and MKs we received constitutive RhoB-deficient mice (further referred to as $RhoB^{-/-}$) from Prof. Ulla Knauß (Trinity University, Dublin, Ireland) (Königs et al., 2014).

		wt		$RhoB^{-/-}$		
		mean	SD	mean	SD	P-value
WBC#	$10^3/mm^3$	7.2	4.0	7.4	1.9	0.89
LYM#	$10^3/mm^3$	4.9	2.5	5.6	1.5	0.53
MON#	$10^3/mm^3$	0.3	0.3	0.3	0.1	0.61
GRA#	$10^3/mm^3$	1.9	1.4	1.5	0.6	0.46
EOS#	$10^3/mm^3$	0.0	0.1	0.0	0.0	0.80
LYM%	%	72.0	6.5	76.6	6.4	0.18
MON%	%	4.9	1.0	4.6	0.8	0.47
GRA%	%	23.1	5.7	18.8	5.8	0.16
EOS%	%	1.2	1.4	08	0.3	0.49
RBC	$10^6/mm^3$	8.6	0.4	8.0	0.5	0.02
HGB	g/dl	15.4	0.9	15.1	1.1	0.48
HCT	%	49.3	3.2	47.9	4.7	0.53
MCV	μm^3	57.3	3.3	60.0	2.8	0.10
MCH	pg	18.0	0.7	18.8	0.5	0.01
MCHC	g/dl	31.3	0.8	31.5	0.9	0.73
RDW	%	14.7	1.6	13.7	0.2	0.10

Table 1 Peripheral blood cell counts of *wt* and *$RhoB^{-/-}$* animals measured at a scil Vet abc Plus+ blood analyzer. Table displays pooled data of at least seven animals per genotype. For statistical evaluation, a Wilcoxon-Mann-Whitney test was applied.

The loss of RhoB on protein level in platelets and MKs was confirmed by Western Blotting of respective protein lysates derived from $RhoB^{-/-}$ mice, while control lysates displayed a distinct band of the RhoB protein at around 23 kDa (Figure 9A). The expression of other important GTPases remained unaffected independently of RhoB protein levels. *Peripheral red* (RBC) and *white blood cell* (WBC) counts of $RhoB^{-/-}$ mice were largely normal compared to *wt* controls (Table 1).
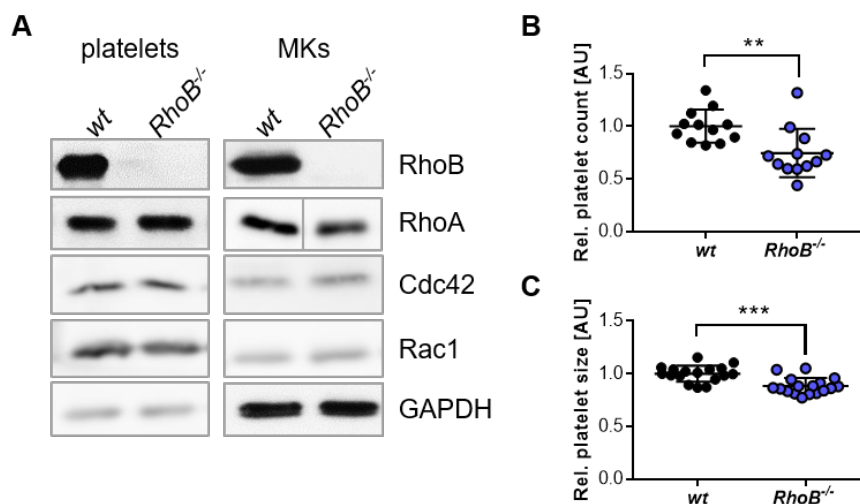
Figure 9 Loss of RhoB in mice has no effect on Rho GTPase protein expression but leads to microthrombocytopenia. (A) Immunoblotting of *wt* and *RhoB⁻/⁻* platelet and MK lysates confirmed the absence of RhoB in *KO* platelets, while the expression of RhoA, Cdc42 and Rac1 was unaffected. GAPDH served as loading control. (B) Relative platelet count (normalized to *wt*) per 30 sec assessed by flow cytometry. Each data point represents one animal (n=12). (C) Relative platelet size (normalized to *wt*) assessed by FSC measurements in flow cytometry. Each data point represents one animal (n=12). Data are presented as mean ± sd. For statistical evaluation, a Wilcoxon-Mann-Whitney test was applied. ** $p < 0.01$; *** $p < 0.001$ indicate statistically significant difference. Data in (A) partly generated by Maximilian Englert.

In contrast to conditional *KOs* of RhoA and Cdc42 in platelets and MKs, which result in macrothrombocytopenia (Pleines et al., 2010; 2012), loss of RhoB led to a reduction in platelet number with a smaller size (microthrombocytopenia) (Figure 9B, C), which was also observed by TEM under resting conditions (Figure 10A, B). TEM analysis further revealed a normal distribution of α- and dense (δ-) granules (Figure 10D, E), but a significant reduction of marginal MT coils. While *wt* platelets usually contain 8 – 12 MT coils (9.48 ± 1.86 MT coils per platelet), which surround the platelet to maintain the spherical shape of resting platelets, *RhoB⁻/⁻* platelets only contained 7.43 ± 2.05 MT coils per platelet (Zoom displayed in Figure 10A right panel; Quantification in Figure 10C). Of note, neither granule count, nor MT numbers were normalized to the platelet sizes.
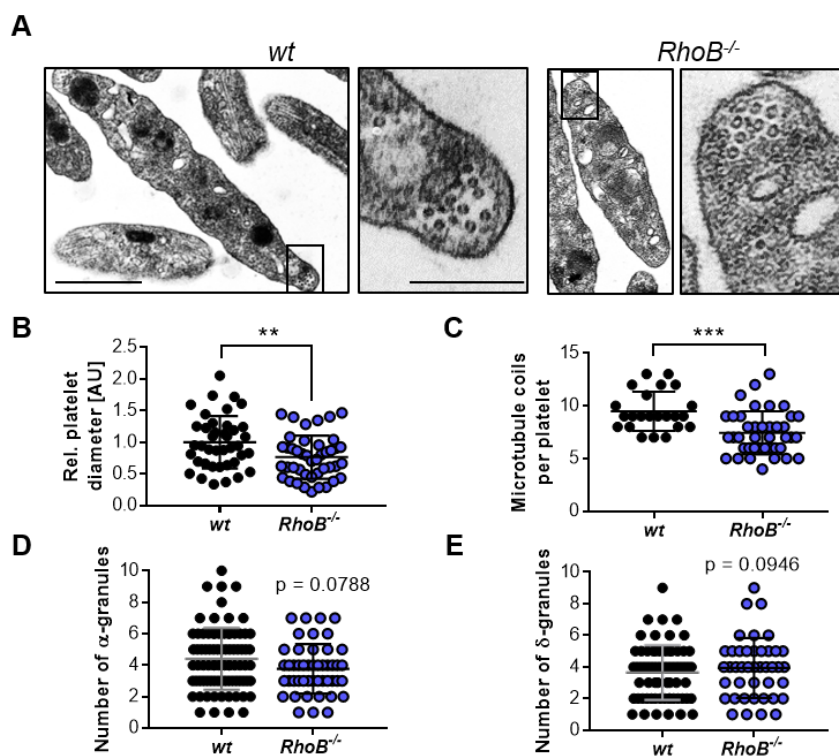
Figure 10 Ultrastructural analysis of resting *RhoB*$^{-/-}$ platelets. (A) Left: Representative picture of *wt* resting platelets by TEM. Right: resting *RhoB*$^{-/-}$ platelets visualized by TEM. Scale bar overview: 1 µm; zoom: 0.5 µm. (B) Quantification of platelet diameter (relation of platelet width to length) relative to *wt* controls (*wt* n=41; *RhoB*$^{-/-}$ n=43). (C) Quantification of MT coils per platelet. MT number was determined by manual count of at least five pictures per genotype. Each data point represents one single platelet (*wt* n=23; *RhoB*$^{-/-}$ n=40). (D, E) Alpha and dense granule number was determined by manual count of at least five pictures per genotype. Each data point represents the granule count of one single platelet (*wt* n=82; *RhoB*$^{-/-}$ n=47). Data are presented in mean ± sd. For statistical evaluation, a Wilcoxon-Mann-Whitney test was applied. ** $p < 0.01$; *** $p < 0.001$ indicate statistically significant differences.

Thrombocytopenia upon deficiency in the Rho GTPases RhoA or Cdc42 is associated with an increased platelet turnover (Pleines et al., 2010, 2012). Therefore, we investigated the in vivo platelet life span of anti-GPIb-labeled *RhoB*$^{-/-}$ and *wt* platelets for a period of five days by flow cytometry, but only observed a minor reduction in platelet turnover between the two genotypes (Figure 11A). The spleen is a site of platelet sequestration and subsequent removal, but besides the previously described splenomegaly (DeWard et al., 2009) (Figure 11B), *RhoB*$^{-/-}$ animals presented with unaltered spleen morphology and MK numbers, which was examined in HE stained paraffin sections (Figure 11C,D). Platelet removal is mediated by desialylation of glycoproteins on their surface, which can be recognized by Ashwell-Morell receptors, which mediates together with *Macrophage galactose lectin* (MGL) clearance of platelets by hepatocytes (Deppermann et al., 2020; Edward Quach et al., 2018). *RhoB*$^{-/-}$ platelets did not show alterations in *Erythrina cristagalli lectin* (ECL) binding to exposed galactose (Figure 11E) and in terminal galactose levels (determined by the ratio of neuraminidase treated platelets versus untreated platelets) (Figure 11F). Moreover, the levels of RNA-rich, *thiazole orange* (TO)-positive platelets, was unaltered in *RhoB*$^{-/-}$ platelets arguing that the loss of RhoB did not

influence platelet turnover (Figure 11G). These results indicate that altered platelet glycoprotein sialylation or platelet age and subsequent increased platelet clearing in spleen or liver are not causative for the thrombocytopenia in *RhoB⁻/⁻* animals.
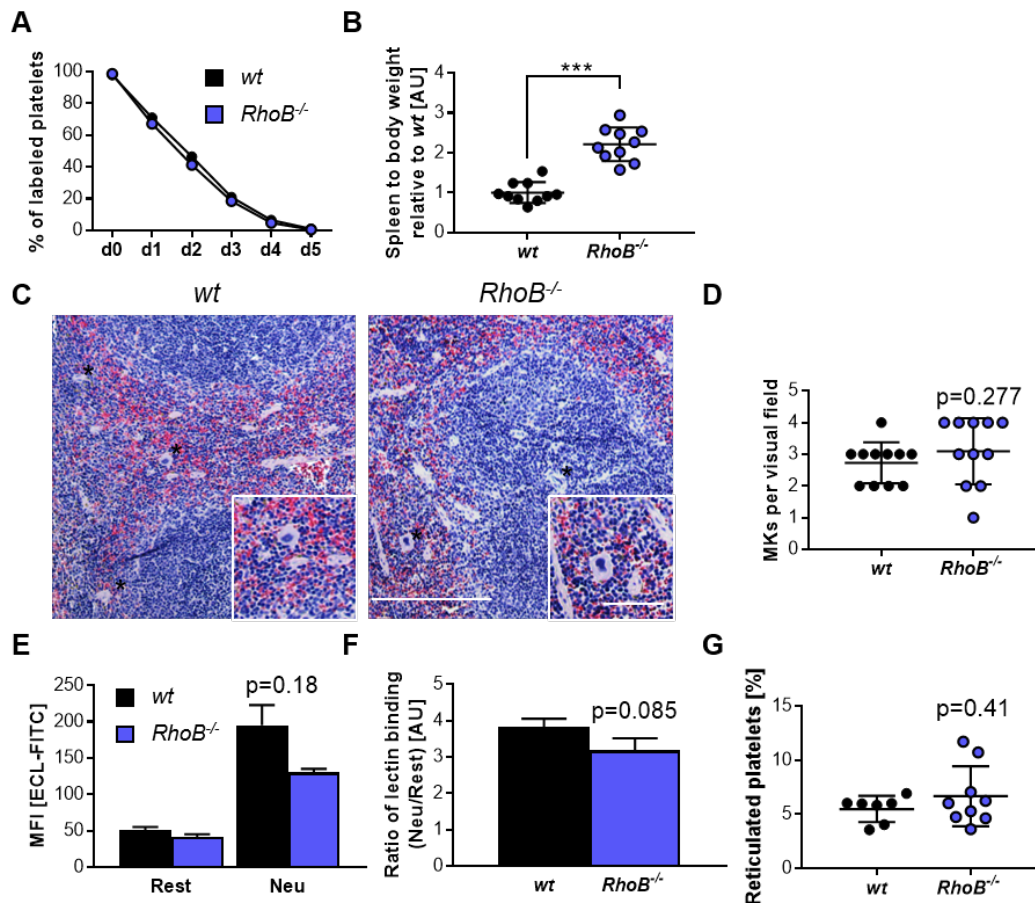

Figure 11 Increased platelet turnover is not causative for the microthrombocytopenia in *RhoB⁻/⁻* mice. (A) For the determination of platelet life span, *wt* and *RhoB⁻/⁻* platelets were labeled with an α-GPIX antibody and the labeled platelet population was analyzed over five consecutive days. Values are mean of five mice per genotype. (B) Ratio of spleen weight (mg) to body weight (mg) relative to *wt* controls. For each genotype 10 mice were analyzed. (C) Native paraffin sections of murine spleens were processed and stained with using HE. Analysis was performed at a Leica DMI4000 B. Scale overview equals 100 µm, zoom 80 µm. (D) Number of MKs per visual field determined in native paraffin sections. (n = 3; 4 visual fields per genotype) (E) Assessment of ECL-FITC binding to *wt* and *RhoB⁻/⁻* platelets by flow cytometry in the resting state (Rest) or upon neuraminidase treatment (Neu) (n=3). (F) Ratio of lectin binding (neuraminidase treated platelets versus untreated platelets) for both genotypes (n=3). (G) Percentage of reticulated (RNA-rich) platelets assessed by TO binding in flow cytometry (*wt* n=7; *RhoB⁻/⁻* n=9). Data are presented in mean ± sd. For statistical evaluation, a Wilcoxon-Mann-Whitney test was applied. *** $p < 0.001$ indicates statistically significant differences.

3.1.2. Distinct signaling defects in RhoB-deficient platelets in vitro

Deficiency for the Rho GTPases RhoA, Cdc42 and Rac1 in platelets is associated with various defects in platelet activation after agonist stimulation in vitro pointing to distinct roles of these proteins in platelet signaling with varying redundancies (Dütting et al., 2017; Pleines et al., 2010, 2012, 2013). Therefore, we next investigated the effect of RhoB deficiency on platelet

activation. In agreement with a smaller platelet size, *RhoB-/-* platelets exhibited reduced levels of glycoproteins on their surface (in particular, the GPIb-V-IX complex and GPVI; Table 2). Whether this was a direct effect of the reduced platelet size or due to a defective receptor shuttling remains to be investigated.

	wt		*RhoB-/-*		
	Mean	SD	Mean	SD	P-value
GPIb	277	29	259	33	0.43
GPV	155	2	135	3	<0.01
GPIX	339	44	317	55	0.26
GPVI	39	8	32	4	0.01
CLEC-2	109	38	125	35	0.30
CD9	970	184	948	234	0.79
α2	37	7	38	8	0.86
β1	108	11	108	4	0.97
αIIbβ3	403	70	407	122	0.93

Table 2 Surface expression of glycoproteins on resting platelets. Levels of the main glycoproteins on the murine platelet surface were analyzed by flow cytometry with FITC-labeled antibodies (n=4). Data are presented in mean MFI ± sd. For statistical evaluation, a Wilcoxon-Mann-Whitney test was applied.

Platelet activation was assessed by flow cytometry using classical platelet agonists. Interestingly, *RhoB-/-* platelets displayed an overall activation defect, which was most striking upon stimulation of the GPVI signaling pathway with either CRP or CVX. This was consistent for both αIIbβ3 integrin activation (assessed by JON/A-PE binding, Figure 12A) as well as degranulation (as assessed by binding of 5C8-FITC to exposed P-Selectin, Figure 12B). Interestingly, this defect in platelet reactivity was different to the results for the related Rho GTPase RhoA, since *RhoA-/-* platelets mainly displayed defect downstream of G-coupled receptors (Pleines et al., 2012).
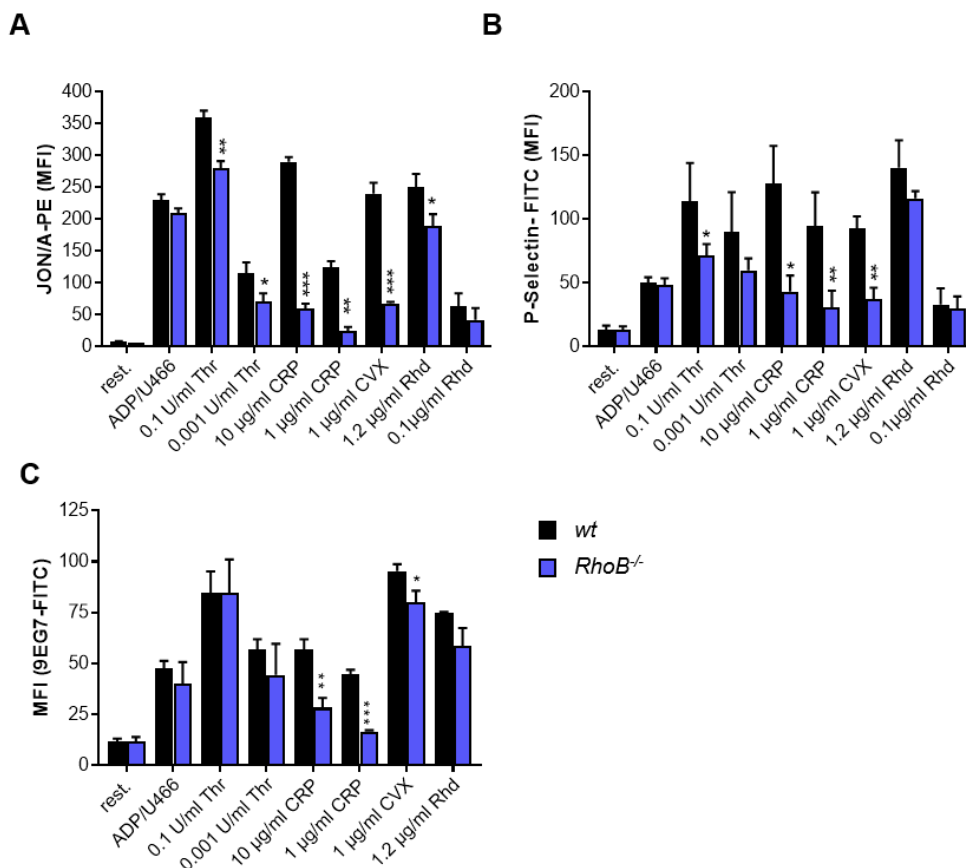
Figure 12 Overall reduced platelet activation of _RhoB-/-_ platelets. (A) Platelet integrin αIIbβ3 activation was investigated by JON/A-PE binding upon stimulation with agonists in different concentrations (n=4). (B) α-granule release was investigated by P-Selectin exposure on platelet surface upon stimulation with agonists in different concentrations (n=4). (C) Platelet integrin β1 activation was assessed by 9EG7-FITC binding upon agonist stimulation in different concentrations (n=4). Data are presented in mean ± sd. For statistical evaluation, a Wilcoxon-Mann-Whitney test was applied. * $p < 0.05$; ** $p < 0.01$; *** $p < 0.001$ indicate statistically significant difference. Rest = resting; ADP/U466 = Adenosine diphosphate/U46619; Thr = thrombin; CRP = collagen-related peptide; CVX = convulxin; Rhd = Rhodocytin.

It was previously demonstrated that _RhoB-/-_ macrophages displayed reduced level of β2 and β3, but not β1 integrins (Wheeler and Ridley, 2007). Since murine platelets do not express β2 integrins, and β3 and β1 surface expression was unaltered in _RhoB-/-_ platelets (Table 2), we additionally investigated platelet β1-integrin activation (assessed by 9EG7-FITC binding) by flow cytometry and found similar activation defects as for αIIbβ3 integrins (Figure 12C). As flow cytometric measurements are static assays, we next investigated platelet aggregation of washed platelets under stirring conditions in the light-aggregometer again using a variety of (hem)ITAM or GPCR agonists. Interestingly, we only observed mild aggregation defects in this assay for all tested agonists and agonist concentrations (Figure 13A-B).
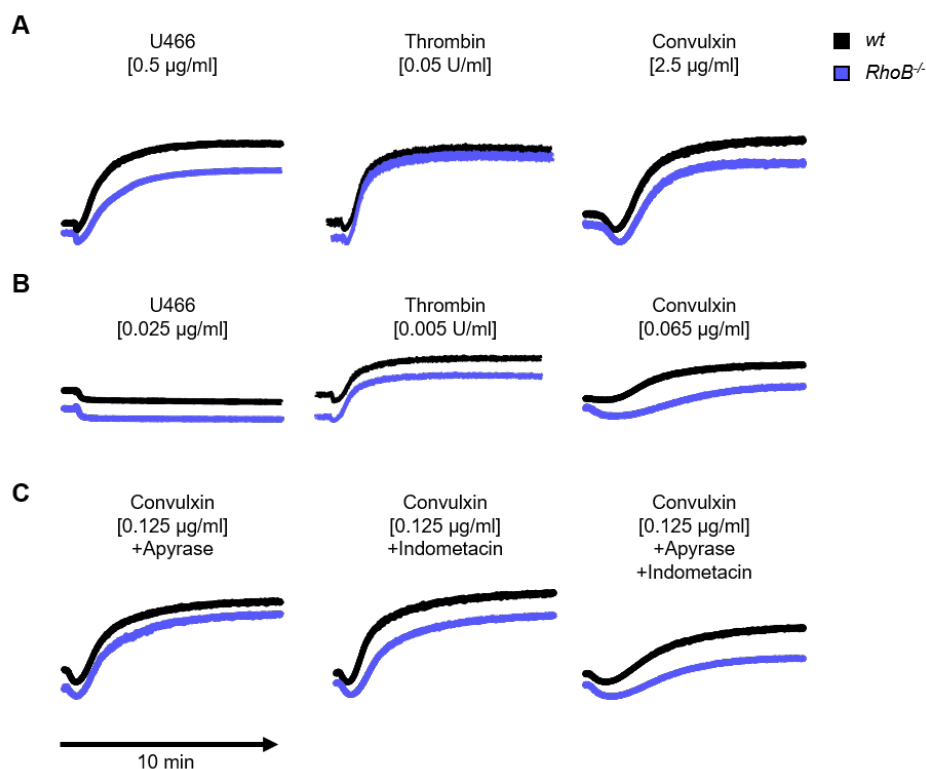
Figure 13 Largely normal aggregation of *RhoB-/-* platelets in vitro. (A) Representative aggregation curves of high dose agonist stimulation of washed *wt* and *RhoB-/-* platelets under stirring conditions for 10 min. (B) Representative aggregation curves of low dose agonist stimulation of washed *wt* and *RhoB-/-* platelets under stirring conditions for 10 min. (C) Representative aggregation curves of second wave inhibition by either Apyrase, Indometacin or a combined treatment stimulation of washed *wt* and *RhoB-/-* platelets under stirring conditions for 10 min. Data were partly generated by Dr. Isabelle Becker.

Since *RhoB-/-* platelets presented with only small defects in aggregation, we speculated that soluble factors released during degranulation (ADP, TxA_2, 5-HTT) induce a second wave of activation leading to a compensation of the above-described activation defects. To evaluate this hypothesis, we blocked second wave aggregation using Indometacin (Cyclo-oxygenase inhibitor) and Apyrase (ADPase) (Figure 13C). *RhoB-/-* platelets displayed aggregate formation similar to *wt* platelets regardless of Indometacin, Apyrase, or a combined treatment (Figure 13C, right panel). Interestingly, determination of ATP release in lysates of activated platelets in the light aggregometer in a CellTiter-Glo® Assay revealed a tendency towards an enhanced release of ATP in Indometacin-treated *RhoB-/-* platelet lysates (Figure 14). This supports the hypothesis that second wave activation factors indeed partly compensate for activation defects under stirring conditions.
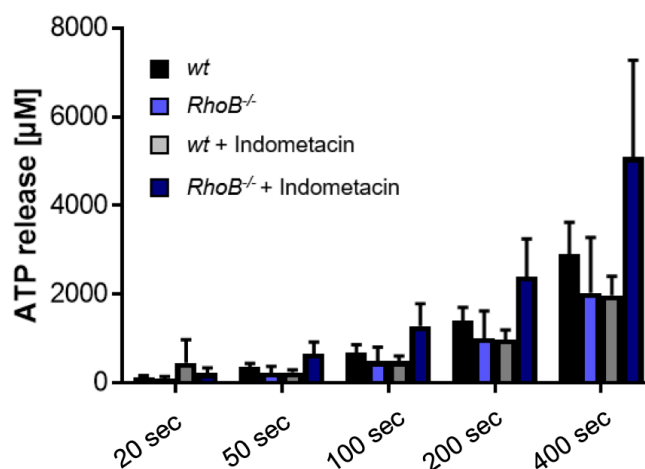
Figure 14 Influence of second wave inhibition on platelet ATP release. *Wt* and *RhoB*$^{-/-}$ platelets were stimulated with 5 µg/ml collagen in the light aggregometer under stirring conditions. Samples were taken at the indicated time points and lysed in RIPA buffer on ice. Hereafter, ATP release was determined by CellTiter-Glo® assay in the lysates. (n=4; Indometacin-treatment n=2).

In order to mimic in vivo thrombus formation, we next performed ex vivo flow chamber assays, in which murine whole blood was perfused over a collagen-coated surface at different shear rates (1000 s^{-1}= intermediate; 1700 s^{-1} = high). *RhoB*$^{-/-}$ platelets were still able to form structured thrombi (Figure 15A, B upper panel) but the overall surface coverage was significantly reduced (Figure 15A, B lower panel) compared to *wt* platelets. This was observed for both intermediate and high shear rates.
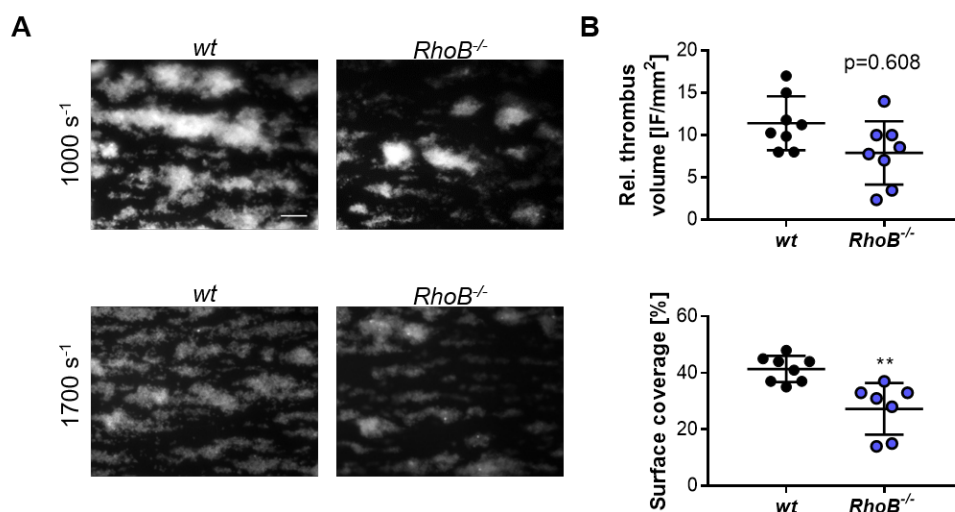

Figure 15 Ex vivo thrombus formation under flow on a collagen-coated surface. (A) Representative pictures of thrombus formation at an intermediate shear of 1000 s^{-1} and at a high shear of 1700 s^{-1}. (B) Upper panel: Formation of 3D structures at 1000 s^{-1} displayed as relative thrombus formation (n=8). Lower panel: Adhesion of platelets to collagen at 1000 s^{-1} assessed by area coverage (n=8). Data are

presented in mean ± sd. For statistical evaluation, a Wilcoxon-Mann-Whitney test was applied. ** p < 0.01 indicates statistically significant difference.

This in vitro defect did not translate into altered in vivo thrombus formation, which was determined by mechanical injury of the abdominal aorta (Figure 16A). Furthermore, hemostasis of *RhoB$^{-/-}$* mice was not affected in a tail bleeding time assay on filter paper (Figure 16B).
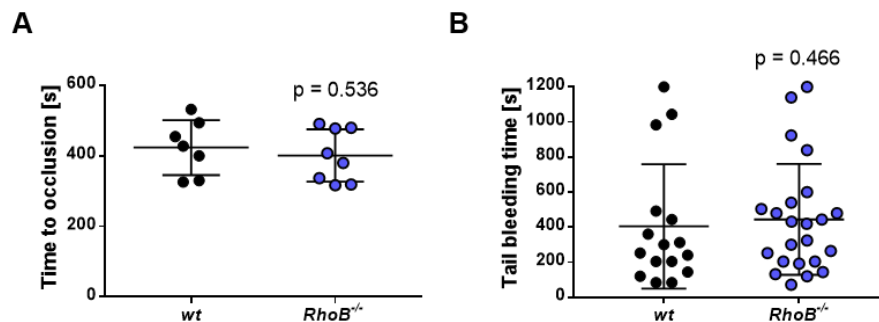

Figure 16 In vivo studies on thrombosis and hemostasis in *RhoB$^{-/-}$* animals. (A) Mechanical injury of the abdominal aorta in vivo. Each data point represents one animal (*wt* n=7; *RhoB$^{-/-}$* n=8). Data was generated by Dr. Ayesha Baig. (B) Tail bleeding time on filter paper in vivo. Each data point represents one animal (*wt* n=15; *RhoB$^{-/-}$* n=23). Data pooled from two independent experiments. Data are presented in mean ± sd. For statistical evaluation, a Wilcoxon-Mann-Whitney test was applied.

3.1.3. RhoB-deficient platelets display altered microtubule organization

Rho GTPases are described as critical regulators of actin and MT dynamics in various cell types. We therefore investigated the influence of the constitutive loss of RhoB in murine platelets regarding cytoskeletal arrangements. To determine platelet outside-in signaling and F-actin dynamics, we incubated *wt* and *RhoB$^{-/-}$* platelets for 5, 15 and 30 min on a fibrinogen-coated surface. We did not detect a difference in spreading between *wt* and *RhoB$^{-/-}$* platelets for all investigated time points (Figure 17A, B quantification), which indicates that outside-in signaling and F-actin rearrangements are functional in *RhoB$^{-/-}$* platelets. In addition, we investigated F-actin content and assembly by measuring the MFI of FITC labeled phalloidin in flow cytometry. In line with the unaltered spreading, we did not find any alterations in F-actin content and assembly neither upon CRP nor upon thrombin stimulation (Figure 17C).
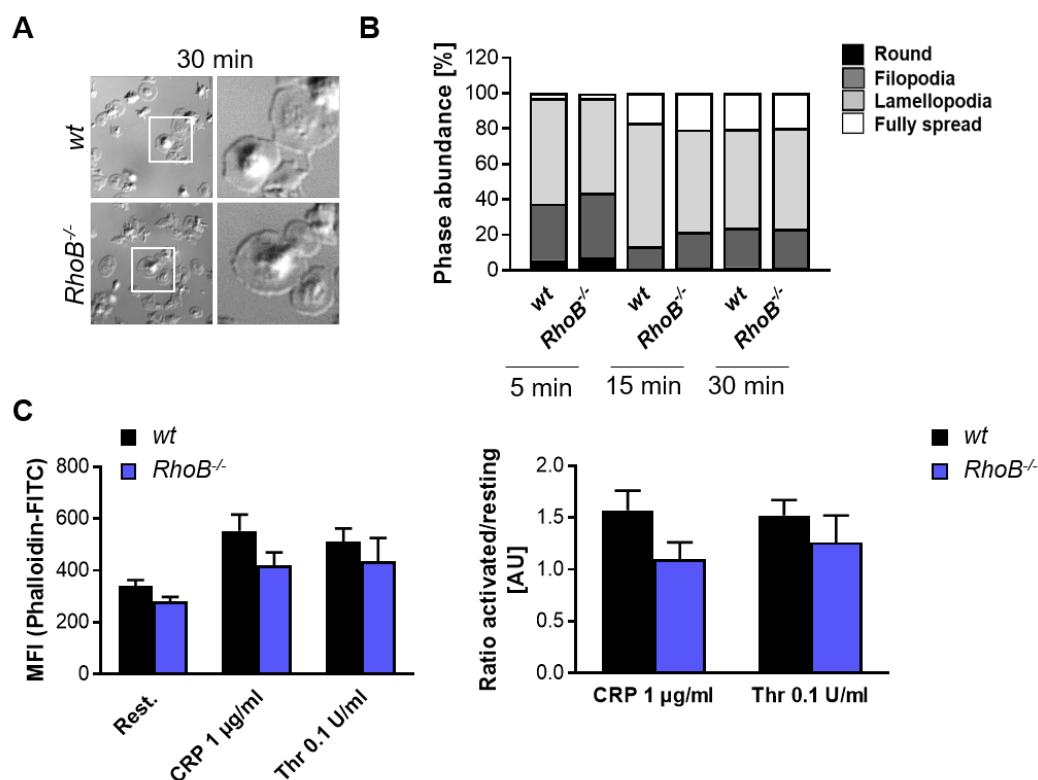
Figure 17 Spreading and F-actin dynamics in *RhoB-/-* platelets. (A) Representative picture of platelets spread on fibrinogen for 30 min. (B) Quantification of platelet spreading on fibrinogen for 5, 10 and 15 min (n=3). (C) Left: MFI of phalloidin-FITC in resting platelets and platelets stimulated with 1 µg/ml CRP and 0.1 U/ml thrombin. Right: Ratio of CRP or thrombin activated and resting values to determine F-actin assembly (n=3). Data are presented in mean ± sd. For statistical evaluation, a Wilcoxon-Mann-Whitney test was applied. Rest. = Resting; CRP = Collagen related peptide; Thr = thrombin; MFI = mean fluorescence intensity.

To further analyze the platelet cytoskeleton, fibrinogen-spread platelets were fixed in 4% PFA, blocked, stained with anti-α-tubulin-Alexa488 antibody and phalloidin-Atto647 which stains F-actin and imaged using a Leica SP8 confocal microscope. The F-actin cytoskeleton was not affected by loss of RhoB, however, the α-tubulin network appeared markedly altered in *RhoB-/-* platelets (Figure 18A). In addition, we imaged platelets spread on fibrinogen and stained solely for α-tubulin in *d*STORM and observed *RhoB-/-* platelets with a disturbed MT network (Figure 18B).
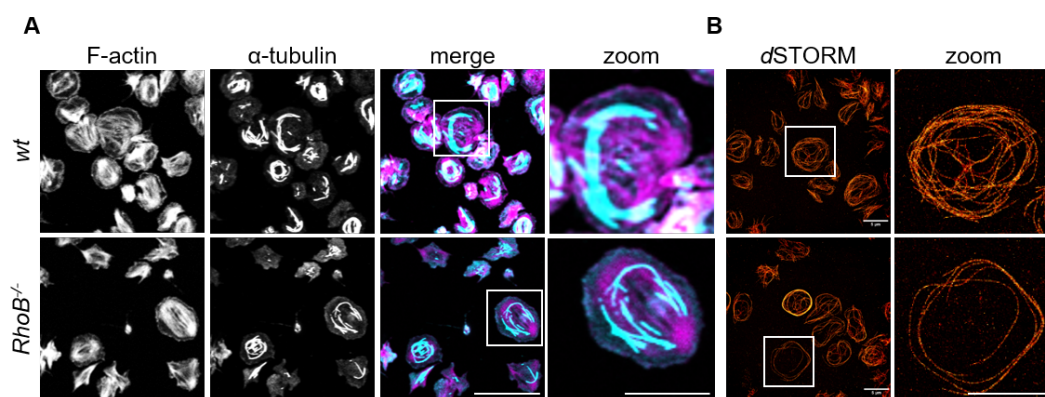
Figure 18 Confocal and *d*STORM analysis of spread platelets on fibrinogen. (A) Representative confocal microscopy pictures of platelets spread on fibrinogen for 30 min, stained with phalloidin-Atto647 (magenta) and α-tubulin-Alexa488 (cyan) and imaged using a Leica TC SP8 confocal microscope. Scale bar in overview equals 10 μm and in zoom 5 μm. (B) Representative *d*STORM images of platelets spread on fibrinogen for 30 min, stained with α-tubulin-Alexa488 (red) and imaged using an EMCCD camera (iXon Ultra 897, Andor, Belfast, UK). Scale bar equals 5 μm. *d*STORM data was generated by Charly Kusch.

MTs are highly dynamic structures that are constantly assembled and disassembled. MT disassembly into dimers can be artificially induced by exposure to cold (4°C) and reassembly into fibers occurs spontaneously at 37°C (Detrich et al., 2000). To further investigate the role of RhoB in MT arrangements and dynamics, we induced MT disassembly in platelets by cold storage (4°C) for 2 h followed by a reassembly at 37°C (Stritt et al., 2017). While *wt* and *RhoB^-/-^* platelets displayed a round MT coil at their periphery at 37°C and disassembled upon cold-storage (Figure 19A, left and middle), *RhoB^-/-^* platelets were not able to reassemble the coils after disassembly and the following reassembly step (*wt*: 83 ± 2% vs. *RhoB^-/-^*: 23 ± 5%) (Figure 19B). Of note, this effect was only observed, when the platelets were spun down onto glass cover slips.
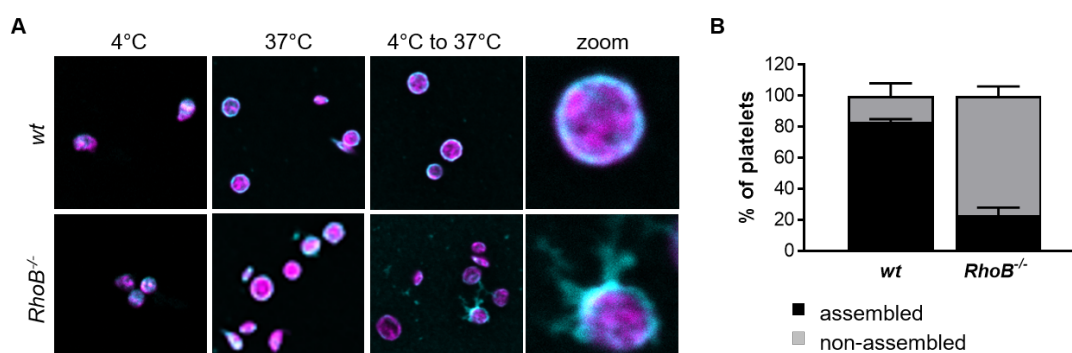

Figure 19 Cold-induced MT disassembly. (A) Representative confocal microscopy images of cold-induced MT organization at 4°C, 37°C and a combination of disassembly at 4°C with following reassembly at 37°C in platelets. After 2 h of incubation at the indicated time points, platelets were spun down onto Poly L-Lysine coated glass slides and stained with phalloidin-Atto647 (magenta) and α-tubulin-Alexa488 (cyan). Scale bar in overview equals 10 μm and in zoom 1 μm. (B) Quantification of MT organization in *wt* and *RhoB^-/-^* platelets after cold-induced MT disassembly and reassembly (4°C to 37°C). At least five pictures per animal were analyzed (n=3). Data are presented in mean ± sd. For statistical evaluation, a Wilcoxon-Mann-Whitney test was applied.

MTs can be modified through PTMs, which serve for a proper adaption to their different cellular functions. In platelets, PTMs of α-tubulin have been reported to be involved in MT rearrangements, including acetylation (of residue K40) and detyrosination/tyrosination (in C-terminal tyrosines, often also called glutaminylation) (Gundersen et al., 1984; Patel-Hett et al., 2008; Webster and Borisy, 1989).

Acetylation and detyrosination are indicators for stable, long-lived MTs, while more dynamic MTs are tyrosinated and deacetylated (Chakraborti et al., 2016). We therefore investigated the acetylation status of the α-tubulin K40 residue by Western blotting in platelet lysates (Figure 20A). *RhoB⁻/⁻* platelets showed a pronounced decrease of acetylated α-tubulin, whereas the expression level of detyrosinated α-tubulin was unaltered (Figure 20B, C). These results strongly suggest that the small Rho GTPase RhoB is involved in MT turnover and dynamics in platelets, which in the deficient platelets results in short-lived MT that are either more unstable or constantly remodeled.
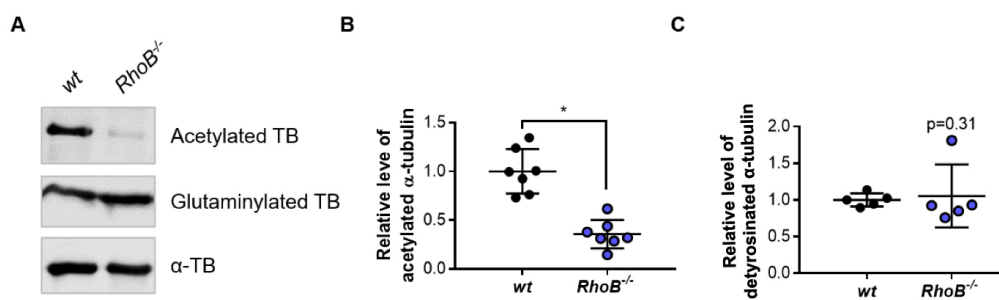

Figure 20 Analysis of acetylation and detyrosination of α-tubulin residues by western blotting. Platelet protein lysates of *wt* and *RhoB⁻/⁻* animals were immunoblotted for PTMs of α-tubulin (acetylated α-tubulin and detyrosinated α-tubulin). Right: Quantification of PTM immunoblots. Each data point represents one animal (Acetylated α-tubulin n=7; detyrosinated α-tubulin n=5). Data are presented in mean ± sd. For statistical evaluation, a Wilcoxon-Mann-Whitney test was applied. * $p < 0.05$ indicates statistically significant difference.

3.1.4. RhoB-deficient MKs display altered microtubule organization

To identify whether the altered MT rearrangements in platelets arouse from differences in cytoskeletal dynamics in the platelet precursors, the MKs, we next investigated the role of RhoB in murine MKs. The constitutive KO of RhoB had no influence on MK localization (Figure 21A, B) and MK number (Figure 21C) which was analyzed in native BM cryosections stained for CD105 (vessel marker) and GPIX (MK marker). Furthermore, in-depth analysis of *wt* and *RhoB⁻/⁻* MKs in the BM by TEM revealed a normally developed DMS in MKs lacking RhoB, thus implicating an unaltered MK maturation in *RhoB⁻/⁻* MKs (Figure 21D).
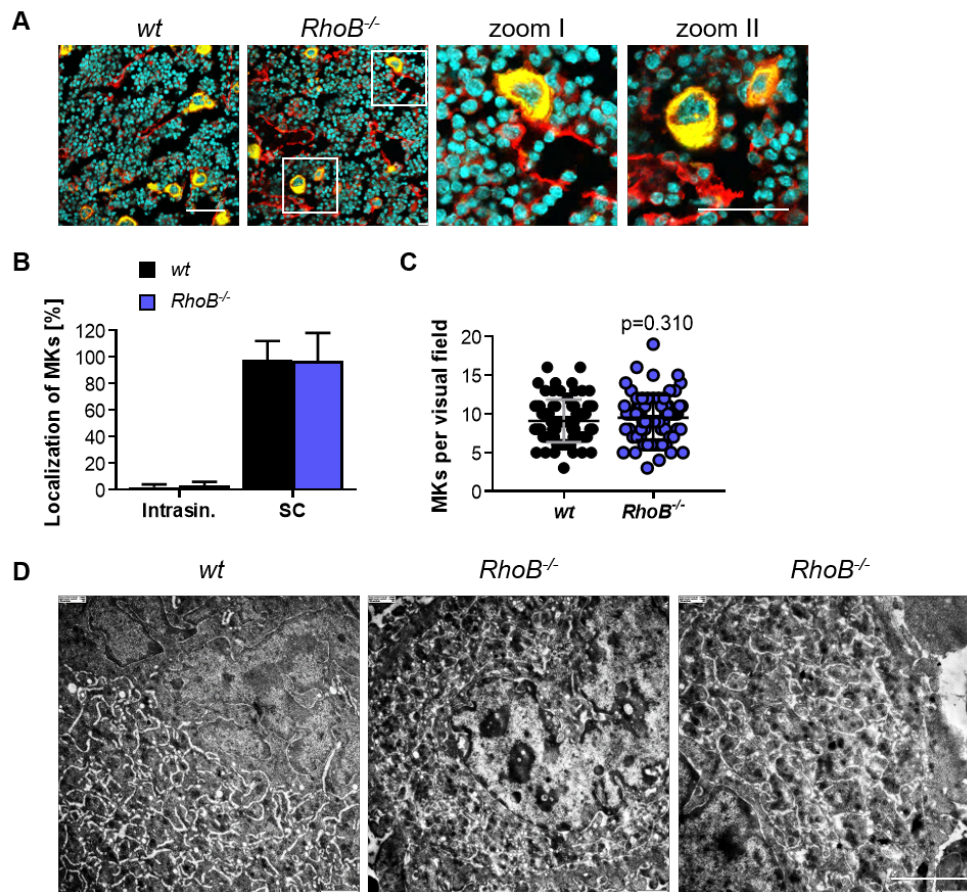
Figure 21 Unaltered localization and ultrastructure of *RhoB⁻/⁻* MKs in situ. (A) Representative confocal microscopy pictures of cryosections of PFA-fixated and dehydrated femora. The femora were processed after the Kawamoto-method for cryosections. Sections were stained with directly labeled anti-CD105 antibody to stain vessel, directly labeled anti-GPIX antibody to visualize MKs and DAPI (nucleus). Scale bar in overview equals 40 µm and in zoom 5 µm. (B) Quantification of MK localization in *wt* and *RhoB⁻/⁻* BM. (C) Quantification of MK numbers in *wt* and *RhoB⁻/⁻* BM. Values present mean of seven animals per genotype. At least 10 pictures per animal were analyzed. Each data point represents one picture n =75). (D) In depth analysis of *wt* and *RhoB⁻/⁻* MKs by TEM. Scale bar equals 4 µm. Data are presented in mean ± sd. For statistical evaluation, a Wilcoxon-Mann-Whitney test was applied. Intrasin. = intrasinusoidal; SC = sinusoidal contact.

A detailed analysis of cultured, BM derived MKs in vitro revealed that RhoB deficiency had no influence on the spreading capacity on HORM collagen (Figure 22A) evident by an unaltered MK spreading area on HORM collagen (quantification Figure 22C). To analyze the actin cytoskeleton more precisely, we stained spread MKs using phalloidin-Atto647 to visualize podosomes, F-actin rich nodules. Interestingly, we neither observed a variation in podosome density (determined by podosome number per MK area, Figure 22B), nor in MFI of F-actin (Figure 22D). Moreover, an additional staining for α-tubulin revealed no alterations in the MT organization in *RhoB⁻/⁻* MKs (Figure 22E).
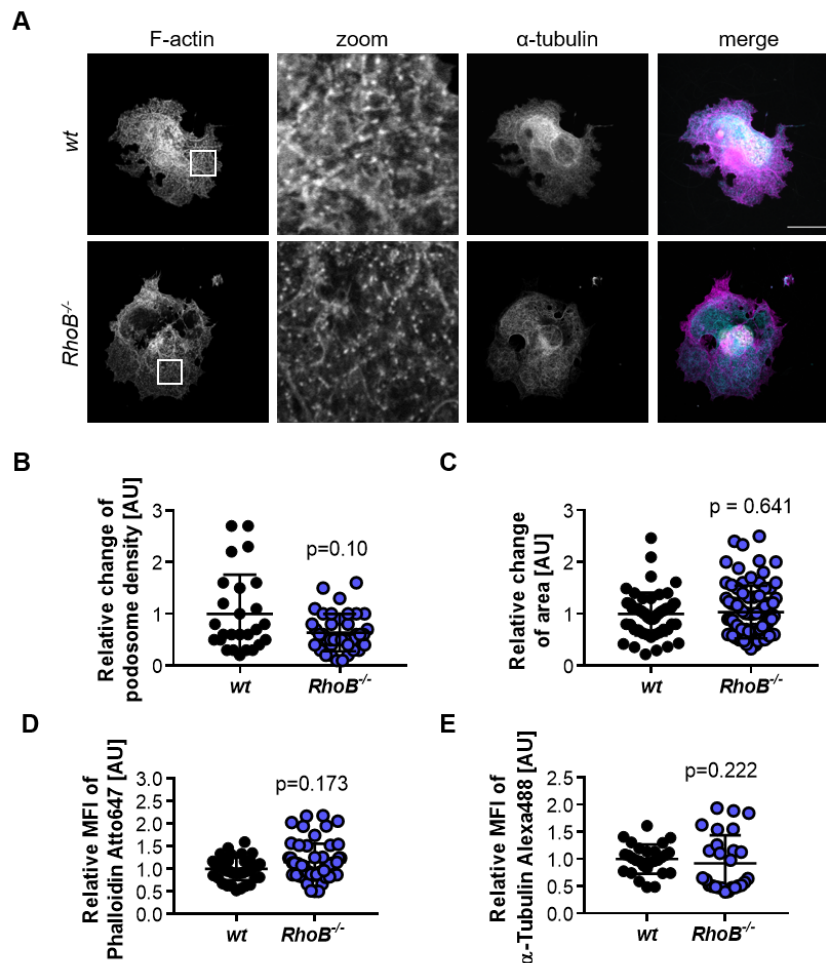
Figure 22 Analysis of cultured BM-MK spreading on collagen in vitro. (A) Representative confocal microscopy pictures of BM derived MKs after BSA gradient were allowed to spread on HORM collagen coated glass slides for 3 h, formaldehyde fixed, blocked and stained with phalloidin-Atto647 (magenta), α-tubulin-Alexa488 (cyan) and DAPI to stain the nucleus. Scale bar in overview equals 40 μm and in zoom 5 μm. (B) Quantification of podosome density in *wt* and *RhoB*$^{-/-}$ MKs spread on HORM collagen (normalized to *wt*). Pooled data of three independent experiments, three animals per genotype were analyzed. Each data point represents one MK (*wt* = 26; *RhoB*$^{-/-}$ = 28). (C) Quantification of spread area on collagen of *wt* and *RhoB*$^{-/-}$ MKs (normalized to *wt*). Pooled data of three independent experiments, values present mean of three animals per genotype. At least 5 pictures per animal were analyzed. Each data point represents one MK (*wt* = 56; *RhoB*$^{-/-}$ = 82). (D) Quantification of F-actin content of *wt* and *RhoB*$^{-/-}$ MKs spread on collagen (normalized to *wt*). Pooled data of three independent experiments, values present mean of three animals per genotype. At least 5 pictures per animal were analyzed. Each data point represents one MK (*wt* = 41; *RhoB*$^{-/-}$ = 56). (E) Quantification of α-tubulin content of *wt* and *RhoB*$^{-/-}$ MKs spread on collagen (normalized to *wt*). Pooled data of two independent experiments, values present mean of three animals per genotype. At least 5 pictures per animal were analyzed. Each data point represents one MK (*wt* = 28; *RhoB*$^{-/-}$ = 27). Data are presented in mean ± sd. For statistical evaluation, a Mann-Whitney test was applied.
** $p < 0.01$; *** $p < 0.001$. AU = arbitrary unit; MFI = mean fluorescence intensity.

Defective thrombopoiesis in the BM is a possible explanation for the observed microthrombo-cytopenia in *RhoB*$^{-/-}$ animals. We therefore analyzed PPF of BM derived MKs cultivated for 3 days in the presence of TPO and hirudin and afterwards stained the proplatelets for F-actin and α-tubulin (Figure 23A). While we could not detect alterations in the PPF capacity between *wt* and *RhoB*$^{-/-}$ MKs during the observation time of 48 h (Figure 23B), we observed a high

proportion (78.1%) of *RhoB$^{-/-}$* MKs with disorganized MT networks (Figure 23A right panel, quantification 23C). This disorganization resulted in irregularly shaped proplatelet tips, with a high proportion of smaller-sized tips and a proportion of big-sized proplatelets shafts. These two populations were not detected in *wt* MKs (Figure 23D), and led in average to smaller tip sizes of *RhoB$^{-/-}$* MKs than *wt* MKs, which could be an explanation for the observed micro-thrombocytopenia.
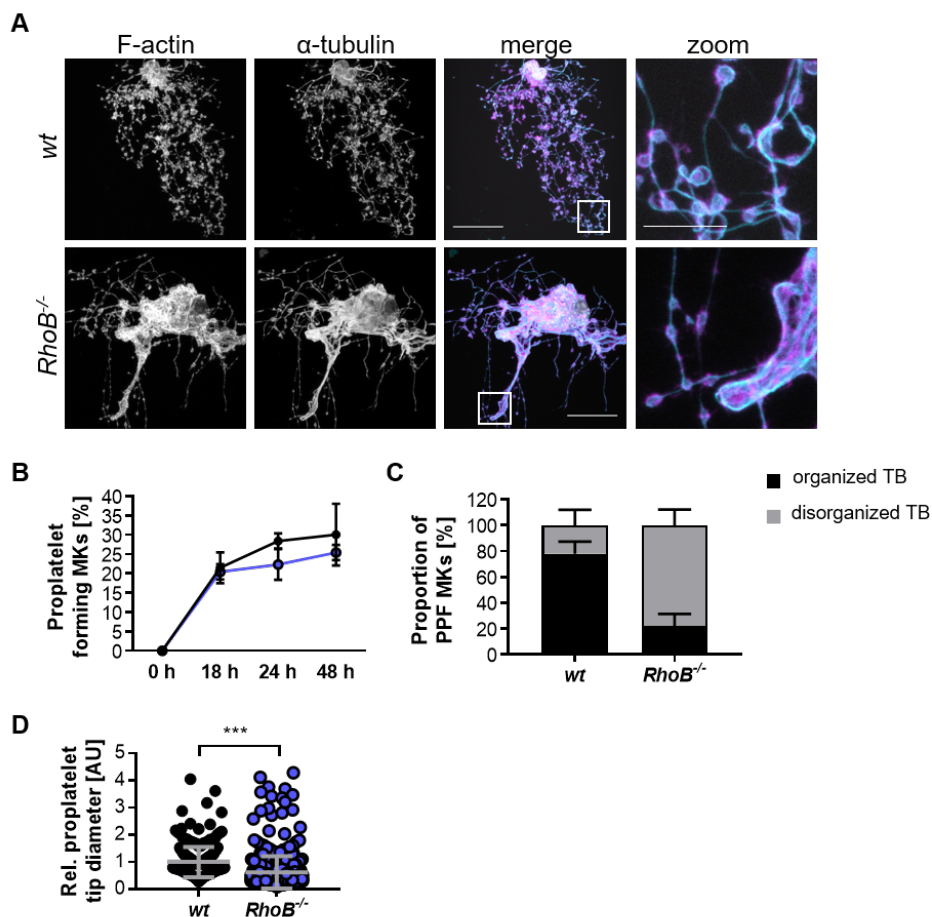

Figure 23 Analysis of PPF of BM derived *RhoB$^{-/-}$* MKs. (A) Representative confocal pictures of BM derived MKs 24 h after BSA gradient. The MKs were spun down to Poly L-Lysine coated glass slides and stained with phalloidin-Atto647 (magenta), α-tubulin-Alexa488 (cyan) and DAPI to visualize the nucleus. Scale bar in overview equals 40 µm and in zoom 5 µm. (B) Quantification of in vitro PPF in an observation period of 18 h, 24 h and 48 h after BSA gradient. Values present mean of three animals per genotype. (C) Quantification of MT organization in *wt* and *RhoB$^{-/-}$* MKs 24 h after BSA gradient. Values present mean of three animals per genotype. At least 13 pictures per animal were analyzed. (D) Quantification of proplatelet tip diameter of *wt* and *RhoB$^{-/-}$* MKs 24 h after BSA gradient (normalized to *wt*). Values present mean of two animals per genotype. At least 11 MKs per animal were analyzed. Each data point represents one proplatelet tip (*wt* = 250; *RhoB$^{-/-}$* = 494). Data are presented in mean ± sd. For statistical evaluation, a Wilcoxon-Mann-Whitney test was applied. *** $p < 0.01$ indicates statistically significant difference. TB = tubulin.

To elucidate possible mechanisms behind the disturbed tubulin network during PPF, we investigated important regulators of the MK cytoskeleton. As expected, actin regulatory proteins as *Non-muscle myosin IIa* (NMIIa) and *IIb* (NMIIb) that are downstream effectors of small Rho

GTPases and influence cell migration and contractility, were unaltered in *RhoB⁻/⁻* BM derived MKs, same as Vinculin and Arp2, which are podosome-associated proteins (Figure 24A). The MT plus-end tracking protein *Adenopolyposis Coli* (APC), which was recently shown as a negative regulator of PPF in mice (Strassel et al., 2018), was also unaltered in *RhoB⁻/⁻* MKs (Figure 24B upper panel). In contrast to platelets, *RhoB⁻/⁻* BM derived MKs displayed unaltered α-tubulin acetylation and detyrosination (Figure 24B middle panel). The levels of α-tubulin and β1-tubulin (exclusively expressed in the MK lineage) were also unaltered (Figure 24B lower panel). Of note, the immune blots were prepared using cultured MKs under resting conditions.
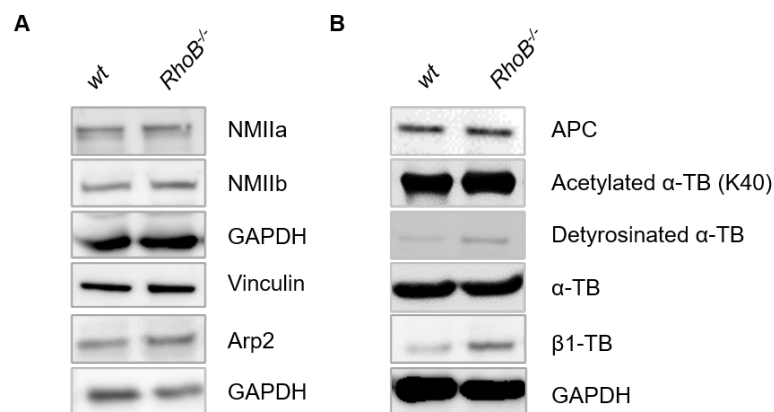

Figure 24 Analysis of important regulator of the actin and tubulin cytoskeleton by western blotting. (A) MK protein lysates of *wt* and *RhoB⁻/⁻* animals were immunoblotted against pivotal regulators of the actomyosin cytoskeleton. GAPDH was used as a loading control. (B) MK protein lysates of *wt* and *RhoB⁻/⁻* animals were immunoblotted against pivotal regulators of the tubulin cytoskeleton, tubulin isoforms and PTM of α-tubulin. GAPDH was used as a loading control. TB = tubulin.

3.2. Redundancies of RhoA and RhoB in platelets and MKs

3.2.1. Impaired platelet function of RhoA/RhoB-deficient platelets

It was previously shown that *RhoA⁻/⁻* platelets display an activation defect mainly upon stimulation of receptors coupled to $G_{\alpha q}$ and $G_{\alpha 13}$, resulting in reduced platelet αIIbβ3 integrin inside-out activation and degranulation in flow cytometric assays (Pleines et al., 2012). The $G_{\alpha 13}$ signaling defects translated into an absence of shape change upon stimulation with low doses of the thromboxane analog U46619, a phenomenon that cannot be recapitulated in *RhoB⁻/⁻* platelets (Figure 25A). These results demonstrate that RhoA and RhoB seem to be involved in different signaling pathways in platelets. We therefore next sought to investigate whether a similar situation was present in MKs. Strikingly, we found that RhoB levels were dramatically upregulated in *RhoA⁻/⁻* MKs compared to the *wt* (Figure 25B). Similarly, protein expression analysis of unstimulated *RhoA^{fl/fl;Pf4-Cre}* (further referred to as *RhoA⁻/⁻*) and *wt* platelets revealed an upregulation of RhoB in the absence of RhoA (Figure 25B), while expression of RhoA was

unaltered in *RhoB^-/-* platelets (Figure 25C). In the light of these results we hypothesized that the increased levels of RhoB may mechanistically contribute to the MK localization and platelet biogenesis defect observed in the BM of *RhoA^-/-* animals in situ and in vivo (Dütting et al., 2017).
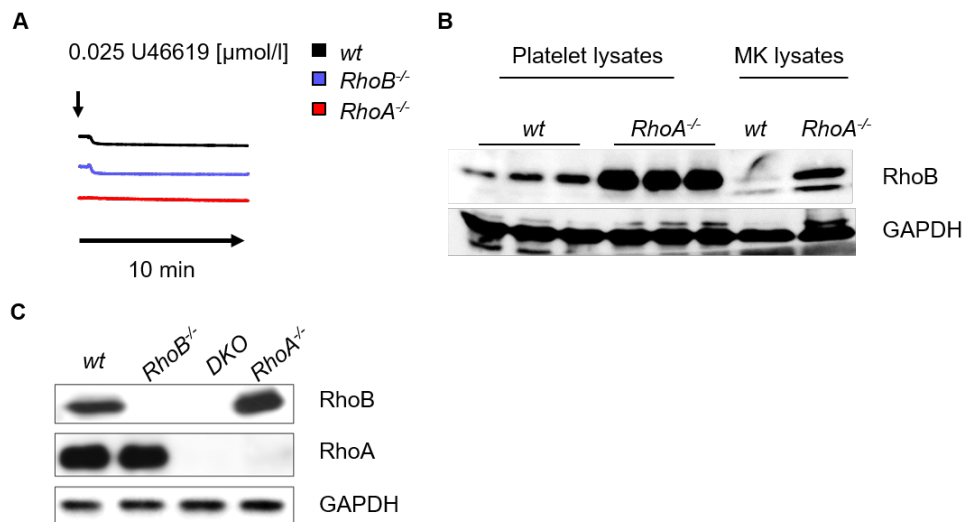

Figure 25 Upregulation of RhoB on proteins level in *RhoA^-/-* platelets and MKs. (A) Representative aggregation curve of low dose U46619 stimulation of washed *wt* and *RhoB^-/-* platelets under stirring conditions for 10 min. (B) Platelet and MK protein lysates of *wt* and *RhoA^-/-* animals were immunoblotted against RhoB. GAPDH was used as a loading control. (C) Platelet protein lysates of *wt*, *RhoB^-/-*, *RhoA^-/-* and *RhoA^fl/fl;Pf4-Cre/RhoB^-/-* (*DKO*) animals were immunoblotted against RhoB and RhoA. GAPDH was used as a loading control.

We therefore deleted RhoB in *RhoA^-/-* mice by intercrossing them with *RhoB^-/-* mice. The resulting *RhoA^fl/fl;Pf4-Cre/RhoB^-/-* mice (further referred as *DKO*) displayed an aggravated macrothrombocytopenia compared to *RhoA^-/-* mice (Figure 26A, B), which was clearly evident in TEM analyses (Figure 26C). All other tested peripheral blood parameters of *RhoB^-/-*, *RhoA^-/-* and *DKO* mice were within a similar range, with only minor significant changes in hemoglobin levels (MCH), which were elevated in *RhoB^-/-* and *RhoA^-/-* animals (Table 3). Of note, *DKO* animals had an increased percentage of lymphocytes and decreased percentage of granulocytes compared to *wt* animals, which was also observed in *RhoB^-/-* animals. These results were not analyzed in more detailed in this thesis.

DKO mice furthermore displayed a moderately increased platelet turnover, which was observed by platelet life span (Figure 26D) as previously described for *RhoA^-/-* animals (Pleines et al., 2012).
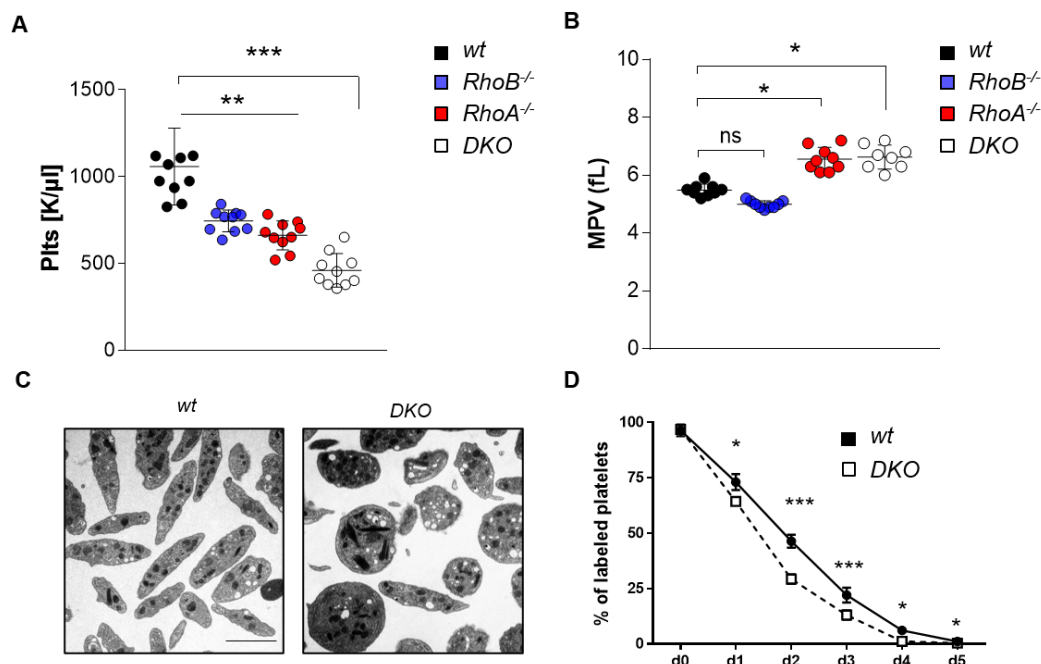
Figure 26 Double deficiency of RhoA and RhoB causes severe macrothrombocytopenia and increased platelet turnover. (A) Platelet count of *wt*, *RhoB-/-*, *RhoA-/-* and *DKO* animals determined by a scil Vet abc Plus+ blood analyzer. Each data point represents one animal (*wt*, *RhoB-/-*, *RhoA-/-* n=9; *DKO* n=8). For statistical evaluation, a two-way ANOVA with Bonferroni correction for multiple comparisons was applied (B) MPV of *wt*, *RhoB-/-*, *RhoA-/-* and *DKO* animals determined by a scil Vet abc Plus+ blood analyzer. Each data point represents one animal (*wt*, *RhoB-/-*, *RhoA-/-* n=9; *DKO* n=8). For statistical evaluation, a two-way ANOVA with Bonferroni correction for multiple comparisons was applied (C) Representative picture of resting platelets by transelectron microscopy. Scale bar in overview equals 2 µm. (D) For the determination of platelet life span, *wt* and *DKO* platelets were labeled with an α-GPIX antibody and analyzed in an observation period of five days. Values are mean of four mice per genotype. For statistical evaluation, a Wilcoxon-Mann-Whitney test was applied and for multiple comparisons a two-way ANOVA with Bonferroni correction was used. Data are presented in mean ± sd. * p < 0.05; ** p < 0.01; *** p < 0.001 indicate statistically significant difference.

Table 3 Peripheral blood cell counts of *wt*, *RhoB*^{-/-}, *RhoA*^{-/-} and *DKO* animals measured by a scil Vet abc Plus+ blood analyzer. Table displays pooled data of at four animals per genotype. For statistical evaluation, a two-way ANOVA with Bonferroni correction was applied.

		wt		*RhoB*^{-/-}		*RhoA*^{-/-}		*DKO*		P-value *DKO-wt*	P-value *DKO-RhoB*^{-/-}	P-value *DKO-RhoA*^{-/-}
		mean	SD	mean	SD	mean	SD	mean	SD			
WBC	$10^3/mm^3$	7.2	4.0	7.4	1.9	6.5	3.8	6.3	2.8	0.81	0.71	0.96
LYM#	$10^3/mm^3$	4.9	2.5	5.6	1.5	4.3	2.5	5.9	2.4	0.84	0.88	0.70
MON#	$10^3/mm^3$	0.3	0.3	0.3	0.1	0.2	0.2	0.1	0.1	0.33	0.47	0.58
GRA#	$10^3/mm^3$	1.9	1.4	1.5	0.6	1.3	1.5	0.9	0.5	0.13	0.22	0.51
EOS#	$10^3/mm^3$	0.0	0.1	0.0	0.0	0.0	0.0	0.0	0.1	0.42	0.34	0.55
LYM%	%	72.0	6.5	76.6	6.4	73.1	7.6	78.1	5.9	0.01	0.20	0.16
MON%	%	4.9	1.0	4.6	0.8	4.8	1.0	3.4	0.8	0.16	0.34	0.17
GRA%	%	23.1	5.7	18.8	5.8	22.3	7.2	15.9	2.5	0.00	0.18	0.16
EOS%	%	1.2	1.4	0.8	0.3	0.9	0.4	0.4	0.3	0.17	0.08	0.12
RBC	$10^6/mm^3$	8.6	0.4	8.0	0.5	8.1	0.5	8.3	0.4	0.37	0.18	0.47
HGB	g/dl	15.4	0.9	15.1	1.1	15.3	0.4	15.0	0.5	0.63	0.80	0.88
HCT	%	49.3	3.2	47.9	4.7	49.1	1.7	49.4	1.2	0.70	0.37	0.56
MCV	μm^3	57.3	3.3	60.0	2.8	60.3	2.1	59.6	0.7	0.09	0.67	0.72
MCH	pg	18.0	0.7	18.8	0.5	18.5	0.3	17.9	0.3	0.93	0.01	0.02
MCHC	g/dl	31.3	0.8	31.5	0.9	27.4	10.4	30.5	0.4	0.05	0.05	0.43
RDW	%	14.7	1.6	13.7	0.2	14.1	0.5	13.6	0.7	0.12	0.66	0.40

Similarly, *DKO* platelets displayed a dose-dependent integrin αIIbβ3 activation defect upon stimulation with thrombin and a severe granule release defect (Figure 27A, B) in addition to their inability to perform shape change upon U46619 stimulation (Figure 27C). Together, these results show that the *DKO* platelets mirror key signaling defects characteristic of *RhoA*^{-/-}, but not *RhoB*^{-/-} platelets. Likewise, *DKO* animals exhibited defective hemostasis as verified by increased tail bleeding tendencies on filter paper in vivo similar to *RhoA*^{-/-} mice (Figure 28).
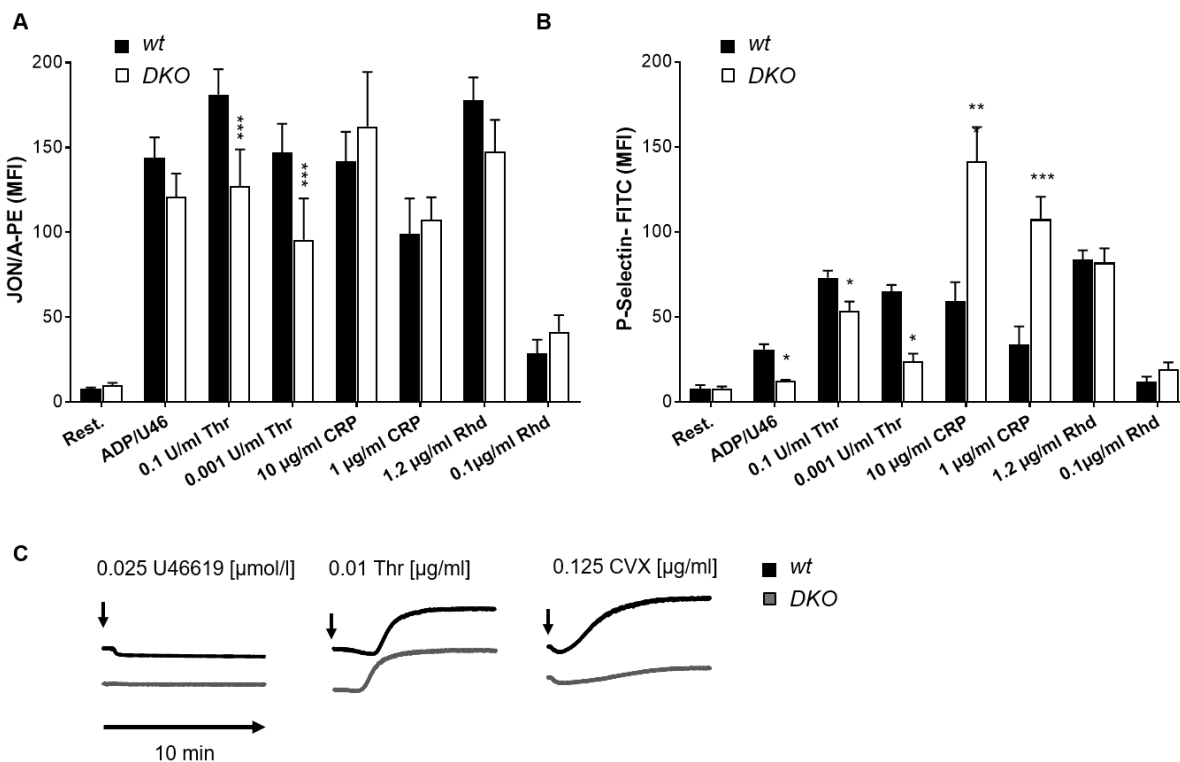
Figure 27 Platelet activation and aggregation of *DKO* platelets in vitro. (A) Platelet integrin αIIbβ3 activation was investigated by JON/A-PE binding upon stimulation with agonists in different concentrations (n=4). (B) α-granule release was investigated by P-Selectin exposure on platelet surface upon stimulation with different agonist concentrations (n=4). (C) Representative aggregation curve of low dose agonist stimulation of washed *wt* and *DKO* platelets under stirring conditions for 10 min. Data are presented in mean ± sd. For statistical evaluation, a Wilcoxon-Mann-Whitney test was applied. * p < 0.05; ** < 0.01 ***; p < 0.001 indicate statistically significant difference. Rest = resting; ADP/U466 = Adenosine diphosphate/U46619; Thr = thrombin; CRP = collagen-related peptide; CVX = convulxin; Rhd = Rhodocytin.

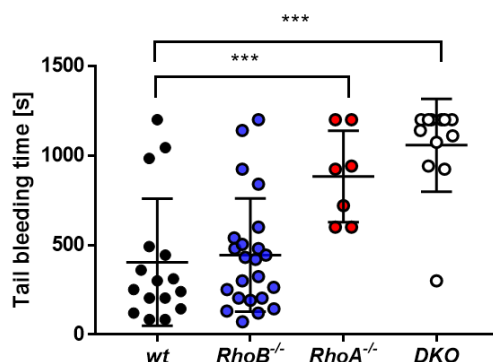**Figure 28 Impaired hemostasis in *DKO* animals.** Tail bleeding time in vivo was assessed using the filter paper method. Each data point represents one animal (*wt* n=16; *RhoB⁻ᐟ⁻* n=24; *RhoA⁻ᐟ⁻* n=7; *DKO* n=10). Data are presented in mean ± sd. For statistical evaluation, a two-way ANOVA with Bonferroni correction for multiple comparisons was applied. *** p < 0.001 indicates statistically significant difference.

3.2.2. Concomitant deficiency of RhoB reverts the localization of RhoA-deficient MKs

We previously described that up to 30% of *RhoA*$^{-/-}$ MKs are able to entirely translocate into the BM sinusoids in a process involving the Rho GTPase Cdc42 (Dütting et al., 2017). To investigate the outcome of RhoB deficiency on MK localization and platelet biogenesis, we generated 2D native BM sections of *wt, RhoB*$^{-/-}$, *RhoA*$^{-/-}$ and *DKO* mice. Consistent with our previous findings, approximately 25% of *RhoA*$^{-/-}$ MKs were localized in the vessel lumen, whereas this phenomenon was hardly observed in the BM of *wt* mice (Figure 29A, B quantification). *RhoB*$^{-/-}$ animals displayed a slightly, but significant reduction of MKs in close contact to the BM vessels and a concomitant increase of MKs in the BM *hematopoietic compartment* (HC). Since the quantification is based solely on 2D sections of the BM, the informative value is limited. Strikingly, concomitant deficiency of *RhoB* was able to revert the intrasinusoidal localization of *RhoA*$^{-/-}$ MKs. This was accompanied by a significant increase in BM derived MK numbers compared to the *wt* and *RhoA*$^{-/-}$ mice, as well as by clustering of *DKO* MKs around the sinusoids (Figure 29C). The *DKO* MKs were less intact, displayed a defective DMS with fewer membrane invaginations, and an increased number of neutrophils inside the cytoplasm, a phenomenon referred to as emperipolesis (Figure 29D). This process was already described for *RhoA*$^{-/-}$ MKs (Dütting et al., 2017) and highlights that *DKO* MKs exhibit some key features of *RhoA*$^{-/-}$ MKs and that RhoB seems solely to be involved in the process of transmigration. Thus, RhoA and RhoB play distinct roles for MK localization in the BM and are possible counter-player in this process.
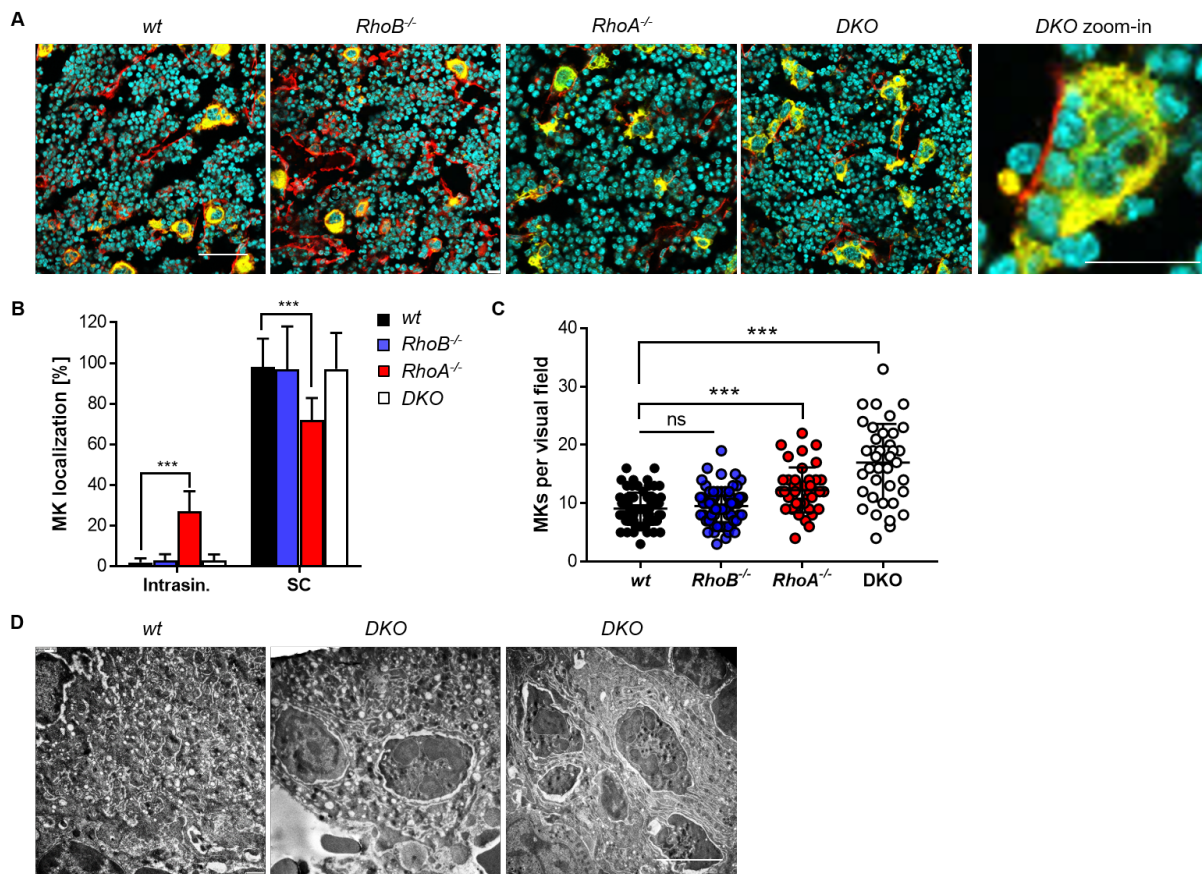
Figure 29 Double deficiency of RhoA and RhoB leads to MK clusters around the sinusoidal endothelium. (A) Representative confocal microscopy pictures of cryosections of PFA-fixated and dehydrated femora. Sections were stained with an Alexa647-labeled anti-CD105 antibody to stain vessel and an Alexa488-labeled anti-GPIX antibody to visualize MKs and DAPI (nucleus). Scale bar in overview equals 40 µm and in zoom 5 µm. (B) Quantification of MK localization in *wt*, *RhoB⁻ᐟ⁻*, *RhoA⁻ᐟ⁻* and *DKO* BM. (C) Quantification of MK number in *wt*, *RhoB⁻ᐟ⁻*, *RhoA⁻ᐟ⁻* and *DKO* BM. Values present mean of seven animals per genotype. At least 10 pictures per animal were analyzed. Each data point represents one picture (*wt* n=75; *RhoB⁻ᐟ⁻* n=75 *RhoA⁻ᐟ⁻* n=41 and *DKO* n=39). (D) In depth analysis of *wt*, *RhoB⁻ᐟ⁻*, *RhoA⁻ᐟ⁻* and *DKO* MKs in transmission electron micrographs. Scale bar equals 3 µm. Data are presented in mean ± sd. For statistical evaluation, a two-way ANOVA with Bonferroni correction for multiple comparisons was applied. Intrasin. = intrasinusoidal; SC = sinusoidal contact.

MK spreading is a process involving the interaction of MK receptors with ECM proteins and the redistribution of the actin and tubulin cytoskeleton upon MK activation. To gain a detailed analysis of the *DKO* MK cytoskeleton under in vitro conditions, we performed spreading experiments on HORM collagen and fibrinogen. Spread *DKO* MKs were able to cover a larger area on the HORM collagen surface than *wt* MKs, implying that the cytoskeleton was altered due to the combined loss of both small GTPases (Figure 30A, B). While the MFI of phalloidin-Atto647, which stains F-actin, was not altered in *DKO* MKs (Figure 30C), the podosome density (number of podosomes per MK area) was significantly reduced. This effect might be explained by an increased spreading area of *DKO* MKs, while the number of podosomes stayed comparable to *wt* numbers (mean podosome number per MKs *wt* = 452 ± 240; *DKO* = 396 ± 212; p value = 0.34; Figure 30D). Interestingly, the MFI of α-tubulin was significantly reduced in

the *DKO* MKs, implicating a defective tubulin cytoskeleton rather than a defective actin cytoskeleton (Figure 30E).
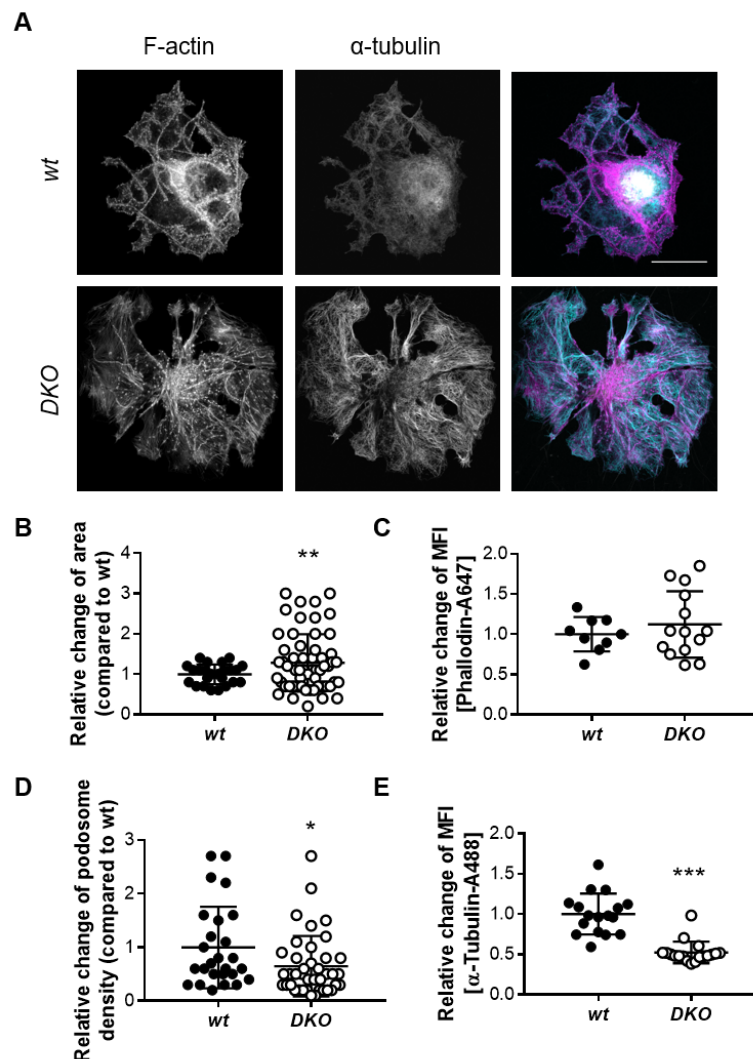

Figure 30 Analysis of cultured *DKO* BM derived MK spreading on HORM collagen in vitro. (A) Representative confocal microscopy pictures of BM derived MKs after BSA gradient were allowed to spread on HORM collagen-coated glass slides for 3 h, PFA-fixed, blocked and stained with phalloidin-Atto647 (magenta), α-tubulin-Alexa488 (cyan) and DAPI to stain the nucleus. Scale bar in overview equals 40 µm. (B) Quantification of spread area on collagen of *wt* and *DKO* MKs (normalized to *wt*). Pooled data of three independent experiments, values present mean of three animals per genotype. At least 5 pictures per animal were analyzed. Each data point represents one MK (*wt* n=24; *DKO* n=58). (C) Quantification of F-actin content of *wt* and *DKO* MKs spread on collagen (normalized to *wt*). Pooled data of three independent experiments, values present mean of three animals per genotype. At least 5 pictures per animal were analyzed. Each data point represents one MK (*wt* n=9; *DKO* n=14). (D) Quantification of podosome density in *wt* and *DKO* MKs spread on HORM collagen (normalized to *wt*). Pooled data of three independent experiments, three animals per genotype were analyzed. Each data point represents one MK (*wt* n=26; *DKO* n=40). (E) Quantification of α-tubulin content of *wt* and *DKO* MKs spread on collagen (normalized to *wt*). Pooled data of three independent experiments, values present mean of three animals per genotype. At least 5 pictures per animal were analyzed. Each data point represents one MK (*wt* n=17; *DKO* n=18). Data are presented in mean ± sd. For statistical evaluation, a Mann-Whitney test was applied. * $p < 0.05$; ** $p < 0.01$; *** $p < 0.001$. MFI = mean fluorescence intensity.

3.2.3. RhoA and RhoB have redundant roles in platelet biogenesis

To gain further insights into the MK cytoskeleton, we performed PPF of BM derived MKs in vitro. Especially the elongation of proplatelets is driven by a Dynein/Dynactin-dependent sliding of MTs and is highly dependent on the MT network (Bender et al., 2015; Patel-Hett et al., 2008) and we therefore speculated that the tubulin defect observed in spread *DKO* MKs would transfer into a defective PPF or shaft elongation. Indeed, *DKO* MKs were smaller in size with less and bigger swellings compared to *wt* control (Figure 31A), yet no differences in the capacity of PPF was detected (Figure 31B). As shown in Figure 22, *RhoB*$^{-/-}$ MKs displayed a high proportion of proplatelet forming MKs with a defective tubulin cytoskeleton. This was even more pronounced in *DKO* MKs (but with no statistical significance in comparison to *RhoB*$^{-/-}$ conditions; Figure 31C), whereas *RhoA*$^{-/-}$ MKs were not as severely affected.

To draw conclusions about the in vivo conditions and the observed macrothrombocytopenia in *DKO* mice, we observed *DKO* and *wt* MKs in the murine skull by two-photon intravital microscopy. *DKO* MKs clustered heavily around the blood vessels but were still able to perform PPF (Figure 31D). Regardless, this experiment needs to be repeated more often to gain deeper insights into in vivo PPF.
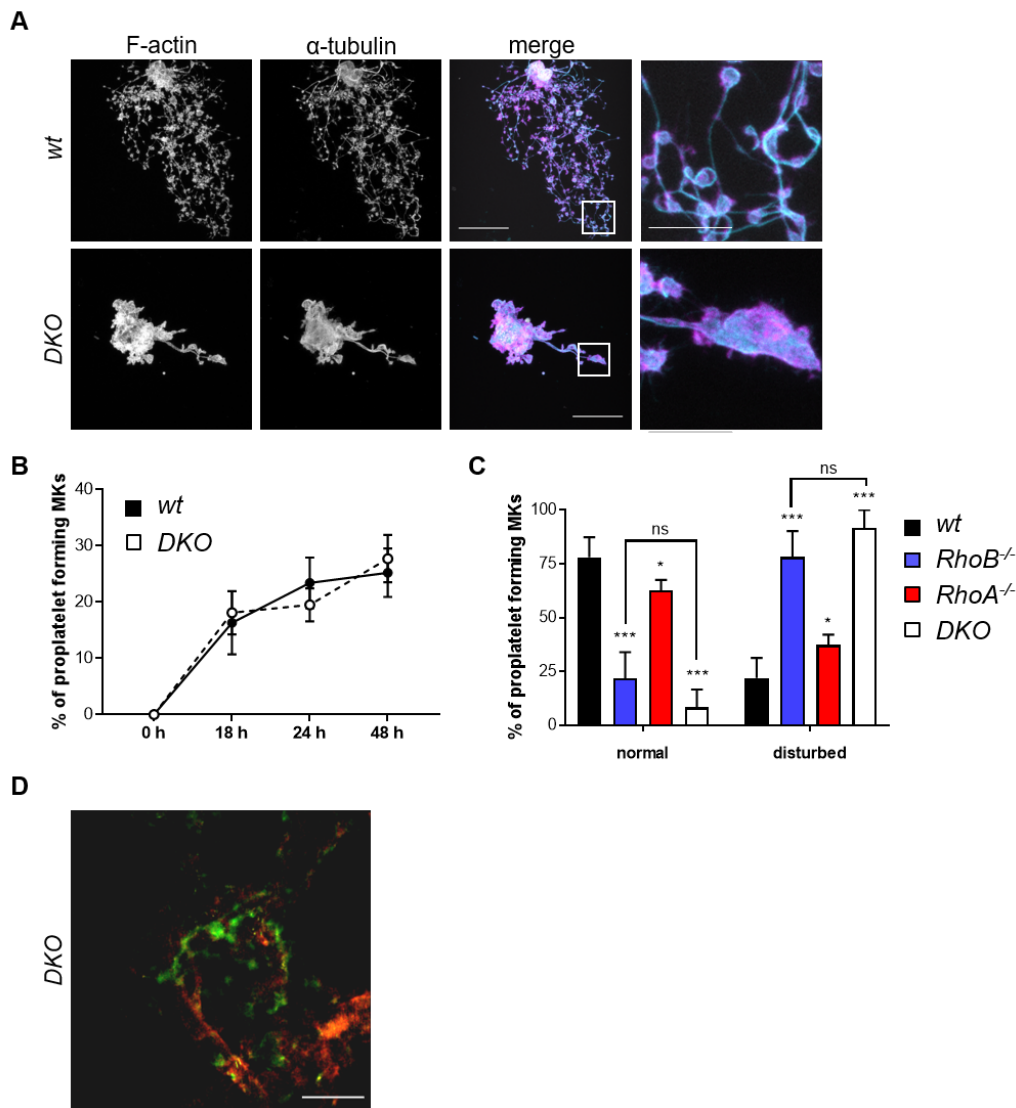
Figure 31 Analysis of PPF of BM derived *DKO* MKs. (A) Representative confocal pictures of BM derived MKs 24 h after BSA gradient. The MKs were spun down to Poly L-Lysine coated glass slides and stained with phalloidin-Atto647 (magenta), α-tubulin-Alexa488 (cyan) and DAPI to visualize the nucleus. Scale bar in overview equals 40 µm and in zoom 5 µm. (B) Quantification of in vitro PPF in an observation period of 18 h, 24 h and 48 h after BSA gradient. Values present mean of three animals per genotype. For statistical evaluation, a Wilcoxon-Mann-Whitney test was applied. (C) Quantification of MT organization in *wt, RhoB⁻/⁻, RhoA⁻/⁻* and *DKO* MKs 24 h after BSA gradient. At least 10 pictures per animal were analyzed (n=3). For statistical evaluation, a two-way ANOVA with Bonferroni correction for multiple comparisons was applied. (D) Intravital two-photon microscopy of BM derived MKs (GPIX; green) in the skull. Blood vessels were visualized with BSA-FITC and CD105-AlexaF488. Scale bar equals 50 µm. Data in (D) were kindly provided by Dr. Isabelle Becker. Data are presented in mean ± sd. For statistical evaluation, a Wilcoxon-Mann-Whitney test was applied. *** $p < 0.001$ indicates statistically significant difference.

Since *RhoB⁻/⁻* platelets, but not cultured MKs, displayed a reduction in acetylated α-tubulin, we next isolated platelets and MKs of *RhoB⁻/⁻-, RhoA⁻/⁻-* and *DKO* mice. The platelets were directly lysed, while the MKs were cultured in media containing TPO and hirudin. Afterwards, the proplatelet forming MKs were spun down and protein lysates were prepared. As observed before, *RhoB⁻/⁻* platelets showed a massively decreased K40 acetylation, while *RhoA⁻/⁻* and *DKO* platelets showed only minor reductions (Figure 32A). Proplatelet-forming MKs showed no

differences in PTMs of α-tubulin (acetylation and detyrosination), leaving the question what caused the tubulin defect in *RhoB⁻ᐟ⁻* and *DKO* MKs. We next investigated important regulator of the actin and tubulin cytoskeleton in proplatelet forming MKs but did not observe any alterations for neither actin regulatory proteins (NMIIa, NMIIb, Vinculin, Arp2) nor APC, α-tubulin, and β1-tubulin (Figure 32B).
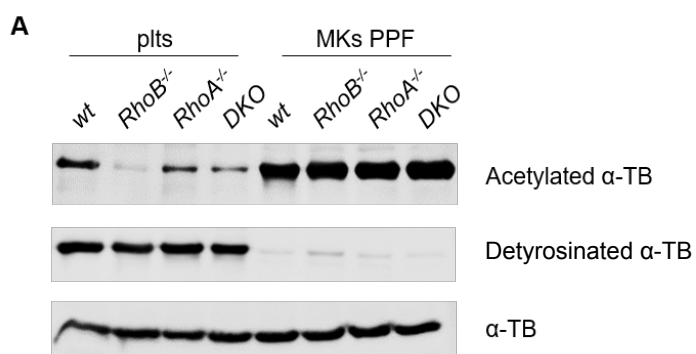

Figure 32 Analysis of proteins involved in the tubulin and actin cytoskeleton. (A) MK protein lysates of *wt*, *RhoB⁻ᐟ⁻*, *RhoA⁻ᐟ⁻* and *DKO* animals were immunoblotted against PTM of α-tubulin. GAPDH was used as a loading control. (B) MK protein lysates of *wt*, *RhoB⁻ᐟ⁻*, *RhoA⁻ᐟ⁻* and *DKO* animals were immunoblotted against pivotal regulators of the actin and tubulin cytoskeleton and tubulin isoforms. GAPDH was used as a loading control. TB = tubulin.
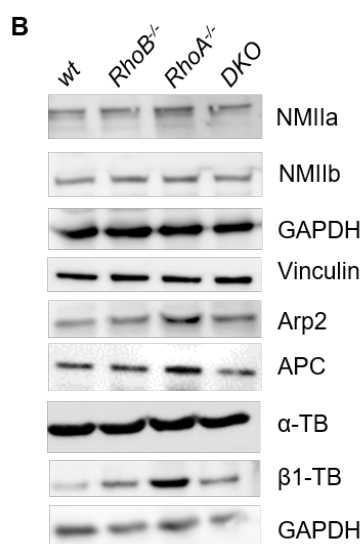
In conclusion, we were able to show that mice with a double deficiency of RhoA and RhoB recapitulated findings from both, *RhoA⁻ᐟ⁻* (macrothrombocytopenia, platelet signaling defects) and *RhoB⁻ᐟ⁻* animals (MK tubulin defect). Most importantly, we were able to show that a double deficiency of RhoA and RhoB was sufficient to revert the intrasinusoidal localization of *RhoA⁻ᐟ⁻* MKs.

3.2.4. Heterozygous KO of RhoB reverts MK translocation of RhoA-deficient mice

Due to the significant increase in RhoB expression in *RhoA⁻ᐟ⁻* MKs, we speculated that the transmigration of *RhoA⁻ᐟ⁻* MKs may not be caused by the loss of RhoA but rather by the

upregulation of RhoB. Therefore, we generated animals that specifically lacked RhoA in platelets and MKs additionally carrying a constitutive heterozygous deletion of RhoB to test whether the level of RhoB in MKs was able to directly influence MK localization upon absence of RhoA. On protein level, RhoB expression was about 330% in *RhoA*-/- MKs compared to *wt* MKs, whereas *RhoA*-/-/*RhoB*+/- MKs contained only 70% of *wt* levels (Figure 33A, B). *RhoA*-/-/ *RhoB*+/- animals displayed a macrothrombocytopenia, which was more severe than in *RhoA*-/- animals but less pronounced than in the *DKO* animals (Figure 33C, D). Of note, the platelet size did not vary between the three different genotypes (only *RhoB*-/- animals displayed smaller platelets; Figure 33D).
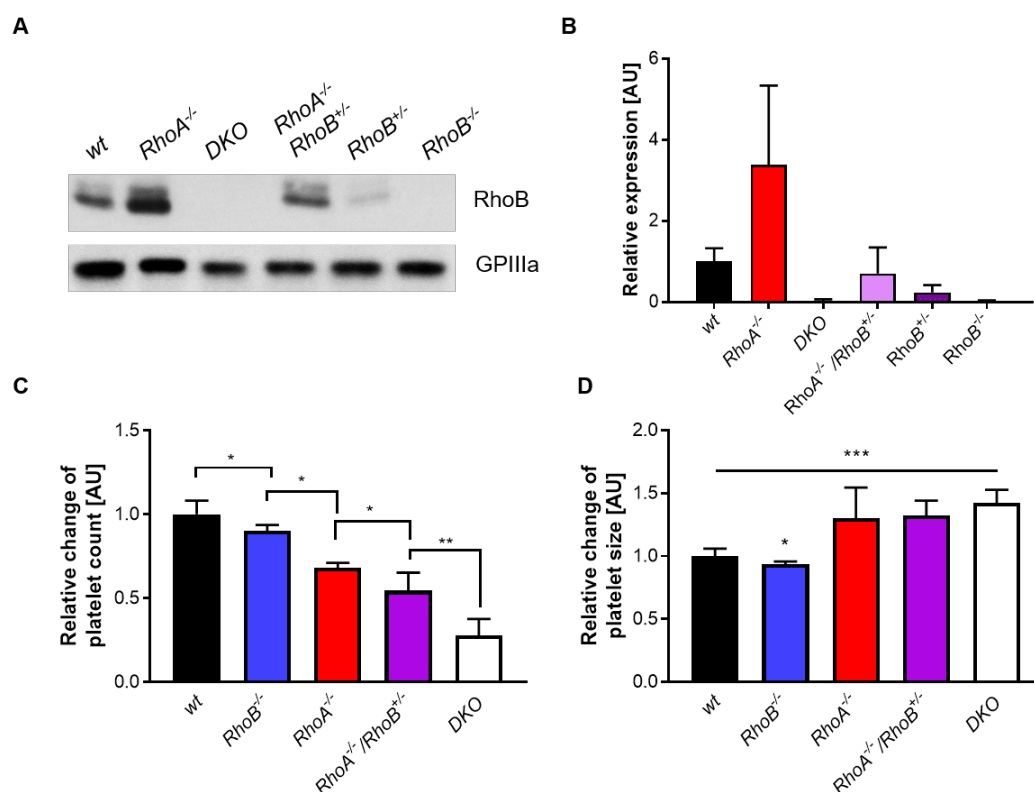
Figure 33 Analysis of *RhoA*-/-/*RhoB*+/- animals. (A) MK protein lysates of *wt*, *RhoB*-/-, *RhoA*-/-, *RhoA*-/-/ *RhoB*+/- and *DKO* animals were immunoblotted against RhoB. GAPDH was used as a loading control. (B) Densitometric analysis of blot densities quantified as ratio of RhoB to GAPDH and calculated as percentage of control; Pooled data of three independent experiments. (C) Relative platelet count (normalized to *wt*) assessed by a scil Vet abc Plus+ blood analyzer (*wt* n = 4; *RhoB*-/- n = 3; *RhoA*-/- n = 2; *RhoA*-/-/*RhoB*+/- n = 5; *DKO* n = 5). (D) Relative platelet size (normalized to *wt*) assessed by a scil Vet abc Plus+ blood analyzer (*wt* n = 4; *RhoB*-/- n = 3; *RhoA*-/- n = 2; *RhoA*-/-/*RhoB*+/- n = 5; *DKO* n = 5). Data are presented in mean ± sd. For statistical evaluation, a two-way ANOVA with Bonferroni correction for multiple comparisons was applied. * $p < 0.05$; ** $p < 0.01$; *** $p < 0.001$ indicates statistically significant difference.

Since the thrombocytopenia of *RhoA*-/-/*RhoB*+/- animals was more drastic than in *RhoA*-/- animals, we prepared cryosections of the native BM to get an insight into MK localization in situ. *RhoA*-/-/*RhoB*+/- MKs looked more intact than *DKO* MKs and did not cluster at the vessel wall (Figure 34A). This finding was supported by TEM, furthermore demonstrating a better

developed DMS with more membrane invaginations compared to *DKO* MKs (Figure 35). On the one hand, *RhoA⁻/⁻/RhoB⁺/⁻* animals showed a significantly reduced number of MKs with intrasinusoidal localization compared to *RhoA⁻/⁻* mice, although a small percentage of MKs was still able to translocate into the vessel lumen (4.8%±3.9 MKs intrasinusoidal, Figure 34B). On the other hand, the *RhoA⁻/⁻/RhoB⁺/⁻* animals displayed a significantly reduced number of MKs localized in the BMHC, thus partially reversing the phenotype observed in *DKO* animals (Figure 34C). These findings highlight that RhoA and RhoB play redundant and non-redundant roles in MKs and platelets and demonstrate the challenges to assign the defects in the *DKO* to a specific mechanism. Nevertheless, these findings indicate that RhoB levels might directly influence the transendothelial migration observed in *RhoA⁻/⁻* mice.

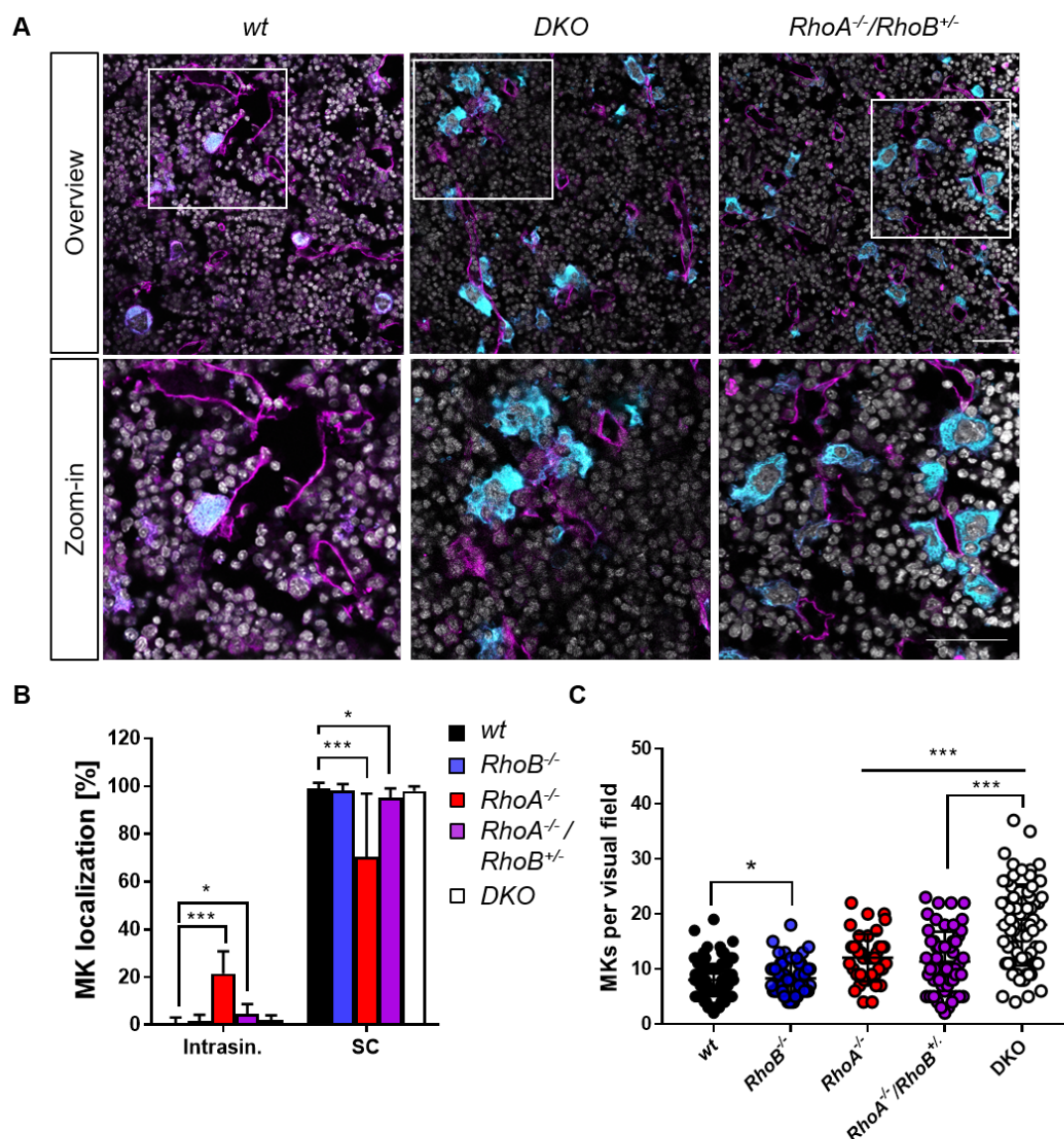**Figure 34 Localization of *RhoA⁻/⁻/RhoB⁺/⁻* MKs in situ.** Representative confocal microscopy pictures of cryosections of PFA-fixated and dehydrated femora. Sections were stained with an Alexa647-labeled anti-CD105 antibody to stain vessel and an Alexa488-labeled anti-GPIX antibody to visualize MKs and DAPI (nucleus). Scale bar in overview equals 40 µm and in zoom 10 µm. (B) Quantification of MK localization in

wt, *RhoB⁻/⁻*, *RhoA⁻/⁻*, *RhoA⁻/⁻/RhoB⁺/⁻*, and *DKO* BM (n=5) (C) Quantification of MK number in *wt*, *RhoB⁻/⁻*, *RhoA⁻/⁻*, *RhoA⁻/⁻/RhoB⁺/⁻*, and *DKO* BM (n=5). At least 10 pictures per animal were analyzed. Each data point represents one picture (*wt* n=120; *RhoB⁻/⁻* n=62, *RhoA⁻/⁻* n=40, *RhoA⁻/⁻/RhoB⁺/⁻* n=58, and *DKO* n=78). Data are presented in mean ± sd. For statistical evaluation, a two-way ANOVA with Bonferroni correction for multiple comparisons was applied. * $p < 0.05$; *** $p < 0.001$ indicates statistically significant difference. Intrasin. = intrasinusoidal; SC = sinusoidal contact.
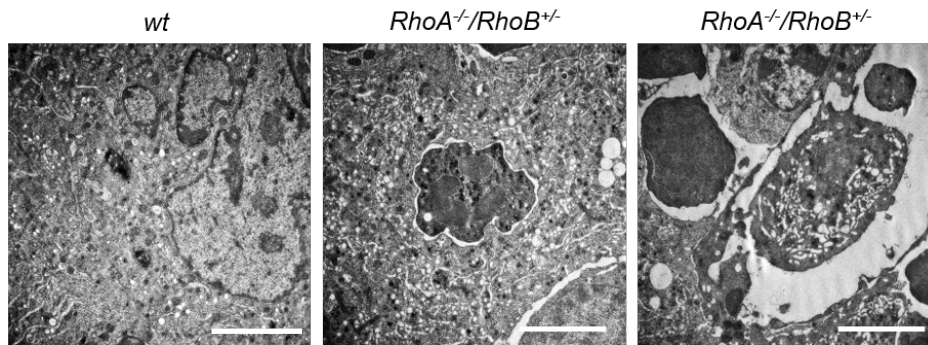
wt	*RhoA⁻/⁻/RhoB⁺/⁻*	*RhoA⁻/⁻/RhoB⁺/⁻*

Figure 35 Analysis of the MK DMS by TEM. In depth analysis of *wt* and *RhoA⁻/⁻/RhoB⁺/⁻* BM in transmission electron micrographs. Scale bar equals 3 µm.

3.3. PDK1 guides proplatelet formation and F-actin rearrangements in murine MKs

3.3.1. Loss of PDK1 in MKs causes altered MK localization

The impact of conditional lack of PDK1 in platelets and MKs on MK biology was assessed in collaboration with the group of Prof. Oliver Borst (University Hospital Tübingen), which provided us with *PDK1^fl/fl Pf4-Cre* mice further referred to as *PDK1⁻/⁻* (Manne et al., 2018; Münzer et al., 2016). To verify the absence of PDK1 in platelets and MKs, mRNA transcript analysis was performed in murine MKs and kidney cells (Figure 36A, left) and protein levels were determined in MK lysates (Figure 36A, right), which both confirmed the loss of PDK1 in MKs. As previously described (Chen et al., 2013; Manne et al., 2018; Münzer et al., 2016) the deficiency of PDK1 resulted in a significant macrothrombocytopenia, which progressively deteriorated with increasing age (Figure 36B). Reductions in platelet counts can be associated with a decreased platelet life span due to enhanced clearance of platelets in the reticulo-endothelial system of the spleen, which prompted us to assess platelet life span in *PDK1⁻/⁻* mice by injecting a DyLight 488-coupled α-GPIX antibody. Interestingly, we found platelet turnover to be significantly increased in *PDK1⁻/⁻* animals (Figure 36C). Since this accelerated clearing of platelets did not fully explain the pronounced thrombocytopenia, we also investigated platelet recovery by intravenous injection of an anti-GPIbα depletion antibody, followed by analysis of platelet counts for seven days in order to assess de-novo platelet generation. The percentage of recovered platelets, however, was restored to the initial level in *wt* and *PDK1⁻/⁻* animals in the course of time suggesting a normal platelet biogenesis (Figure 36D).
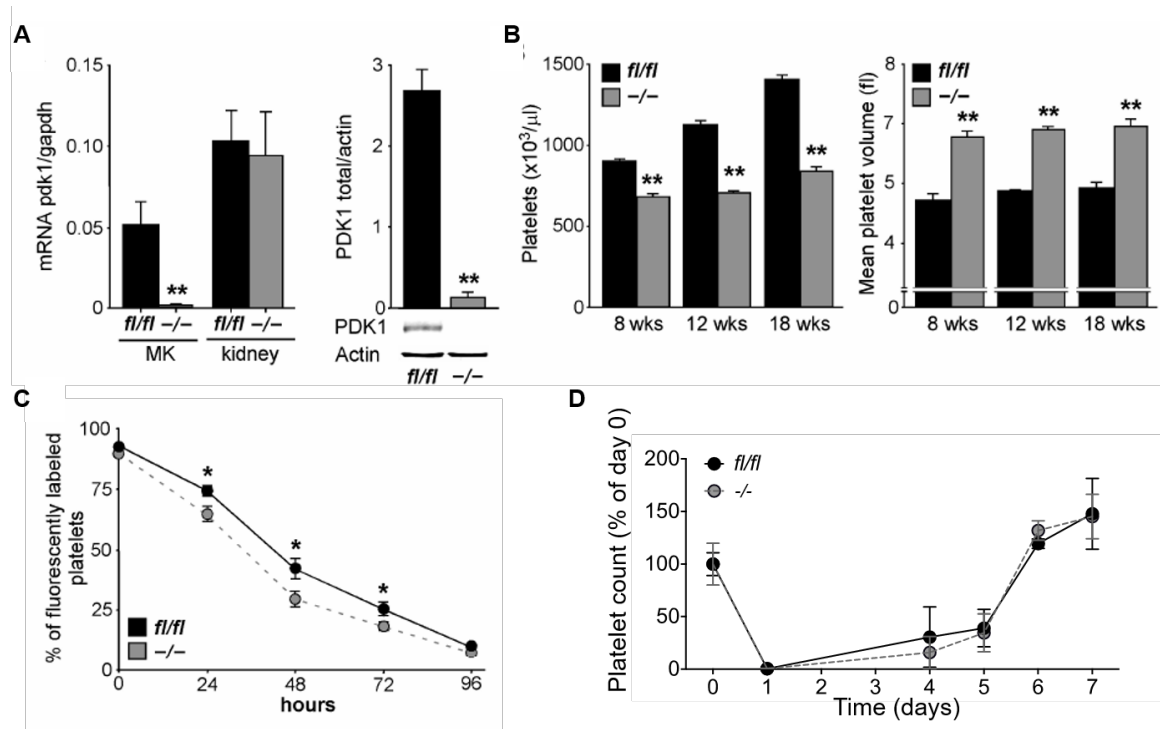
Figure 36 Loss of PDK1 in MKs results in macrothrombocytopenia and a reduced life span. (A) Left: mRNA transcript levels of PDK1 in murine platelets and kidneys from *wt* and *PDK1*$^{-/-}$ animals (n=6). Right: representative immunoblots and densitometric analysis of total PDK1 protein levels in *wt* and *PDK1*$^{-/-}$ MKs (n=5). (B) Platelet count and size of 8 weeks (n=13), 12 weeks (n=22) and 18 weeks (n=10) old *wt* and *PDK1*$^{-/-}$ animals. (C) Determination of platelet life span by injection of a DyLight488-labeled α-GPIX antibody. Fluorescently labeled platelets were followed up for 96 hours (n=6). (D) Relative platelet count (in comparison to respective platelet count on day 0) after depletion by intravenous injection of rat anti-GPIbα antibody. Platelet recovery was observed over a period of seven days by flow cytometry. Data in (A) to (C) were generated in the laboratory of Prof. Oliver Borst. Data in (D) were kindly provided by Dr. Irina Pleines-Meinhold. Data in (A) to (C) are presented in mean ± sem. Data in (D) are presented in mean ± sd. For statistical evaluation, a Wilcoxon-Mann-Whitney test was applied. * $p < 0.5$; ** $p < 0.01$ indicate statistically significant difference. Data modified after Geue and Aurbach et al., 2019.

To further evaluate megakaryopoiesis, we investigated the BM structure of *PDK1*$^{-/-}$ animals by anti-GPIX immunostaining of BM cryosections (Figure 37A, B). Strikingly, *PDK1*$^{-/-}$ exhibited a distinct megakaryocytosis reflected by increased numbers of GPIX-positive MKs within the BM (Figure 37C). However, the MKs appeared intact and showed no signs of fragmentation. Detailed evaluation of MK localization in the BM revealed that the majority of MKs localized in close contact to the sinusoids, whereas the number of *PDK1*$^{-/-}$ MKs next to the vessels was significantly reduced (Figure 37D). Despite their increased number, *PDK1*$^{-/-}$ MKs accumulated in the BMHC indicating insufficient transendothelial platelet biogenesis.
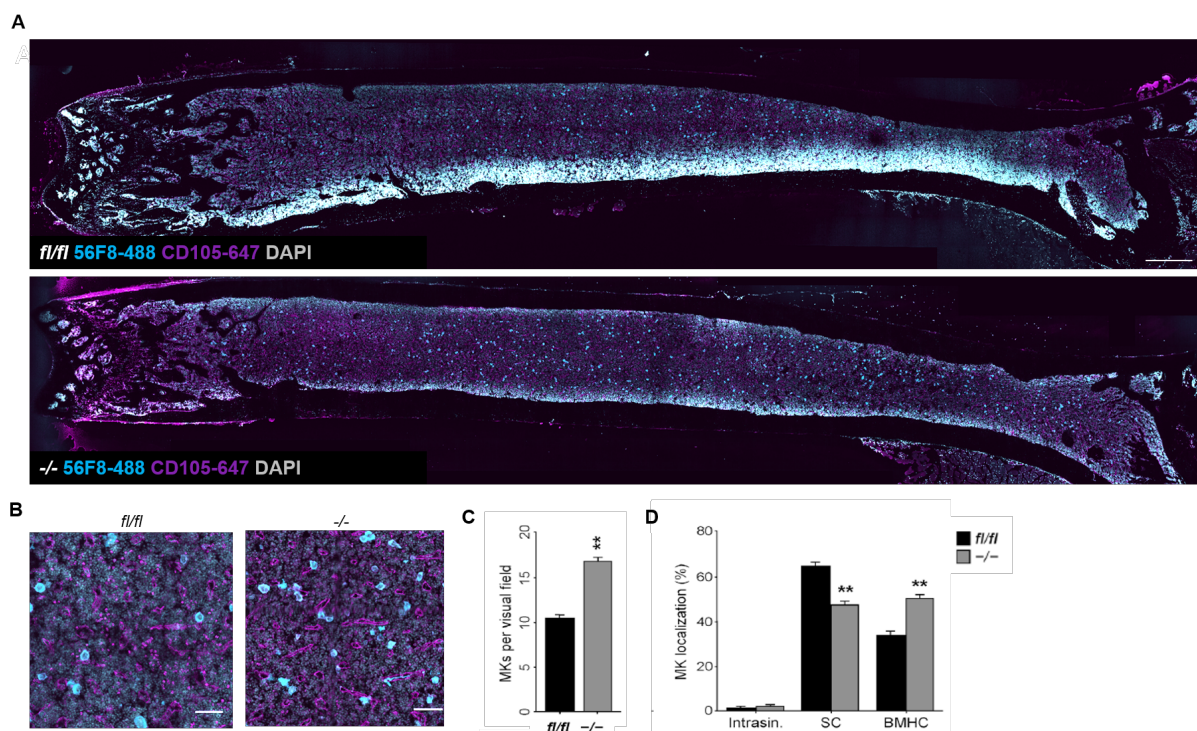
Figure 37 Altered distribution of *PDK1-/-* MKs in the BM. (A) Cryo-conserved whole femora of *wt* and *PDK1-/-* animals were sectioned and imaged using a Leica TC SP8 confocal microscope equipped with the Leica Application Software (LAS) X Navigator (n=3). Scale bar equals 500 μm. (B) Representative visual fields of the murine BM *wt* and *PDK1-/-* animals (n=3). Scale bar equals 50 μm. (C) Determination of MK number per visual field (n=6). For statistical evaluation, a Wilcoxon-Mann-Whitney test was applied. (D) Percentage of MK localization in the BM (n=6). For statistical evaluation, a two-way ANOVA with Bonferroni correction for multiple comparisons. Sections were stained with an Alexa647-labeled anti-CD105 antibody to stain vessel and an Alexa488-labeled anti-GPIX antibody to visualize MKs and DAPI (nucleus). Data in (C) and (D) were generated in the laboratory of Prof. Oliver Borst. Data are presented in mean ± sem. ** $p < 0.01$ indicates statistically significant difference. Data modified after Geue and Aurbach et al., 2019. Intrasin. = intrasinusoidal; SC = sinusoidal contact; BMHC = Bone marrow hematopoietic compartment

3.3.2. PDK1 influences the F-actin cytoskeleton and DMS development

As it is hypothesized that MK localization towards the BM vessels is driven by maturation steps leading to directed transendothelial PPF of mature polarized MKs (Antkowiak et al., 2016), we analyzed the morphology of BM derived MKs in their native environment by TEM and their polarization capacity in vitro in solution. While *wt* MKs displayed a fully developed DMS, *PDK1-/-* MKs had less membrane invaginations in the periphery and around the nucleus (Figure 38A). Furthermore, the *PDK1-/-* MKs displayed a reduced number of granules indicating a disturbed maturation process within the BM. Thus, we examined whether PDK1 deficiency resulted in alterations of polyploidization, a process driven by cycles of DNA replication without cytokinesis ('endomitosis'). Analyses of DNA content in CD41+ BM derived MKs revealed that *PDK1-/-* MKs presented a shift of ploidization with reduced <8N populations and increased 16N, 32N and >32N populations (Figure 38B, C) indicating an altered maturation process. MK maturation and DMS organization highly rely on F-actin dynamics to polarize membranes and nuclei territories

that end in directed platelet biogenesis at the BM sinusoids. To further determine MK polarization capacity, we used immunofluorescence confocal microscopy with consecutive 3D surface rendering of BM derived MKs after 5 days of culture in solution. Interestingly, *PDK1^{-/-}* MKs displayed an increased non-polarized population in comparison to *wt* MKs (71.5±4.62% vs. 46.35±2.58%) with a concomitant decreased polarized MK population and decreased diameter in solution (Figure 38D, E).
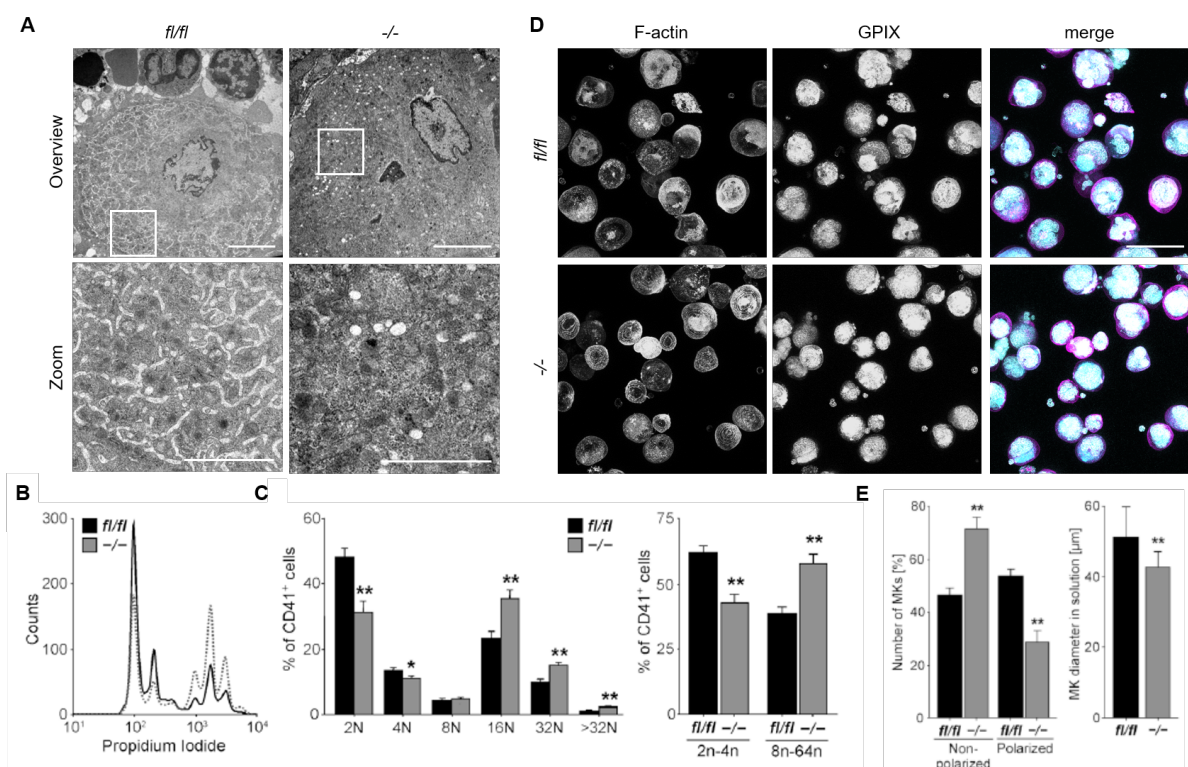

Figure 38 PDK1-deficiency in MKs results in disturbed DMS development, increased poly-ploidization and defective polarization. (A) Representative TEM images of *wt* and *PDK1^{-/-}* BM show less developed DMS and large zones without granula in *PDK1^{-/-}* MKs. Overview: Scale bar equals 5 μm; zoom scale bar equals 2 μm. (B) Representative ploidy histogram of *wt* and *PDK1^{-/-}* CD41+ BM derived MKs after 5 days of culture (n=6). For statistical evaluation, a two-way ANOVA with Bonferroni correction for multiple comparisons was applied. (C) Left: Percental distribution of DNA content in *wt* and *PDK1^{-/-}* CD41+ BM derived MKs. Right: Percentage of CD41+ BM derived MKs with a DNA content below or over 8N (n=6). For statistical evaluation, a two-way ANOVA with Bonferroni correction for multiple comparisons was applied. (D) Representative confocal images depicted in maximum projection of BM derived *wt* and *PDK1^{-/-}* MKs cultured for five days imaged using a Leica TC SP8 confocal microscope. Scale bar equals 40 μm. Color code for merge: Magenta F-actin (phalloidin Atto-647), cyan DMS (GPIX, 56F8-A488), grey nuclei (DAPI). (E) Left: Quantification of polarization of BM derived *wt* and *PDK1^{-/-}* MKs cultured for five days. Right: MK diameter (μm) in solution, for statistical analysis, images in (D) were analyzed by ImageJ. Data in (B) and (C) were generated in the laboratory of Prof. Oliver Borst and are presented in mean ± sem. Data in (D) are presented in mean±sd (n=6, at least 100 MKs per genotype were analyzed). For statistical evaluation, a Wilcoxon-Mann-Whitney test was applied. * $p < 0.05$; ** $p < 0.01$ indicates statistically significant difference. Data modified after Geue and Aurbach et al., 2019.

MK polarization is a process mainly driven by the actin cytoskeleton and altered actin dynamics may be causative for the underlying defects in *PDK1^{-/-}* MKs. To further investigate the role of the cytoskeleton in *PDK1^{-/-}* MKs, we examined the cytoskeletal network in cultured *wt* and *PDK1^{-/-}*

BM derived MKs by letting them adhere to a collagen-coated glass surface for 3 h at 37°C (Figure 39A). Analysis of *PDK1$^{-/-}$* MKs revealed a disturbed assembly of F-actin with regions of F-actin accumulations and a decreased MFI of phalloidin-Atto647N, while the MFI of α-tubulin-A488 remained unaffected (Figure 39B).

Figure 39 Analysis of cytoskeletal structures in spread *wt* and *PDK1$^{-/-}$* BM derived MKs spread on collagen. (A) Representative confocal images of BM derived *wt* and *PDK1$^{-/-}$* MKs cultured for 5 days, then let to adhere to collagen (50 µg/ml) for 3 h and stained for F-actin and α-tubulin. Images were acquired using a Leica TCS SP8 confocal microscope. Scale bar equals 40 µm. Color code for merge: Magenta F-actin (phalloidin Atto-647), cyan α-tubulin (α-tubulin -A488), grey nuclei (DAPI). (B) Left: Mean fluorescence intensity of phalloidin-Atto647N quantified by ImageJ in *wt* and *PDK1$^{-/-}$* MKs (n=36-59). Left: Mean fluorescence intensity of α-tubulin-Alexa488 quantified by ImageJ in *wt* and *PDK1$^{-/-}$* MKs (n= 40-48). (C) Quantification of MK spreading area after 3 h on collagen at 37°C by ImageJ (n=74-86). (D) Absolute number of podosomes per MK quantified by ImageJ (n=38-57). Data are presented in mean±sd (n=5). For statistical evaluation, a Wilcoxon-Mann-Whitney test was applied. ** $p < 0.01$ indicates statistically significant difference. Data modified after Geue and Aurbach et al., 2019.

As a consequence of the defective actin cytoskeletal dynamics, *PDK1$^{-/-}$* MKs displayed a reduced spreading area on collagen and a significantly reduced number of podosomes, F-actin rich structures that mediate interactions between MKs and matrix proteins (Figure 39C, D). Of

note, podosomes density, which is determined by podosomes per area was not altered between *wt* and *PDK1⁻/⁻* MKs. Since F-actin assembly in podosomes is dependent on the core proteins WASP and the Arp2/3 complex, we were interested whether these components were also disturbed in *PDK1⁻/⁻* MKs. Consistently, WASP as well as Arp2 MFI were altered in KO MKs (Figure 40A, B), thereby highlighting the impaired formation of podosomes.

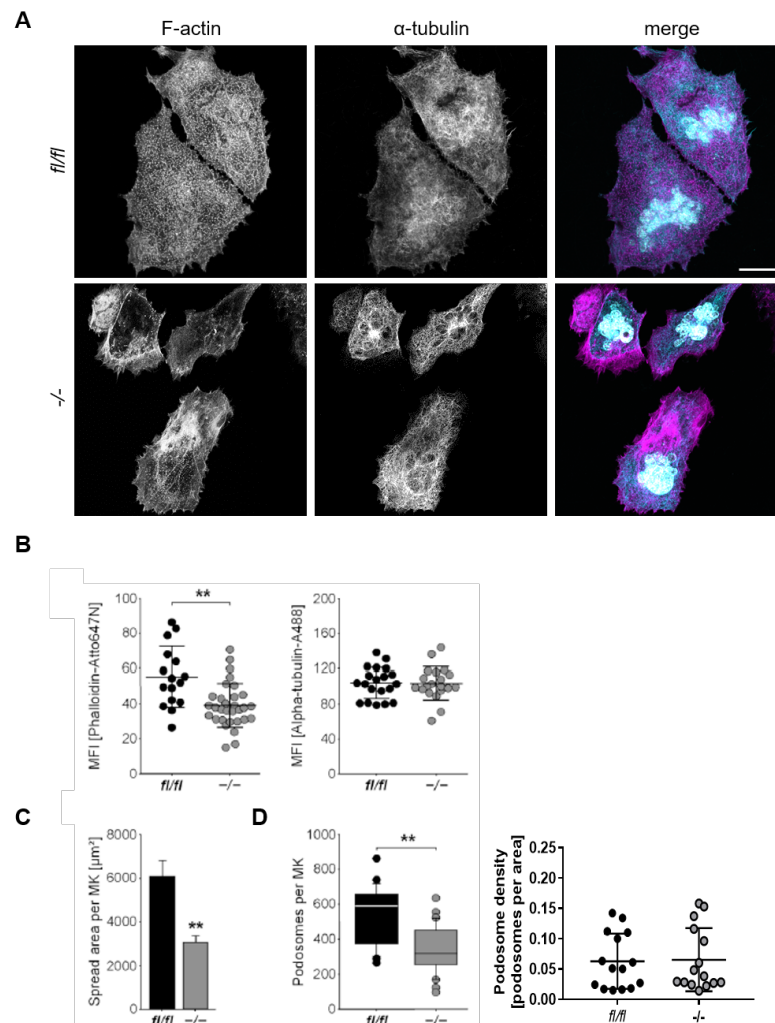**Figure 40 Analysis of podosome structures in spread *wt* and *PDK1⁻/⁻* BM derived MKs spread on collagen.** (A) Representative confocal images of BM derived *wt* and *PDK1⁻/⁻* MKs cultured for 5 days, spread on collagen (50 µg/ml) for 3 h and stained for F-actin and Arp2. Color code for merge: Magenta F-actin (phalloidin Atto-647), cyan Arp2 (primary Arp2 antibody stained with secondary Alexa488 antibody), grey nuclei (DAPI). (B) Representative confocal images of BM derived *wt* and *PDK1⁻/⁻* MKs cultured for 5 days, then spread on collagen (50 µg/ml) for 3 h and stained for F-actin and WASP. Color code for merge: Magenta F-actin (phalloidin Atto-647), cyan WASP (primary WASP antibody stained with secondary Alexa488 antibody), grey nuclei (DAPI). Images were acquired using a Leica TCSP8 confocal microscope. Scale bar equals 40 µm. Modified after Geue and Aurbach et al., 2019.

Of note, *PDK1⁻/⁻* MKs spread comparable to *wt* MKs on fibrinogen (Figure 41A, C) and did not display cytoskeletal alterations regarding F-actin assembly and α-tubulin polymerization (Figure 41B). This finding is in contrast to findings using *PDK1⁻/⁻* platelets, which exhibited a clear spreading defect on immobilized fibrinogen in vitro (Chen et al., 2013).
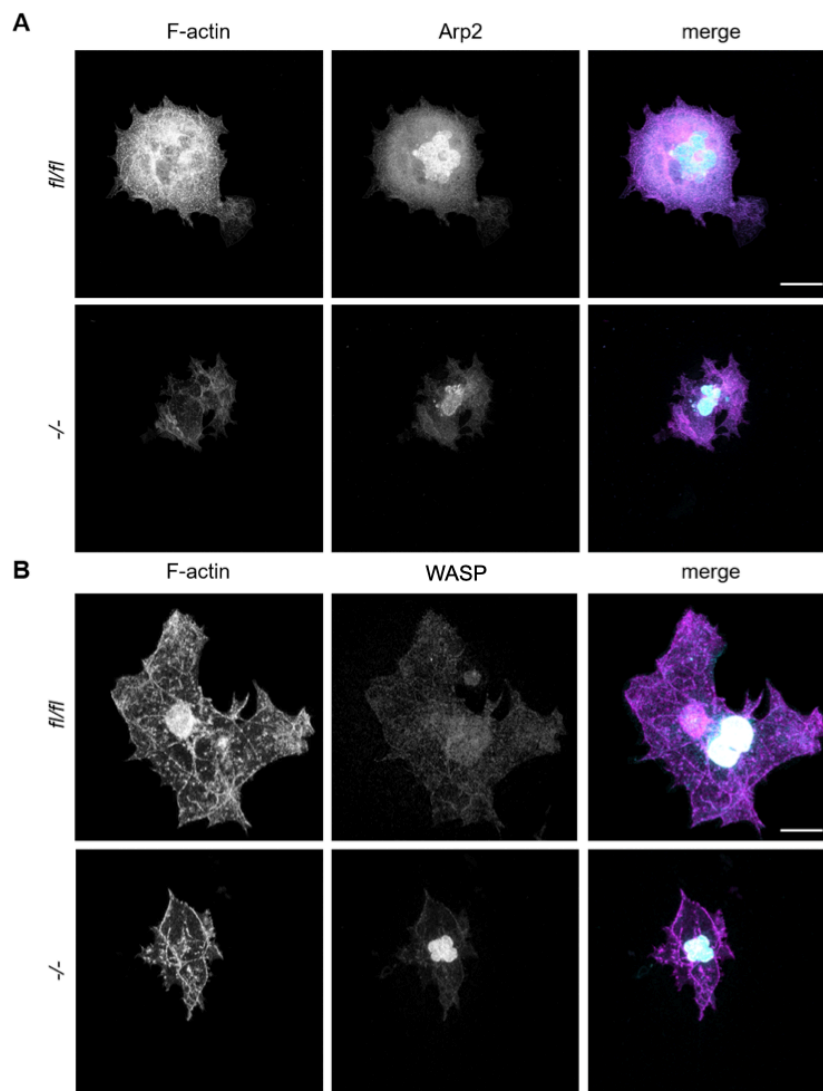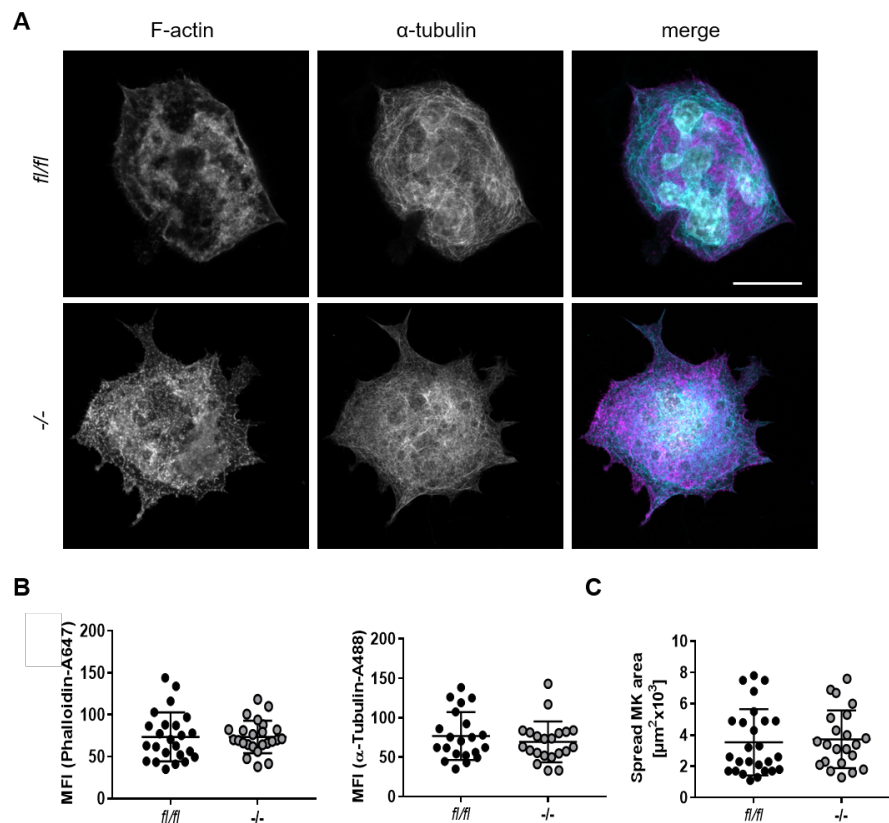

Figure 41 Analysis of cytoskeletal structure in spread *wt* and *PDK1⁻/⁻* BM derived MKs spread on fibrinogen. (A) Representative confocal images of BM derived *wt* and *PDK1⁻/⁻* MKs cultured for 5 days, then let to adhere to fibrinogen (100 µg/ml) for 3 h and stained for F-actin and α-tubulin. Images were acquired using a Leica TCSP8 confocal microscope. Scale bar equals 40 µm. Color code for merge: Magenta F-actin (phalloidin Atto-647), cyan α-tubulin (α-tubulin-A488), grey nuclei (DAPI). (B) Left: Mean fluorescence intensity of phalloidin-Atto647N quantified by ImageJ in *wt* and *PDK1⁻/⁻* MKs (n=24). Left: Mean fluorescence intensity of α-tubulin-Alexa488 quantified by ImageJ in *wt* and *PDK1⁻/⁻* MKs (n= 21). (C) Quantification of MK spreading area after 3 h on collagen at 37°C by ImageJ (n=22-26). Data are presented in mean±sd (n=4). For statistical evaluation, a Wilcoxon-Mann-Whitney test was applied. Data modified after Geue and Aurbach et al., 2019.

To elucidate the mechanism behind the pronounced F-actin cytoskeletal defect observed upon *PDK1* deletion in murine MKs, we investigated protein expression of potential downstream candidates involved in actin cytoskeleton organization, regulation, MK maturation or PPF. Dütting et al. previously identified that the small Rho GTPases RhoA and Cdc42 have opposing roles in MK signaling and are required for transendothelial PPF in the BM (Dütting et al., 2017). Therefore, we investigated the activity of RhoA and Cdc42 in cultured *wt* and *PDK1⁻/⁻* MKs but did not find any alterations in Rho GTPase activity (Figure 42A, B). *p21-activated kinase* (PAK) was described as a potential downstream target of PDK1 (King et al., 2000) and genetic

deletion of PAK2 in mice resulted in an increased number of MKs in the BM, elevated numbers of polyploid MKs, which was accompanied by a severe macrothrombocytopenia caused by defective PPF and an impaired activation of the PAK substrate *LIM kinase* (LIMK) (Kosoff et al., 2015). Following up on this signaling pathway, we found a significant reduction phosphorylation of PAK1/2 and LIMK (Thr$_{508}$), which are pivotal for kinase activation, in *PDK1$^{-/-}$* BM derived MKs (Figure 42C, D). Reduced LIMK activity can result in enhanced Cofilin activity and subsequently increased F-actin severing, since Cofilin is active in a non-phosphorylated state. Immunoblotting revealed a significant reduction in Cofilin phosphorylation (Ser$_3$), supporting the hypothesis that increased Cofilin activity in *PDK1$^{-/-}$* MKs results in a decreased abundance of polymerized actin (Figure 42C, D). Cell polarity in neurons was previously associated with an interaction of PI3K signaling and atypical PKC (Chen et al., 2006), which are also potentially involved in MK polarization during thrombopoiesis (Dütting et al., 2017). We found that PDK1-deficiency in MKs resulted in a decreased phosphorylation of *atypical protein kinase C* (PKCζ) at the activation site Thr$_{410}$ (Figure 42C, D), which suggests its involvement in MK polarization.
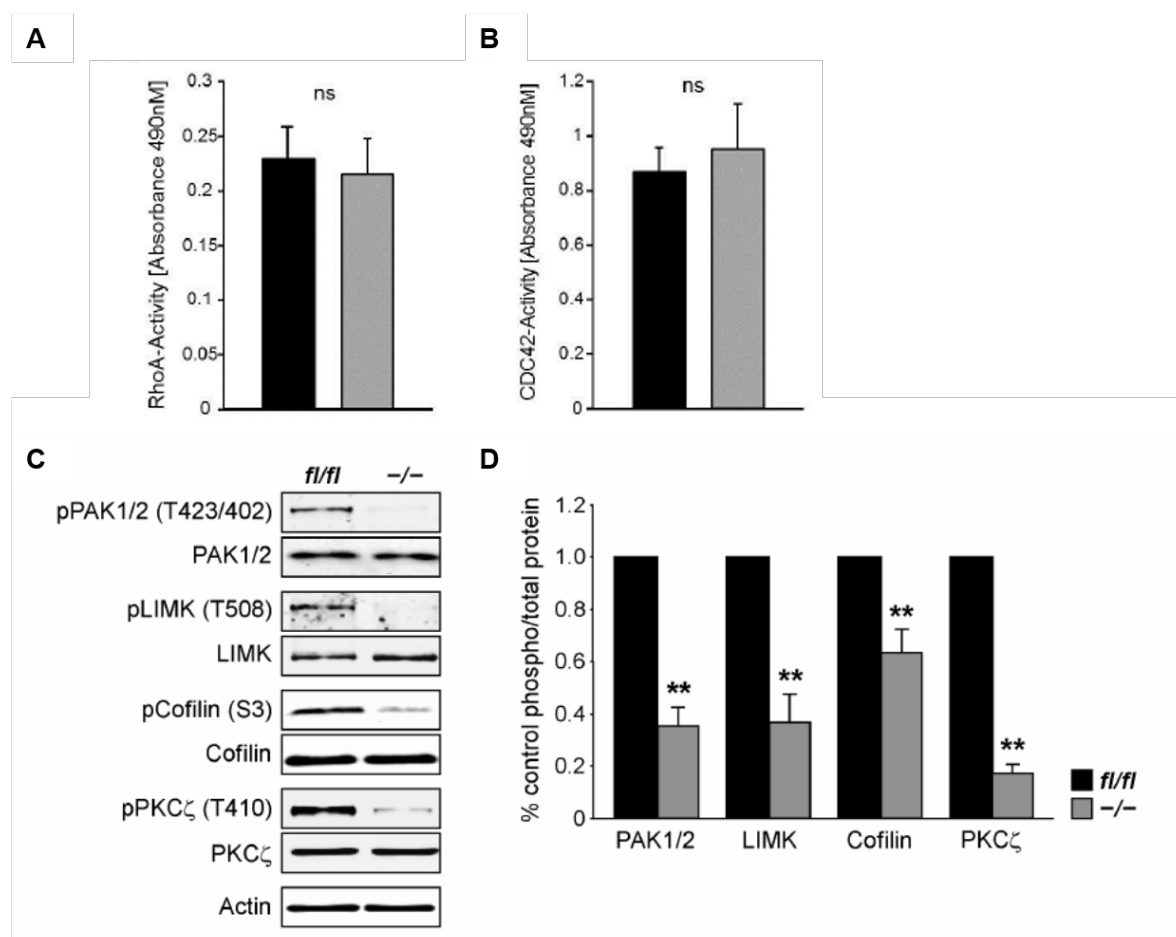
Figure 42 Investigation of potential signaling proteins involved in actin cytoskeletal organization. (A) Determination of RhoA activity in cultured *wt* and *PDK1$^{-/-}$* MKs (n=6). (B) Determination of Cdc42 activity in cultured *wt* and *PDK1$^{-/-}$* MKs (n=6). (C) Representative immunoblots of phosphorylation state of the actin regulatory proteins PAK1/2 at residue Thr$_{423/402}$, LIMK1 at residue Thr$_{508}$, Cofilin at residue Ser$_3$ and PKCζ at Thr$_{410}$ in cultured *wt* and *PDK1$^{-/-}$* MKs (n=5). (D) Densitometric analysis of blot densities

quantified as ratio of phosphorylated to total protein and calculated as percentage of control (n=5). Data were generated in the laboratory of Prof. Oliver Borst. Data are presented in mean±sem For statistical evaluation, a Wilcoxon-Mann-Whitney test was applied. ** p < 0.01 indicates statistically significant difference. Data modified after Geue and Aurbach et al., 2019.

3.3.3. Proplatelet formation in vitro and in vivo is partly regulated by PDK1

As macrothrombocytopenia can be caused by defective platelet biogenesis, we next investigated the capacity of *PDK1*$^{-/-}$ MKs to produce platelets in vitro and in vivo. Consistent with previous findings, PDK1-deficiency resulted in a slight defect in PPF of BM derived MKs in vitro within the observation period of 48 h (Figure 43A). Furthermore, visualization of the MK cytoskeleton in proplatelets revealed fewer proplatelet branches and increased size of swellings and tips (Figure 43B) again revealing an important role of PDK1 in cytoskeletal rearrangement, as branching and tip size are highly dependent on the F-actin and tubulin network (Italiano et al., 1999; Patel-Hett et al., 2008). Besides clear in vitro evidence for reduced PPF, we investigated in vivo PPF by 2P-IVM of the BM in the skull. In line with the in vitro results, PDK1-deficiency resulted in a reduced capacity of MKs to form proplatelets into vessel sinusoids in vivo (Figure 43C).
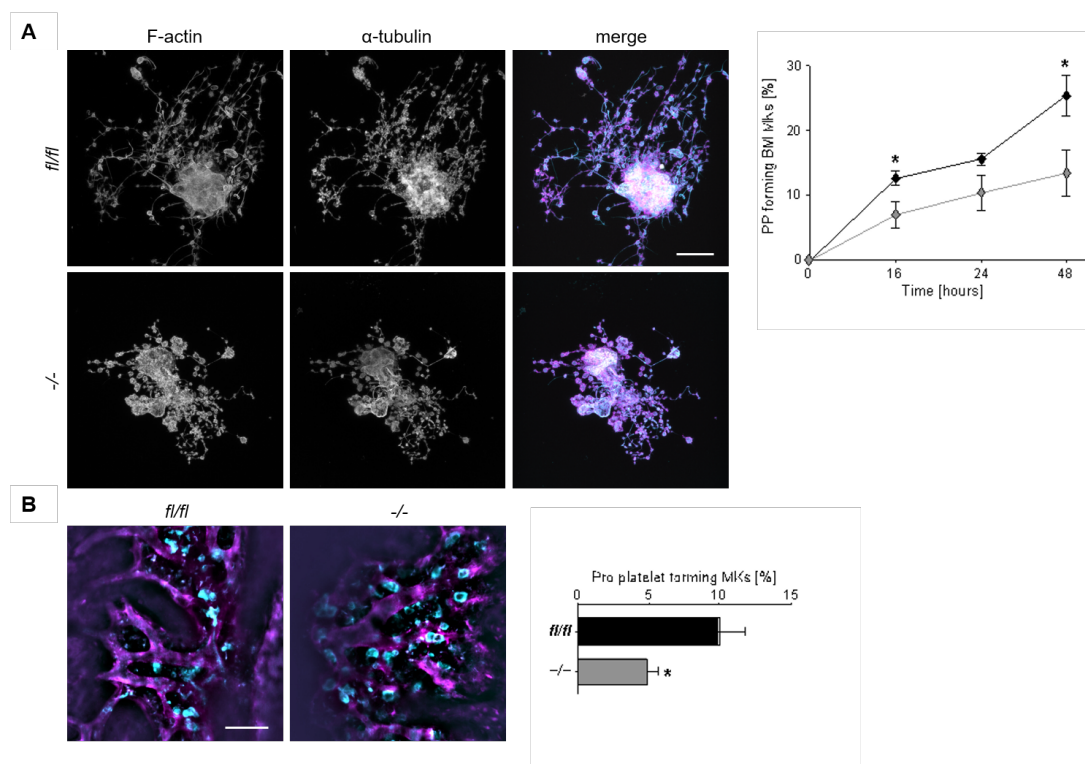
Figure 43 Impaired PPF of BM derived *PDK1*$^{-/-}$ MKs In vitro and in vivo. (A) Left: Representative confocal images of BM derived *wt* and *PDK1*$^{-/-}$ MKs that were cultured for three days in the presence of TPO and hirudin and then incubated for 48 h solely with hirudin to promote PPF. After 24 h, MKs were stained for F-actin and α-tubulin. Images were acquired using a Leica TCS SP8 confocal microscope. Scale bar equals 40 µm. Color code for merge: Magenta F-actin (phalloidin Atto-647), cyan α-tubulin (α-tubulin -A488), grey nuclei (DAPI). Right: Quantification of PPF during the time course of 48 h. Data are presented in mean±sd (n=3, at least 3-4 visual fields were analyzed per genotype). For statistical evaluation, a Wilcoxon-Mann-Whitney test was applied. (B) 2P-IVM indicates reduced PPF in vivo in *PDK1*$^{-/-}$ MKs. Left: Representative median projection of 30 µm z-stacks from *wt* and *PDK1*$^{-/-}$ murine BM.

MKs and platelets were stained with anti-GPIX antibody (green) and the vessel lumen was labeled using BSA-FITC and an Alexa488-labeled anti-CD105 antibody (red). Scale bar equals 100 µm. Right: Quantification of in vivo PPF. Data are presented in mean±sem (n=5-6, 4-10 z-stacks per mouse were analyzed). For statistical evaluation, a Welch´s test was applied. Data in (B) were kindly provided by Dr. David Stegner.* p < 0.05 indicates statistically significant difference. Data modified after Geue and Aurbach et al., 2019.

3.3.4. PDK1 guides release of platelet like particles in human CD34⁺ cell-derived MKs

To assess the reproducibility of our findings in the human system, we investigated how a partial downregulation of PDK1 in CD34⁺ cell-derived MKs affected the formation of platelet-like particles. The knockdown was mediated using a *PDK1* shRNA (shRNA-bearing pGIPZ lentiviral vector), while a non-silencing shRNA (sh_ctrl) was used as control. To assess the knockdown efficiency of the three target shRNAs, we performed a knockdown within K562 cells (Figure 44A) and chose the most efficient shRNA vector (sh3_PDK1) for the subsequent transduction of human CD34⁺ *hematopoietic stem and progenitor cells* (HSPCs) derived from two different donors in direct comparison. Even though we did not observe any alterations when the cytoskeleton of the *proplatelet-like particles* (PLPs) was analyzed (data not shown), the partial knockdown of *PDK1* negatively influenced the production of PLPs (Figure 44B), which was determined by flow cytometry. Additionally, we detected that *PDK1* depletion resulted in markedly more mature MKs after 14 days of liquid culture, depicted by an elevated CD41/ CD42b double positive cell fraction as assessed by flow cytometry (Figure 44C).
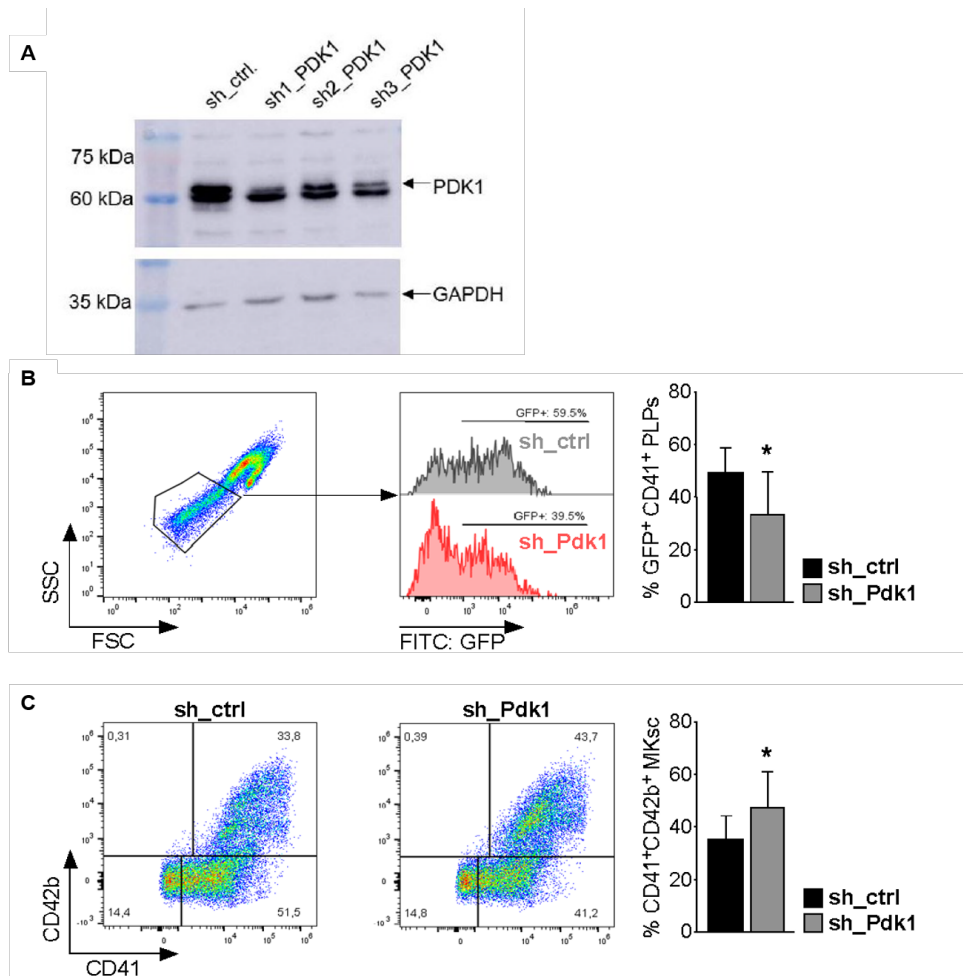
Figure 44 Downregulation of PDK1 in human CD34+ HSP cells. (A) Analysis of knockdown efficiency of the three target shRNA constructs (shRNA-bearing pGIPZ lentiviral vector) and a non-silencing shRNA control (sh_ctrl) in K562 cells by Western Blotting. (B) Left: Representative scatterplot of GFP+ CD41+ PLPs (gate adjusted on peripheral blood platelets) of day 14 in cultivation and respective histograms indicate the percentage of GFP+ PLPs. Right: Quantification of GFP+ CD41+ PLPs in the platelet gate assessed in three independent experiments with CD34+ cells from two different donors. (C) Left: Representative scatterplot of differentiation potency of CD34+ HSP cells of one donor using GPIb (CD41) and GP1bα (CD42b) as markers for mature MKs. Right: Quantification of mature CD41+/CD42b+ double positive MKs assessed in three independent experiments with CD34+ cells derived from two different donors. Data are presented in mean±sd (n=2). Data were kindly provided by Dr. Georgi Manukjan. For statistical evaluation, a Wilcoxon-Mann-Whitney test was applied. * $p < 0.05$ indicates statistically significant difference. Data modified after Geue and Aurbach et al., 2019.

These findings clearly demonstrate that PDK1 is not only an important regulator of PPF in mice, but also in humans, thus verifying how observations in the murine system can be reproduced in the human system and vice versa.

4. Discussion

4.1. Function of RhoB in platelets and MKs

4.1.1. RhoB and GPVI

As described previously, RhoB is dispensable for murine development, as *RhoB-/-* animals are viable, fertile and displayed a mendelian inheritance (Liu et al., 2001). Additionally, *RhoB-/-* mice exhibited a reduced thymus weight and cellularity accompanied by increased TGFβ1 signaling in the thymic medullary epithelium implicating a pivotal role for RhoB in thymic development by regulation of TGFβRII expression (Bravo-Nuevo et al., 2011). According to Zhao and colleagues, MK-derived TGFβ1 contributes to stem cell quiescence and increased TGFβ1 levels were shown to suppress hematopoietic cell differentiation (Zhao et al., 2014). The influence of RhoB on MK-derived TGFβ1 and consequently on MK maturation, however, still needs to be investigated. Moreover, *RhoB-/-* mice exhibit a retarded vascular development and vessel sprouting in the retina (Adini et al., 2003), a process which might be dependent on GPVI and partly CLEC-2, as the *retinopathy of prematurity* (ROP) outcome in mice is worsened by blockade or loss of these receptors in mice (Dr. Isabelle C. Becker, doctoral thesis 2020). Interestingly, *RhoB-/-* platelets displayed pronounced GPVI-dependent and mild CLEC-2-dependent activation defects in flow cytometric analysis and moderate GPVI-dependent aggregation defects in vitro. So far, there is no evidence directly linking RhoB to collagen-related signaling in any cell types. It is speculative whether loss of RhoB is directly causative for the activation defect in platelets.

Interestingly, RhoB activity was associated with Rac1 translocation and localization to endosomes in endothelial cells (Marcos-Ramiro et al., 2016). We therefore hypothesized that loss of RhoB influences Rac1 localization in platelets causing GPVI-related signaling defects, since Rac1 was postulated as a pivotal regulator of PLCγ2 activation, a downstream effector of GPVI (McCarty et al., 2005; Pleines et al., 2009). Unfortunately, neither RhoB activity nor RhoB (or Rac1) localization studies were performed in platelets or MKs in this study due to insufficient antibody availability. In addition, we neither detected altered levels of Rac1, PLCγ2, Syk or LAT in *RhoB-/-* platelets nor did we observe defective lamellipodia formation as seen in *Rac1-/-* platelets (McCharty et al., 2005). Moreover, Vega and colleagues showed that downregulation of RhoB led to spreading defects similar to Rac1 depletion and affected surface expression of β1 integrins in prostate cancer cells (Vega et al., 2012), a finding that could not be recapitulated in *RhoB-/-* platelets. For further evaluation, Rho activity within in platelets and MKs needs to be investigated by *fluorescence resonance energy transfer* (FRET) experiments, as the regulation of Rho GTPases by GAPs and GEFs and the spatial-temporal distribution of the kinase ROCK

markedly affects Rho signaling in diverse cell types (Bidaud-Meynard et al., 2019; Truebestein et al., 2016).

RhoB and the small GTPase *ADP-ribosylation factor 6* (Arf6), a downstream target of GPVI in platelets, were shown to form a complex. Arf6 not only increases RhoB protein stability but further induces localization of RhoB to the plasma membrane and to endosomes. This interaction could help unraveling the observed GPVI signaling defect in *RhoB$^{-/-}$* platelets, Arf6 expression was not examined in the course of this thesis, though. Depletion of Arf6 results in the degradation of RhoB, defective actin adhesion dynamics and increased cancer cell migration (Zaoui et al., 2019). Notably, RhoB has mostly been associated with the actin cytoskeleton in diverse cell types and is a main regulator of stress fiber formation (Gottesbühren et al., 2013; Sabatel et al., 2011) and cell migration (Reymond et al., 2012; Vega et al., 2012). Nevertheless, the actin cytoskeleton of *RhoB$^{-/-}$* MKs and platelets appeared rather unaltered, as F-actin content and assembly in platelets as well as phalloidin-Atto647 MFI in MKs were comparable to *wt* conditions. In summary, this thesis demonstrated the involvement of RhoB either directly or (more likely) indirectly in GPVI integrin signaling in platelets. Further experiments concerning the interaction of Rac1, Arf6 and GPVI signaling proteins with RhoB will promote the understanding of the underlying mechanism.

4.1.2. RhoB and microtubule organization

In this study, we show for the first time that RhoB is involved in MT cytoskeletal dynamics and stability. In platelets, RhoB deficiency resulted in disturbed MT organization, hindered MT reassembly after cold-induced disassembly and decreased levels of acetylated α-tubulin at Lys$_{40}$, but unaltered actin organization and distribution. Notably, it was previously demonstrated that α-tubulin is heavily acetylated in platelets and contributes to the kinetics of platelet spreading (Patel-Hett et al., 2008; Sadoul et al., 2012). Furthermore, acetylation levels of Lys$_{40}$ of α-tubulin are associated with an increased tubulin longevity (Song and Brady, 2015; Wloga et al., 2017) suggesting that decreased acetylation levels might correspond to short-lived MT that are either more unstable or constantly remodeled. This gives us a hint for our findings in spread platelets, as RhoB deficiency resulted in disturbed α-tubulin distribution compared to *wt* platelets, which might be caused by increased filament turnover. Additionally, *RhoB$^{-/-}$* platelets were not able to rebuild MT coils after disassembly, which suggests that these MT coils are more prone to stress and may be why the MT coil depolymerized more quickly.

Tubulin filaments are deacetylated by deacetylases with *Histone deacetylase 6* (HDAC6) as the most prominent one in platelets. Overexpression of HDAC6 resulted in MT deacetylation, while its inhibition induced MT hyperacetylation (Esteves et al., 2019; Sadoul et al., 2012). Recently, Massoudi and colleagues showed that HDAC6 had no influence on murine MKs, while human HDAC6 interacted with Cortactin and not on tubulin (Messaoudi et al., 2017). Interestingly, HDAC1 and HDAC6 are closely linked to suppression of RhoB and inhibition of HDAC with

Farnesyltransferase and *Geranylgeranyl transferase inhibitors* (FTIs and GGTIs) induced RhoB transcription mediated by p300, a histone acetyltransferase (Ahn et al., 2011; Delarue et al., 2007). As p300 together with *NAD-dependent deacetylase sirtuin-2* (SIRT2) were closely associated with α-tubulin acetylation in Parkinson's and Alzheimer's disease (Esteves et al., 2019), this might draw a link to the observed MT phenotype in *RhoB$^{-/-}$* platelets and MKs. Loss of RhoB might indirectly influence the activity of its regulator p300 and lead to altered PTM of α-tubulin.

Considering possible signaling pathways that link RhoB to MT dynamics, the formin mDia and RhoB were shown to interact in endosomes by control of actin dynamics that were necessary for vesicle trafficking (Wallar et al., 2007). Moreover, mice deficient for mDia and RhoB had abnormally shaped erythrocytes, splenomegaly, and extramedullary hematopoiesis (not present in the single KOs), which implies a role for RhoB and mDia in the regulation of *hematopoietic progenitor cells* (HPCs) (DeWard et al., 2009). Recently, Green and colleagues observed that treatment of human and murine platelets with the *Formin homolog 2* (FH2) domain inhibitor SMIFH2 resulted not only in the disruption of platelet actin dynamics but also in MT organization and dynamics (Green et al., 2020). It was presented that MT networks failed to form while platelet spreading, resting platelets were reduced in size and α-tubulin was less acetylated when FH2 domains were inhibited. These results resemble the MT phenotype in *RhoB$^{-/-}$* platelets. As mDia is a downstream effector of small Rho GTPases and induces actomyosin contractility by NMIIa activation, we investigated NMIIa and NMIIb expression in murine platelets and MKs. Neither did we detect altered levels of mDia nor of NMIIa and NMIIb in *RhoB$^{-/-}$* platelets. Of note, the active phosphorylated forms of these proteins were not investigated thus allowing the possibility that loss of RhoB influenced the activation status.

Loss of the MT plus end tracking protein APC in mice also led to decreased α-tubulin acetylation at Lys$_{40}$ (Strassel et al., 2018). As *RhoB$^{-/-}$* MKs had normal protein levels of APC we ruled an influence of this protein on MT dynamics out under KO conditions. Additional target proteins linking RhoB to the MT cytoskeleton could be *Twinfilin 1* (Twf1) and Cofilin1, which were recently shown as modulators of the actin/tubulin crosstalk during platelet biogenesis (Becker et al., 2020).

Together, these results show, that RhoB is involved in MT turnover, which in turn may be causative for the observed microthrombocytopenia in *RhoB$^{-/-}$* animals. These results could highly benefit from additional studies on PTM of α-tubulin and the mediators of acetylation/ deacetylation in murine platelets.

4.1.3. Microthrombocytopenia in RhoB-deficient mice

Microthrombocytopenia is a rare clinical incidence and a common feature of diseases such as the *Wiskott-Aldrich Syndrome* (WAS), a rare X-linked recessive disease caused by mutations in the *WAS* gene (Massaad et al., 2013) or CARST, a congenital auto-recessive disease caused

by mutations in *ADAP* (Hamamy et al., 2014; Levin et al., 2015), which are both associated with mutations in genes involving F-actin cytoskeletal dynamics. Microthrombocytopenia is often accompanied by an increased risk of intracranial, gastrointestinal, or oral bleeding. Similarly, in mice the loss of F-actin regulatory proteins such as Arp2, WASP, ADAP, and *Profilin1* (Pfn1) are associated with microthrombocytopenia together with a premature ectopic platelet release into the BM (Bender et al., 2014; Paul et al., 2017; Sabri et al., 2006; Spindler et al., 2018). Here, we show for the first time that loss of the small Rho GTPase RhoB results in micro-thrombocytopenia, which is not concomitant with ectopic platelet release into the BM hematopoietic department. In contrast to platelets and MKs lacking ADAP, Arp2 or WASP, which display pronounced defects in F-actin dynamics and aberrant podosome formation, *RhoB⁻/⁻* platelets and MKs presented with normal F-actin organization in vitro. As described in this thesis, *RhoB⁻/⁻* platelets display a severe MT assembly defect as confirmed by an inability to rearrange tubulin coils after cold-induced disassembly, altered α-tubulin distribution in spread platelets, and decreased MT stability observed by altered PTM in α-tubulin. Similar results of aberrant tubulin rings in resting platelets in IF and TEM were also previously obtained when Arp2-deficient platelets were analyzed (Paul et al., 2017). Moreover, platelets lacking the small actin monomer-binding protein Pfn1 were identified to exhibit increased number of tubulin coils in the marginal band accompanied by aberrantly twisted and bend MTs (Stritt et al., 2018). However, Arp2 as well as Pfn1 localization were not affected in *RhoB⁻/⁻* platelets and MKs. These results implicate that the microthrombocytopenia in *RhoB⁻/⁻* animals is independent of F-actin phenotypes and rather dependent on alterations in the MT cytoskeleton. Since MTs are pivotal for later stages of PPF, we thus speculate that *RhoB⁻/⁻* MKs are not able to release normally sized proplatelets into the bloodstream resulting in both, smaller and bigger MK fragments as observed in vitro by proplatelet tip size measurements. This hypothesis needs to be further investigated by advanced microscopy techniques as three dimensional microscopy approaches seen in Eckly et al., 2020.

Notably, we only solely observed a significant microthrombocytopenia *RhoB⁻/⁻* animals when diluted blood samples were examined using a flow cytometer (Figure 9). Platelets in undiluted whole blood samples of *RhoB⁻/⁻* animals measured in a blood analyzer were only moderately smaller than *wt* platelets (Figure 26). These results are in agreement with the results of Aurbach and Spindler et al., 2019.

In summary, our results indicate different origins of microthrombo-cytopenia in *RhoB⁻/⁻* animals as in Arp2, WASP, ADAP, and Pfn1-deficient mice due to a more prominent involvement in rearrangements of the tubulin cytoskeleton during platelet biogenesis.

4.2. The role of RhoB in MK transmigration

RhoA and RhoB belong to the family of small Rho GTPases and share an amino acid sequence homology of 87% (Wheeler and Ridley, 2004). While *RhoB⁻/⁻* MKs and platelets exhibit unaltered

levels of RhoA protein, loss of RhoA resulted in an upregulation of RhoB on protein level. The negative regulation of RhoA by RhoB and vice versa has already been shown in various cell types: Silencing of RhoB by siRNA in *human umbilical vein endothelial cells* (HUVEC) resulted in increased RhoA activity regulating cell viability and migration (Howe and Addison, 2012), loss of RhoA in keratinocytes emanates in an upregulation of RhoB and decreased directed cell migration (Jackson et al., 2011), and RhoA-depleted macrophages displayed an increase of RhoB protein and concomitant impaired tail retraction, but unaltered macrophage migration (Königs et al., 2014). These results suggest that RhoA and RhoB might have compensatory roles and reciprocally regulate one another. In vitro experiments demonstrated that silencing of RhoA induced upregulation of total and active RhoB and that RhoB protein stability was dependent not on the active, but on the GDP-bound form of RhoA and required *Rho GDP-dissociation inhibitor 1 alpha* (RhoGDIα) (Ho et al., 2008). To date, the importance of Rho GAPs and GEFs in platelet and MK biology is increasingly recognized and they were shown to be critical regulators of platelet aggregation, thrombus formation, α-granule release and αIIbβ3 integrin activation in response to thrombin and TxA$_2$ (Beck et al., 2014; Elvers et al., 2012; Lu et al., 2017; Ngo et al., 2017; Williams et al., 2015). Nevertheless, the regulatory network and interactions between small Rho GTPases, GAPs and GEFs are still barely understood and need to be investigated in more detail.

Following up on the question whether RhoA and RhoB withhold similar functions in platelets and MKs, we performed aggregation studies using the TxA$_2$ analog U46619. Strikingly, *RhoB$^{-/-}$* platelets performed shape change and displayed unaltered aggregation after stimulation with low doses of U46619, whereas *RhoA$^{-/-}$* platelets were unable to change their shape under these conditions. Together with the more prominent actin phenotype observed in platelets and MKs and the macrothrombocytopenia of *RhoA$^{-/-}$* animals, these results pinpoint to different roles for RhoA and RhoB in these cells. To further elucidate the compensatory or non-compensatory roles of these two proteins, we generated RhoB/RhoA *DKO* animals. These mice exhibited an even more pronounced macrothrombocytopenia than RhoA-deficient animals and had immense defects in PPF and DMS development. Most notably, double-deficiency for RhoA and RhoB reverted the intrasinusoidal location of *RhoA$^{-/-}$* MKs described by Dütting and colleagues (Dütting et al., 2017) and led to a clustering of MKs around the vessels. Dütting and colleagues also proposed that MK localization in the BM is driven by a regulatory feedback loop of RhoA and Cdc42, as the respective DKO also presented with heavy MK clusters around the sinusoids. They suggested STOP (RhoA) and GO (Cdc42) mechanisms guiding the MKs towards the vessel (Dütting et al., 2017). This mechanism is highly dependent on the genetic background, as *RhoA$^{-/-}$* animals with mixed SV129/C57BL/6J background showed higher numbers of intrasinusoidal MKs compared to *RhoA$^{-/-}$* mice with a pure C57BL/6J background, thus highlighting the relevance of genetic backgrounds and the importance of matching *wt* controls (Dr. Tobias Heib, doctoral thesis 2020).

Recent publications questioned the efficiency of the *Pf4-Cre* KO mouse model (Nagy et al., 2019), as endogenous Pf4 is not exclusively expressed in MKs and platelets, but is also found in a variety of immune cells (Eberlein et al., 2010; Kioon et al., 2018; Lasagni et al., 2007; Schaffner, 2005; Shi et al., 2014b) and outside the hematopoietic lineage in intestinal epithelial cells (Lapchak et al., 2012). Intriguingly, BM transplantation experiments using *wt* and *RhoA⁻/⁻* animals accentuated that the phenotypes observed in *RhoA⁻/⁻* animals are not influenced by *Pf4-Cre*-mediated off-target effects (Dr. Tobias Heib, doctoral thesis 2020). To elucidate the impact of RhoB protein levels on MK transmigration, we generated mice deficient for RhoA and with a heterozygous deficiency for RhoB, referred as *RhoA⁻/⁻/RhoB⁺/⁻* animals. In theory, these animals should carry half of the protein levels of *wt* animals, however, *RhoA⁻/⁻/RhoB⁺/⁻* MKs displayed around 30% reduction in total RhoB levels compared to control MK lysates. In general, phenotype severity in these animals ranged between *RhoA⁻/⁻* and *DKO* mice meaning that e.g. the macrothrombocytopenia was not as severe as in *DKO* animals but more pronounced than in *RhoA⁻/⁻* mice. Similar results were shown when DMS development and MK localization were analyzed. MKs with 30% reduced RhoB levels and concomitant loss of RhoA (*RhoA⁻/⁻/RhoB⁺/⁻*)were still able to transmigrate into the vessel lumen and to stay attached to the endothelium best observed by TEM pictures, but to a lesser extent than *RhoA⁻/⁻* MKs. This highlights the potential direct importance of RhoB in the process of transendothelial MK migration. To follow up on this hypothesis, we generated MK- and platelet-specific RhoB knock-in animals (*RhoBᵏⁱⁿ*) that present with increased RhoB levels, while RhoA is expressed normally. This project is ongoing and needs to carefully investigate Rho activity. Especially RhoB-GTP antibodies or FRET experiments are crucial to rule out the activity status of upregulated RhoB in the *RhoBᵏⁱⁿ* animals.

In the meantime, various hypotheses remain to explain the observed transmigration and its reversion:

1. Alteration of adhesion receptors

Around 1 – 2% of *wt* MKs are found in the vessel lumen. It is possible that MKs per se are able to transmigrate in a podosome-dependent manner, as they are able to protrude bigger fragments into the vessel lumen (Eckly et al., 2020). Additionally, under physiological conditions, the lung was described as a site of platelet biogenesis as MKs migrate from the BM into the bloodstream and circulate through the lungs releasing platelets (Lefrançais et al., 2017).

Under physiological conditions MKs may subsequently be flushed away by the bloodstream but *RhoA⁻/⁻* MKs might be capable to stick to the endothelium through an upregulation of adhesion receptors. Dr. Tobias Heib already ruled out integrin β1 and G6b-B as mediators of MK transmigration, as concomitant deletion of *RhoA* and *Itgb1*, or *RhoA* and *Mpig6b* did not interfere with the intrasinusoidal translocation of *RhoA* single KOs (Dr. Tobias Heib, doctoral thesis 2020). However, *RhoA⁻/⁻* MKs showed increased spreading capacity on fibrinogen

associated with increased GPVI and αIIbβ3 levels on the platelet surface (Lou M. Wackerbarth, master thesis 2020). These receptors are pivotal for platelet and MK activation and regulate adhesion to the ECM components collagen and fibrinogen. An upregulation of the receptors might lead to increased adhesion of platelets and MKs to the vessel wall, which explains why *RhoA⁻ᐟ⁻* MKs are increasingly found adherent to the vessel walls. Nevertheless, according to this theory, these animals should display higher proportions of platelets stuck to the sinusoidal endothelium, which would eventually affect thrombus formation. The reduced thrombus formation and protection against ischemic stroke observed in *RhoA⁻ᐟ⁻* animals in vivo, however, contradicts this hypothesis (Pleines et al., 2012).

Double deficiency of RhoA and RhoB may revert the MK stickiness and MKs are either not able to migrate into the bloodstream and rather cluster around the vessel or migrate into the vessel and are immediately flushed away. Thus, according to the second hypothesis, the lungs of RhoA/B double-deficient animals should contain an increased number of MKs. These findings are highly discussed in the literature as *wt* MKs are barely observed to migrate into the vessel lumen and the current view is that MK maturation and PPF mainly takes place in the BM, while the lung microvasculature serves as a vascular bed for final platelet maturation (Gorelashvili et al., 2020; Stegner et al., 2017). With this notion in mind, the analysis of *DKO* lungs would be of great interest. Initial experiments couldn't show MKs in the lungs of *DKO* animals, though (data not shown).

2. Involvement of Metalloproteinases

Metalloproteinases (MMPs) are pivotal mediators of matrix degradation and divided into collagenases (MMP1, 8, 13 and 18), and gelatinases (MMP2 and 9). So far, transcripts for MMP1, 11, 14, 15, 17, 19, 24 and 25 were identified by RNAseq screen in primary human MKs (Cecchetti et al., 2011). Already 20 years ago it was shown, that MMP-9 induction by *stromal derived factor 1* (SDF-1) modulates MK migration towards the BM sinusoids and subsequent platelet release (Lane et al., 2000). Interestingly,FLC derived MKs incubated with prostate cancer cell releasates upregulated MMP2 and MMP3, which are both stored in α-granules (Roweth et al., 2019). A prostate cancer study hypothesized a connection of upregulated RhoB protein levels with an increase of MMP1 transcripts and increased cell motility (Yoneda et al., 2010). This points to an interesting role of MMPs in MK migration, and should be carefully evaluated in *RhoA⁻ᐟ⁻* animals. The upregulation of RhoB in *RhoA⁻ᐟ⁻* MK could induce the upregulation of MMPs and hereby promote MK migration into the blood vessels.

3. Biomechanical parameters

Previous studies indicate that the cytoskeleton has a major impact on cellular biomechanical parameters such as cellular flexibility or stiffness (Scheller et al., 2020). These biomechanical/ biophysical properties of MKs are highly relevant and could be partly an explanation for MK transmigration: Due to reduced MLC levels, *RhoA⁻ᐟ⁻* MKs might be more flexible and may

therefore be able to squeeze completely through the BM endothelium. Previous studies showed already that MKs are able to progress large fragments through the sinusoidal endothelium, thus it is possible that whole intact MKs can transmigrate in a podosome-dependent manner and without influence of MT bundles (Brown et al., 2018; Eckly et al., 2020). These MKs could then attach to the endothelium and are not flushed away due to their flexible biomechanical properties. Double deficiency of RhoA and RhoB may thus result stiffer MKs that cluster around the vessel and display massively disturbed DMS structures. Measurements of MK biomechanical properties together with the collaboration partners at the University of Greifswald (TR240 ´Platelets´; Palankar/Otto/Bender) are indispensable for answering this question.

4. MK emperipolesis

Emperipolesis is a process of interaction between MKs and other hematopoietic lineages. Already 50 years ago, the ingestion of other hematopoietic cells by MKs was observed, with neutrophils being to most prominent ones (Larsen, 1970). Emperipolesis is present in the healthy BM but increases in disease-states such as myelofibrosis (Spangrude et al., 2016), gray platelet syndrome (Di Buduo et al., 2016; Larocca et al., 2015) or hemorrhagic shock (Dziecioł et al., 1995; Sahebekhtiari and Tavassoli, 1976). Nevertheless, the significance and the mechanism of emperipolesis remains unknown. MKs are able to sense inflammation through *toll-like receptors* (TLRs) (Andonegui et al., 2005; Beaulieu et al., 2011; D'Atri et al., 2015) and were shown to interact with several subsets of immune cells (Cunin et al., 2017). A recent study by Cunin and colleagues stated that neutrophils enter MKs in membrane-bound vesicles through β2-integrin – ICAM-1 interactions and subsequently develop membrane continuity with the DMS in an actin-dependent manner (Figure 45). Hereby neutrophils transfer membrane and proteins to MKs and vice versa, upon which intact neutrophils are able to obtrude (Cunin et al., 2019).
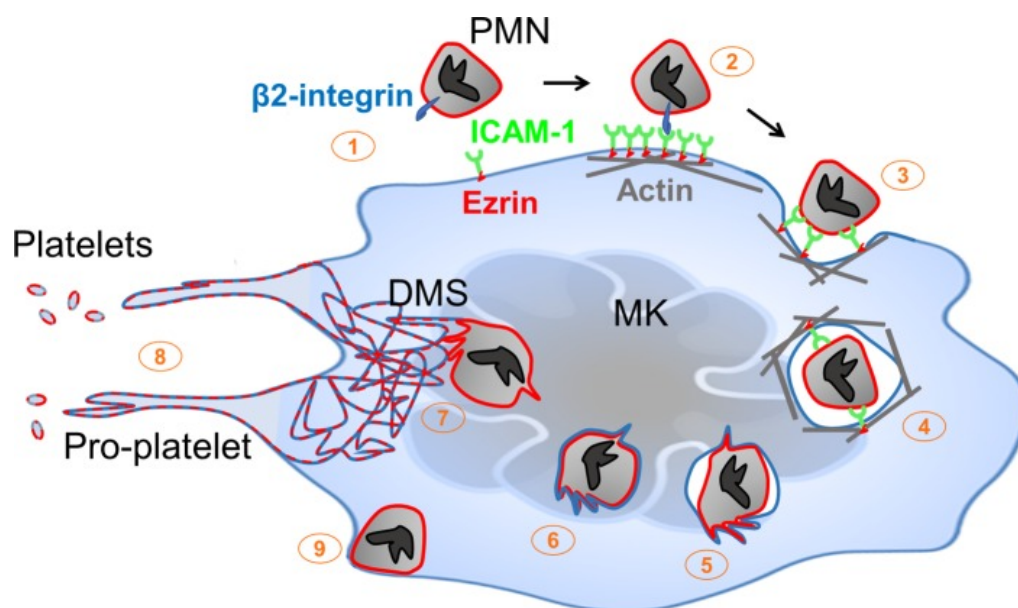
Figure 45 The process of emperipolesis. (1) – (3): MK-neutrophil interaction, involvement of β2-integrin and ICAM-1, Ezrin and the actin cytoskeleton. (4) – (7) Neutrophil entry through emperisome and final entry of neutrophil into the MK DMS. (8) – (9) Production of platelets with neutrophil membrane and release of intact neutrophil. Modified after Cunin et al., 2019.

Intriguingly, *RhoA*$^{-/-}$ MKs display an increase in emperipolesis, which was observed by TEM (Pleines et al., 2012). Similar results were observed in *DKO*, but not *RhoB*$^{-/-}$ MKs. Increased emperipolesis could lead to a higher portion of MKs that obtain neutrophilic membrane and protein, which might enable them to transmigrate into the sinusoidal lumen in a diapedesis-like manner through neutrophilic receptors on their surface. As *wt* MKs already perform emperipolesis and transmigrate to a small proportion this could mean that only MKs that previously underwent emperipolesis are able to transmigrate. This assumption is however contradicted by G6b-B and RhoA/RhoB *DKO* MKs, which undergo emperipolesis, but do not transmigrate.

Nevertheless, the process of emperipolesis needs to be studied more closely to answer the following questions: Which proteins are transferred to the MKs? What does this transfer change within the MK signaling? Do transmigrated MKs contain neutrophilic membrane and/or proteins?

5. Endothelial barrier function

Rho GTPases are described as regulators of endothelial cell barrier function. Endothelial cell-cell contacts are linked by tight junctions and adherens junctions. Adherens junctions are formed by the adhesion molecule *vascular endothelial cadherin* (VE-cadherin), which clusters at endothelial cell-cell contacts. Through differential signaling from VE-cadherin to the actin cytoskeleton, endothelial integrity is granted (Taha et al., 2014). Pronk and colleagues recently identified RhoB as a negative regulator of human endothelial cell permeability in resting endothelium (Pronk et al., 2019). RhoB knockdown resulted in an increased barrier resistance by augmentation of VE-cadherin cell-cell interactions. Following up on this, increased RhoB

activity in MKs might influence endothelial barrier function. If Pronk and colleagues results were transferred into our *RhoA^-/-* mouse model, increased RhoB expression would have led to decreased MK transmigration. As this is not the case, either endothelial barrier function has no influence on MK transmigration, or RhoB has the opposite function in murine endothelial cells.

In summary, the potential mechanism behind MK transmigration is barely understood. Further studies in vitro and in vivo will hopefully give insights into the exact role of Rho GTPases in driving MK translocation. Especially advanced in vivo imaging techniques will be of great help for a deeper understanding. Of note, a combination of the above mentioned mechanisms is conceivable and should be considered.

4.3. Pivotal role of PDK1 in megakaryocyte cytoskeletal dynamics

Mild to severe bleeding episodes are often accompanied by thrombocytopenia, which can be caused by either a reduced platelet life span due to accelerated platelet clearance or by defective platelet biogenesis (Eckly et al., 2010; Spindler et al., 2018; Stritt et al., 2017). The mechanisms underlying these processes are poorly understood and need to be further defined. In this thesis, we identified PDK1 and PDK1-dependent signaling as important key components for platelet production under physiological conditions. As displayed in Figure 46, loss of PDK1, which is accompanied by a reduction in the PAK/LIMK/Cofilin/PKC isoform ζ (PKCζ), phosphorylation, results in increased MK ploidy, defective DMS development and polarization, and impaired PPF. These effects are due to the prominent role of PDK1 in F-actin cytoskeletal dynamics that influence MK maturation, podosome formation, and DMS polarization. Furthermore, PDK1 was identified as a regulator of human megakaryopoiesis and thrombopoiesis, as downregulation of PDK1 by shRNA in CD34^{+} HSCs resulted in a higher number of mature MKs but a reduced production of PLPs in vitro.
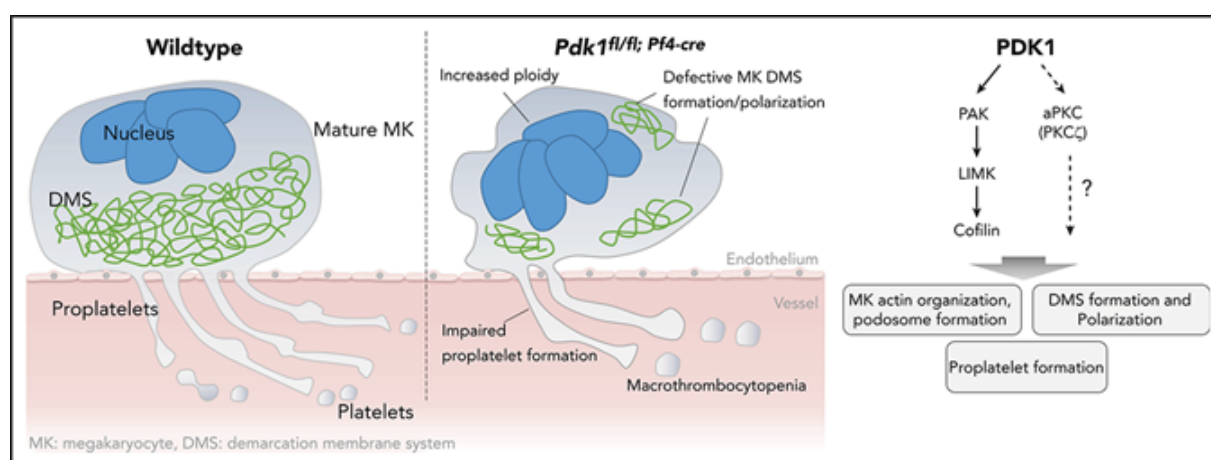

Figure 46 Role of PDK1 in MK maturation, polarization and PPF. Left panel: Under *wt* conditions, mature MKs form proplatelets into the BM blood vessels and platelets are released into the bloodstream.

Middle panel: Due to the loss of PDK1 specifically in the MK lineage, MKs display maturation defects and an impaired proplatelet release into the bloodstream. Right panel: PDK1 downstream signaling under physiological conditions that influence PPF. After Geue and Aurbach et al., 2019.

Thrombocytopenia and bleeding episodes are a well-known side effect of cancer-treatment in many patients. Interestingly, PDK1 inhibitors are widely considered for the long-term therapeutic use for cancer and leukemia treatment (Raimondi and Falasca, 2011; Weisberg et al., 2008) due to the pivotal role of PDK1 in malignant tumors (Maurer et al., 2009) and acute myeloid leukemia (Zabkiewicz et al., 2014), where it was shown to drive tumor invasion and metastasis (Du et al., 2016). Thus, our findings have important implications for potential patients treated with PDK1 inhibitors that are likely affecting MK maturation and subsequently platelet counts.

In mice, genetic deletion of *PDK1* in the MK lineage under the *Pf4* promotor results in an altered MK ultrastructure albeit increased ploidy in vivo and in vitro. PDK1 was described as a key player in Akt-dependent signaling, which influences cell growth, proliferation, and survival. In human platelets, inhibition of PDK1 by BX795 resulted in abolished Thr_{308} phosphorylation on Akt, which in turn resulted in reduced clot retraction and inhibition of 2−methylthio−ADP (2-MeSADP)-induced aggregation (Dangelmaier et al., 2013). Manne and colleagues reproduced these results using human and murine platelets, thus demonstrating that treatment with BX795 abrogated TxA_2 generation. Loss of PDK1 in mice led to similar results highlighting the importance of the PDK1-Akt signaling axis for platelet function (Manne et al., 2018). Furthermore, PDK1 together with BAD was implicated as an important regulator of MK apoptosis during PPF (Machlus et al., 2016). Nonetheless, genetic deletion of *PDK1* in murine MKs had neither influence on expression or phosphorylation of Akt, nor on apoptosis in MKs suggesting that PDK1 is dispensable for Akt signaling and apoptosis in MKs (Geue and Aurbach et al., 2019). $PDK1^{-/-}$ platelets did not exhibit enhanced apoptosis (Chen et al., 2013) and platelet life span as well as recovery after platelet depletion in vivo were only mildly affected upon *PDK1* deletion. Anyhow, these results are not sufficient to explain the pronounced thrombocytopenia observed in $PDK1^{-/-}$ mice. As stated previously, thrombocytopenia can be the result of defective MK maturation and PPF. During the final steps of platelet release, MKs undergo various cytoskeletal alterations of both the actin and the MT cytoskeleton that are pivotal for the MK fate, eventually leading to the release of platelets into the bloodstream. Loss of PDK1 had no influence on the MT cytoskeleton during MK spreading on collagen in vitro, whereas F-actin was aberrantly distributed within the MKs.

Of note, the MT cytoskeleton is implicated in later steps of platelet biogenesis, namely proplatelet elongation and platelet release into the bloodstream (Bender et al., 2015; Patel-Hett et al., 2008; Patel et al., 2005; Thon et al., 2010). In the present study, we investigated PPF in vitro and in vivo and found PPF to be reduced under both experimental settings indicating at least an influence of PDK1 on the tubulin organization in MKs. This needs to be further assessed by measurement of proplatelet tip number and size in vitro, in-depth analysis of in vitro PPF and

staining of tubulin PTM (acetylation and detyrosination) and isoforms (tubulin α2 and tubulin β1).

The actin cytoskeleton is essential for DMS formation and concomitant MK polarization during MK maturation, proplatelet formation and branching as well as transendothelial pore formation (Antkowiak et al., 2016; Dütting et al., 2017; Eckly et al., 2020; Schulze et al., 2006). In line with previous findings showing that F-actin organization is crucial for DMS formation (Antkowiak et al., 2016; Dütting et al., 2017), we found that defective F-actin organization results in a disrupted DMS structure in $PDK1^{-/-}$ MKs. Proper DMS development together with functional F-actin dynamics are pivotal for MK polarization during platelet biogenesis and hereby caused aberrant polarization in $PDK1^{-/-}$ MKs in vitro. Notably, the actual impact of MK polarization on in vivo MK maturation and directed PPF remains elusive, as this model still lacks in vivo evidence. Nevertheless, the classification of polarized MKs in maturation stages as shown in Antkowiak et al. or Spindler et al., might be of relevance but needs to be further verified by site directed PPF experiments with e.g. ECM proteins.

Loss of PDK1 resulted in reduced MK spreading on collagen (but not fibrinogen) and fewer podosomes in line with decreased WASP and Arp2 expression. The podosome density, defined as podosome number per MK area, however, was not altered. Podosomes are described to penetrate the endothelial barrier through pore formation in endothelial cells enabling an MK passage into the blood circulation during later stages of platelet biogenesis (Eckly et al., 2020; Schachtner et al., 2013; Thomas et al., 2017). We speculate, that the F-actin cytoskeleton impacts the thrombocytopenia in $PDK1^{-/-}$ mice due to impaired transendothelial platelet formation. Similarly, Dütting and colleagues recently showed that the small GTPases RhoA and Cdc42 act in a regulatory circuit and hereby regulate MK localization and polarization (Dütting et al., 2017). Loss of each protein results in a thrombocytopenia, moderately altered platelet life span, but defective PPF (Pleines et al., 2010, 2012). These findings are comparable to the here presented phenotype in $PDK1^{-/-}$ mice, however, the activity of the GTPases Cdc42 and RhoA was not altered in $PDK1^{-/-}$ MKs. This leads to the assumption that PDK1 might either act downstream of small Rho GTPases or independently of these signaling pathways. PAK is an important downstream effector of Cdc42, is activated by PDK1 (King et al., 2000) and deficiency of PAK2 in MKs results in impaired actin cytoskeleton dynamics and maldeveloped DMS (Kosoff et al., 2015). In line with these results, $PDK1^{-/-}$ MKs were not able to activate PAK1/2 by phosphorylation at $Thr_{423/402}$ and subsequently reduced phosphorylation of the PAK downstream effectors LIMK and Cofilin. Phosphorylated Cofilin at Ser_3 is an indicator for Cofilin inactivation. Consequently, decreased Cofilin phosphorylation promotes F-actin severing and depolymerization leading to a slower rate of F-actin recovery and F-actin distribution through the cells, which is seen in PDK1-deficient MKs. Interestingly, little is published about the role of LIMK in MKs. Kauskot and colleagues showed that an upregulation of the LIMK/Cofilin pathway in a murine knockin model for von Willebrand disease (VWD)-type 2B resulted in macrothrombocytopenia and MKs with disorganized F-actin. A concomitant inhibition of this LIMK/Cofilin pathway then restored normal platelet

counts and actin turnover. These results stand in contrast to our findings, in which the inactivation of LIMK and activation of Cofilin is associated with thrombocytopenia and aberrant actin distribution. Another direct substrate for phosphorylation by PDK1 is the atypical PKCζ (Le Good et al., 1998). Reduced levels of PKCζ in *PDK1⁻/⁻* MKs are in line with previous findings and implicate that PKCζ might be involved in MK polarity, as PKCs are involved in epithelial cell polarization (Mashukova et al., 2012; Whyte et al., 2010).

This thesis demonstrated that PDK1 is an essential regulator of the F-actin cytoskeleton in murine MKs. Together with previous publications concerning PDK1 in platelets (Manne et al. 2018; Münzer et al., 2016; Chen et al., 2013) we are able to highlight the importance of PDK1 in the MK lineage not only in mice but also in human cells. More-detailed studies concerning PDK1 inhibition in cancer patients, the accompanied thrombocytopenia and MK maturation are indispensable.

5. Concluding remarks and future perspectives

This thesis investigated the role of Rho GTPases RhoA and RhoB, and the signaling protein PDK1 downstream of Rho GTPases in cytoskeletal rearrangements in platelet biogenesis. Hereby, we identified an important function for RhoB in MT dynamics and stability, and a potential role for MK localization together with RhoA. As *RhoA$^{-/-}$* MKs showed an upregulation of RhoB transmigrated into the vessel lumen, *DKO* animals strikingly reverted this phenotype. The dependency of RhoB protein levels of MK migration into the blood vessel through the endothelial layer got clear by studies with animals lacking RhoA and heterozygous RhoB. During this thesis, mice with an upregulation of RhoB, while RhoA was still present, were generated to follow up on this hypothesis (*RhoB^{kin}*). Nevertheless, the analysis of these mice is still ongoing and the results for platelet count and size as well as MK localization are unknown to date. In theory, *RhoB^{kin}* animals should mimic the *RhoA$^{-/-}$* phenotype, resulting in a macrothrombocytopenia and an increased portion of intrasinusoidal MKs. Of note, the upregulation of RhoB needs to be carefully investigated. As only RhoB is upregulated in *RhoB^{kin}* animals, while Rho GEFs and GAP expression should be unaffected, we cannot be certain that higher RhoB levels correspond to increased RhoB activity.

While *RhoB^{kin}* mice are analyzed, these animals can be intercrossed with *RhoA$^{-/-}$* animals in parallel to increase RhoB expression even more while RhoA is absent. With these animals, we are capable to investigate whether the phenotype of *RhoA$^{-/-}$* animals is exclusively caused by RhoB upregulation. Deciphering of these processes will be crucial for a better understanding of MK maturation, migration and proplatelet formation in mice and a translation into the human system. The Rho kinase inhibitor Fasudil, which inhibits ROCK, the downstream effector of Rho GTPases, is widely used in clinics for stroke, pulmonary hypertension, Parkinson, and *amyotrophic lateral sclerosis* (ALS). Nevertheless, the underlying mechanisms are poorly understood. Additionally, this thesis unveiled, how important the establishment of Rho activity assays is to further gain in depth information about Rho GTPase function in platelets and MKs.

Importantly, our studies in *PDK1$^{-/-}$* mice, that display macrothrombocytopenia due to an actin driven PPF defect, were translatable into the human system, as we showed that a knockdown of *PDK1* in human CD34$^+$ cells resulted in reduced PLPs. These findings are pivotal for studies with PDK1 inhibitors for cancer and leukemia treatment, that are likely to develop thrombocytopenia and bleeding episodes.

6. References

Adini, I., Rabinovitz, I., Sun, J.F., Prendergast, G.C., and Benjamin, L.E. (2003). RhoB controls Akt trafficking and stage-specific survival of endothelial cells during vascular development. Genes Dev.

Aguilar, A., Pertuy, F., Eckly, A., Strassel, C., Collin, D., Gachet, C., Lanza, F., and Léon, C. (2016). Importance of environmental stiffness for megakaryocyte differentiation and proplatelet formation. Blood.

Ahn, J., Choi, J.H., Won, M., Kang, C.M., Gyun, M.R., Park, H.M., Kim, C.H., and Chung, K.S. (2011). The activation of p38 MAPK primarily contributes to UV-induced RhoB expression by recruiting the c-Jun and p300 to the distal CCAAT box of the RhoB promoter. Biochem. Biophys. Res. Commun.

Akbar, H., Shang, X., Perveen, R., Berryman, M., Funk, K., Johnson, J.F., Tandon, N.N., and Zheng, Y. (2011). Gene targeting implicates Cdc42 GTPase in GPVI and non-GPVI mediated platelet filopodia formation, secretion and aggregation. PLoS One.

Andonegui, G., Kerfoot, S.M., McNagny, K., Ebbert, K.V.J., Patel, K.D., and Kubes, P. (2005). Platelets express functional Toll-like receptor-4. Blood.

Antkowiak, A., Viaud, J., Severin, S., Zanoun, M., Ceccato, L., Chicanne, G., Strassel, C., Eckly, A., Leon, C., Gachet, C., et al. (2016). Cdc42-dependent F-actin dynamics drive structuration of the demarcation membrane system in megakaryocytes. J. Thromb. Haemost.

Arnold, T.R., Stephenson, R.E., and Miller, A.L. (2017). Rho GTPases and actomyosin: Partners in regulating epithelial cell-cell junction structure and function. Exp. Cell Res.

Aurbach, K., Spindler, M., Haining, E.J., Bender, M., and Pleines, I. (2019). Blood collection, platelet isolation and measurement of platelet count and size in mice—a practical guide. Platelets.

Baker, G.R., Sullam, P.M., and Levin, J. (1997). A simple, fluorescent method to internally label platelets suitable for physiological measurements. Am. J. Hematol.

Ballmaier, M., Germeshausen, M., Schulze, H., Cherkaoui, K., Lang, S., Gaudig, A., Krukemeier, S., Eilers, M., Strauß, G., and Welte, K. (2001). c-mpl mutations are the cause of congenital amegakaryocytic thrombocytopenia. Blood.

Bartley, T.D., Bogenberger, J., Hunt, P., Li, Y.S., Lu, H.S., Martin, F., Chang, M.S., Samal, B., Nichol, J.L., Swift, S., et al. (1994). Identification and cloning of a megakaryocyte growth and development factor that is a ligand for the cytokine receptor Mpl. Cell.

Beaulieu, L.M., Lin, E., Morin, K.M., Tanriverdi, K., and Freedman, J.E. (2011). Regulatory effects of TLR2 on megakaryocytic cell function. Blood.

Beck, S., Fotinos, A., Gawaz, M., and Elvers, M. (2014). Nadrin GAP activity is isoform- and target-specific regulated by tyrosine phosphorylation. Cell. Signal.

Becker, I.C., Scheller, I., Wackerbarth, L.M., Beck, S., Heib, T., Aurbach, K., Manukjan, G., Gross, C., Spindler, M., Nagy, Z., et al. (2020). Actin/microtubule crosstalk during platelet biogenesis in mice is critically regulated by Twinfilin1 and Cofilin1. Blood Adv.

Bender, M., Eckly, A., Hartwig, J.H., Elvers, M., Pleines, I., Gupta, S., Krohne, G., Jeanclos, E.,

Gohla, A., Gurniak, C., et al. (2010). ADF/n-Cofilin-dependent actin turnover determines platelet formation and sizing. Blood.

Bender, M., Stritt, S., Nurden, P., Van Eeuwijk, J.M.M., Zieger, B., Kentouche, K., Schulze, H., Morbach, H., Stegner, D., Heinze, K., et al. (2014). Megakaryocyte-specific Profilin1-deficiency alters microtubule stability and causes a Wiskott-Aldrich syndrome-like platelet defect. Nat. Commun.

Bender, M., Thon, J.N., Ehrlicher, A.J., Wu, S., Mazutis, L., Deschmann, E., Sola-Visner, M., Italiano, J.E., and Hartwig, J.H. (2015). microtubule sliding drives proplatelet elongation and is dependent on cytoplasmic dynein. Blood.

Bergmeier, W., Rackebrandt, K., Schröder, W., Zirngibl, H., and Nieswandt, B. (2000). Structural and functional characterization of the mouse von Willebrand factor receptor GPIb-IX with novel monoclonal antibodies. Blood.

Bergmeier, W., Schulte, V., Brockhoff, G., Bier, U., Zirngibl, H., and Nieswandt, B. (2002). Flow cytometric detection of activated mouse integrin αIIbβ3 with a novel monoclonal antibody. Cytometry.

Bernstein, B.W., and Bamburg, J.R. (1982). Tropomyosin binding to F–actin protects the F–actin from disassembly by brain actin–depolymerizing factor (ADF). Cell Motil.

Bidaud-Meynard, A., Binamé, F., Lagrée, V., and Moreau, V. (2019). Regulation of Rho GTPase activity at the leading edge of migrating cells by p190RhoGAP. Small GTPases.

Blair, P., and Flaumenhaft, R. (2009). Platelet α-granules: Basic biology and clinical correlates. Blood Rev.

Bornert, A., Boscher, J., Pertuy, F., Eckly, A., Stegner, D., Strassel, C., Gachet, C., Lanza, F., & Léon, C. (2020). Cytoskeletal-based mechanisms differently regulate in vivo and in vitro proplatelet formation. Haematologica.

Bravo-Nuevo, A., O'Donnell, R., Rosendahl, A., Chung, J.H., Benjamin, L.E., and Odaka, C. (2011). RhoB deficiency in thymic medullary epithelium leads to early thymic atrophy. Int. Immunol.

Brown, E., Carlin, L.M., Nerlov, C., Lo Celso, C., and Poole, A.W. (2018). Multiple membrane extrusion sites drive megakaryocyte migration into bone marrow blood vessels. Life Sci. Alliance.

Di Buduo, C.A., Alberelli, M.A., Glembostky, A.C., Podda, G., Lev, P.R., Cattaneo, M., Landolfi, R., Heller, P.G., Balduini, A., and De Candia, E. (2016). Abnormal proplatelet formation and emperipolesis in cultured human megakaryocytes from gray platelet syndrome patients. Sci. Rep.

Calvi, L.M., Adams, G.B., Weibrecht, K.W., Weber, J.M., Olson, D.P., Knight, M.C., Martin, R.P., Schipani, E., Divieti, P., Bringhurst, F.R., et al. (2003). Osteoblastic cells regulate the haematopoietic stem cell niche. Nature.

Cecchetti, L., Tolley, N.D., Michetti, N., Bury, L., Weyrich, A.S., and Gresele, P. (2011). Megakaryocytes differentially sort mRNAs for matrix metalloproteinases and their inhibitors into platelets: A mechanism for regulating synthetic events. Blood.

Cerecedo, D., Martínez-Vieyra, I., Mondragõn, R., Mondragõn, M., González, S., and Galván, I.J. (2013). Haemostatic role of intermediate filaments in adhered platelets: Importance of the membranous system stability. J. Cell. Biochem.

Chakraborti, S., Natarajan, K., Curiel, J., Janke, C., and Liu, J. (2016). The emerging role of the Tubulin code: From the Tubulin molecule to neuronal function and disease. Cytoskeleton.

Chen, X., Zhang, Y., Wang, Y., Li, D., Zhang, L., Wang, K., Luo, X., Yang, Z., Wu, Y., and Liu, J. (2013). PDK1 regulates platelet activation and arterial thrombosis. Blood.

Chen, Y.M., Wang, Q.J., Hu, H.S., Yu, P.C., Zhu, J., Drewes, G., Piwnica-Worms, H., and Luo, Z.G. (2006). microtubule affinity-regulating kinase 2 functions downstream of the PAR-3/PAR-6/ atypical PKC complex in regulating hippocampal neuronal polarity. Proc. Natl. Acad. Sci. U. S. A.

Cherfils, J., and Zeghouf, M. (2013). Regulation of small GTPases by GEFs, GAPs, and GDIs. Physiol. Rev.

Choi, E.S., Hokom, M., Bartley, T., Li, Y. −S, Nichol, J.L., Skrine, J., Knudten, A., Chen, J., Hornkohl, A., Grampp, G., et al. (1995). Recombinant human megakaryocyte growth and development factor (rhumgdf), a ligand for c−mpl, produces functional human platelets in vitro. Stem Cells.

Cunin, P., Penke, L.R., Thon, J.N., Monach, P.A., Jones, T., Chang, M.H., Chen, M.M., Melki, I., Lacroix, S., Iwakura, Y., et al. (2017). Megakaryocytes compensate for Kit insufficiency in murine arthritis. J. Clin. Invest.

Cunin, P., Bouslama, R., Machlus, K.R., Bonet, M.M., Lee, P.Y., Wactor, A., Maney, N.N., Morris, A., Guo, L., Weyrich, A., et al. (2019). Megakaryocyte emperipolesis mediates membrane transfer from intracytoplasmic neutrophils to platelets. Elife.

D'Atri, L.P., Etulain, J., Rivadeneyra, L., Lapponi, M.J., Centurion, M., Cheng, K., Yin, H., and Schattner, M. (2015). Expression and functionality of Toll-like receptor 3 in the megakaryocytic lineage. J. Thromb. Haemost.

Da, Q., Behymer, M., Correa, J.I., Vijayan, K.V., and Cruz, M.A. (2014). Platelet adhesion involves a novel interaction between vimentin and von Willebrand factor under high shear stress. Blood.

Dangelmaier, C., Manne, B.K., Liverani, E., Jin, J., Bray, P., and Kunapuli, S.P. (2013). PDK1 selectively phosphorylates Thr(308) on Akt and contributes to human platelet functional responses. Thromb. Haemost.

Delarue, F.L., Adnane, J., Joshi, B., Blaskovich, M.A., Wang, D.A., Hawker, J., Bizouarn, F., Ohkanda, J., Zhu, K., Hamilton, A.D., et al. (2007). Farnesyltransferase and geranylgeranyltransferase I inhibitors upregulate RhoB expression by HDAC1 dissociation, HAT association and histone acetylation of the RhoB promoter. Oncogene.

Deppermann, C., Kratofil, R.M., Peiseler, M., David, B.A., Zindel, J., Silva Castanheira, F.V.E., van der Wal, F., Carestia, A., Jenne, C.N., Marth, J.D., et al. (2020). Macrophage galactose lectin is critical for Kupffer cells to clear aged platelets. J. Exp. Med.

Detrich, H.W., Parker, S.K., Williams, J., Nogales, E., and Downing, K.H. (2000). Cold adaptation of microtubule assembly and dynamics. Structural interpretation of primary sequence changes present in the α- and β-Tubulins of antarctic fishes. J. Biol. Chem.

DeWard, A.D., Leali, K., West, R.A., Prendergast, G.C., and Alberts, A.S. (2009). Loss of RhoB expression enhances the myelodysplastic phenotype of mammalian diaphanous-related formin mDia1 knockout mice. PLoS One.

Du, J., Yang, M., Chen, S., Li, D., Chang, Z., and Dong, Z. (2016). PDK1 promotes tumor

growth and metastasis in a spontaneous breast cancer model. Oncogene.

Dütting, S., Gaits-Iacovoni, F., Stegner, D., Popp, M., Antkowiak, A., Van Eeuwijk, J.M.M., Nurden, P., Stritt, S., Heib, T., Aurbach, K., et al. (2017). A Cdc42/RhoA regulatory circuit downstream of glycoprotein Ib guides transendothelial platelet biogenesis. Nat. Commun.

Dzieciol, J., Debek, W., Chyczewski, L., Szynaka, B., Kisielewski, W., and Sulkowski, S. (1995). Megakaryocytes in the acute stage of experimental hemorrhagic shock. Part II. Megakaryocytic regulation of cell release from the bone marrow. Rocz. Akad. Med. w Białymstoku.

Eberlein, J., Nguyen, T.T., Victorino, F., Golden-Mason, L., Rosen, H.R., and Homann, D. (2010). Comprehensive assessment of chemokine expression profiles by flow cytometry. J. Clin. Invest.

Eckly, A., Rinckel, J.Y., Laeuffer, P., Cazenave, J.P., Lanza, F., Gachet, C., and Léon, C. (2010). Proplatelet formation deficit and megakaryocyte death contribute to thrombocytopenia in Myh9 knockout mice. J. Thromb. Haemost.

Eckly, A., Scandola, C., Oprescu, A., Michel, D., Rinckel, J., Proamer, F., Hoffmann, D., Receveur, N., Léon, C., Bear, J.E., et al. (2020). Megakaryocytes use in vivo podosome−like structures working collectively to penetrate the endothelial barrier of bone marrow sinusoids . J. Thromb. Haemost.

Edward Quach, M., Chen, W., and Li, R. (2018). Mechanisms of platelet clearance and translation to improve platelet storage. Blood.

Elvers, M., Beck, S., Fotinos, A., Ziegler, M., and Gawaz, M. (2012). The GRAF family member oligophrenin1 is a RhoGAP with BAR domain and regulates Rho GTPases in platelets. Cardiovasc. Res.

Essler, M., Amano, M., Kruse, H.J., Kaibuchi, K., Weber, P.C., and Aepfelbacher, M. (1998). Thrombin inactivates myosin light chain phosphatase via Rho and its target Rho kinase in human endothelial cells. J. Biol. Chem.

Esteves, A.R., Palma, A.M., Gomes, R., Santos, D., Silva, D.F., and Cardoso, S.M. (2019). Acetylation as a major determinant to microtubule-dependent autophagy: Relevance to Alzheimer's and Parkinson disease pathology. Biochim. Biophys. Acta - Mol. Basis Dis.

Etienne-Manneville, S., and Hall, A. (2002). Rho GTPases in cell biology. Nature.

Fernandez-Borja, M., Janssen, L., Verwoerd, D., Hordijk, P., and Neefjes, J. (2005). RhoB regulates endosome transport by promoting actin assembly on endosomal membranes through Dia1. J. Cell Sci.

Gagliardi, P.A., di Blasio, L., Puliafito, A., Seano, G., Sessa, R., Chianale, F., Leung, T., Bussolino, F., and Primo, L. (2014). PDK1-mediated activation of MRCKα regulates directional cell migration and lamellipodia retraction. J. Cell Biol.

Gelfand, V. (1995). microtubules edited by Jeremy S. Hyams and Clive W. Lloyd, Wiley-Liss, 1994. $89.95 (439 pages) ISBN 0 471 56193 2. Trends Cell Biol.

Gerald, D., Adini, I., Shechter, S., Perruzzi, C., Varnau, J., Hopkins, B., Kazerounian, S., Kurschat, P., Blachon, S., Khedkar, S., et al. (2013). RhoB controls coordination of adult angiogenesis and lymphangiogenesis following injury by regulating VEZF1-mediated transcription. Nat. Commun.

Geue, S., Aurbach, K., Manke, M.-C., Manukjan, G., Münzer, P., Stegner, D., Brähler, C.,

Walker-Allgaier, B., Märklin, M., Borst, C.E., et al. (2019). Pivotal Role of PDK1 in Megakaryocyte Cytoskeletal Dynamics and Polarization during Platelet Biogenesis. Blood.

Golebiewska, E.M., and Poole, A.W. (2015). Platelet secretion: From haemostasis to wound healing and beyond. Blood Rev.

Le Good, J.A., Ziegler, W.H., Parekh, D.B., Alessi, D.R., Cohen, P., and Parker, P.J. (1998). Protein kinase C isotypes controlled by phosphoinositide 3-kinase through the protein kinase PDK1. Science (80-.).

Gorelashvili, M.G., Angay, O., Hemmen, K., Klaus, V., Stegner, D., and Heinze, K.G. (2020). Megakaryocyte volume modulates bone marrow niche properties and cell migration dynamics. Haematologica.

Gottesbühren, U., Garg, R., Riou, P., McColl, B., Brayson, D., and Ridley, A.J. (2013). Rnd3 induces stress fibres in endothelial cells through RhoB. Biol. Open.

Green, H.L.H., Zuidscherwoude, M., Alenazy, F., Smith, C.W., Bender, M., and Thomas, S.G. (2020). SMIFH2 inhibition of platelets demonstrates a critical role for formin proteins in platelet cytoskeletal dynamics. J. Thromb. Haemost.

Gundersen, G.G., Kalnoski, M.H., and Bulinski, J.C. (1984). Distinct populations of microtubules: Tyrosinated and nontyrosinated alpha Tubulin are distributed differently in vivo. Cell.

Gunning, P., O'Neill, G., and Hardeman, E. (2008). Tropomyosin-based regulation of the actin cytoskeleton in time and space. Physiol. Rev.

Gurney, A.L., Carver-Moore, K., De Sauvage, F.J., and Moore, M.W. (1994). Thrombocytopenia in c-mpl-deficient mice. Science (80-.).

Hamamy, H., Makrythanasis, P., Al-Allawi, N., Muhsin, A.A., and Antonarakis, S.E. (2014). Recessive thrombocytopenia likely due to a homozygous pathogenic variant in the FYB gene: Case report. BMC Med. Genet.

Herman, I.M. (1993). Actin isoforms. Curr. Opin. Cell Biol.

Hitchcock-DeGregori, S.E., Sampath, P., and Pollard, T.D. (1988). Tropomyosin Inhibits the Rate of Actin Polymerization by Stabilizing Actin Filaments. Biochemistry.

Ho, T.T.G., Merajver, S.D., Lapière, C.M., Nusgens, B. V., and Deroanne, C.F. (2008). RhoA-GDP regulates rhob protein stability potential involvement of RhoGDIα. J. Biol. Chem.

Howe, G.A., and Addison, C.L. (2012). RhoB controls endothelial cell morphogenesis in part via negative regulation of RhoA. Vasc. Cell.

Howell, W.H., and Donahue, D.D. (1937). The production of blood platelets in the lungs. J. Exp. Med.

Ihara, K., Ishii, E., Eguchi, M., Takada, H., Suminoe, A., Good, R.A., and Hara, T. (1999). Identification of mutations in the c-mpl gene in congenital amegakaryocytic thrombocytopenia. Proc. Natl. Acad. Sci. U. S. A.

Italiano, J.E., Lecine, P., Shivdasani, R.A., and Hartwig, J.H. (1999). Blood platelets are assembled principally at the ends of proplatelet processes produced by differentiated megakaryocytes. J. Cell Biol.

Jackson, S.P. (2011). Arterial thrombosis-insidious, unpredictable and deadly. Nat. Med.

Jackson, B., Peyrollier, K., Pedersen, E., Basse, A., Karlsson, R., Wang, Z., Lefever, T., Ochsenbein, A.M., Schmidt, G., Aktories, K., et al. (2011). RhoA is dispensable for skin development, but crucial for contraction and directed migration of keratinocytes. Mol. Biol. Cell.

Jaffe, A.B., and Hall, A. (2005). RHO GTPASES: Biochemistry and Biology. Annu. Rev. Cell Dev. Biol.

Kahr, W.H.A., Pluthero, F.G., Elkadri, A., Warner, N., Drobac, M., Chen, C.H., Lo, R.W., Li, L., Li, R., Li, Q., et al. (2017). Loss of the Arp2/3 complex component ARPC1B causes platelet abnormalities and predisposes to inflammatory disease. Nat. Commun.

Kalebic, N., Sorrentino, S., Perlas, E., Bolasco, G., Martinez, C., and Heppenstall, P.A. (2013). αTAT1 is the major α-Tubulin acetyltransferase in mice. Nat. Commun.

Karlsson, R., Pedersen, E.D., Wang, Z., and Brakebusch, C. (2009). Rho GTPase function in tumorigenesis. Biochim. Biophys. Acta - Rev. Cancer.

Kaufman, R.M., Airo, R., Pollack, S., Crosby, W.H., and Doberneck, R. (1965). Origin of pulmonary megakaryocytes. Blood.

Kiel, M.J., and Morrison, S.J. (2006). Maintaining Hematopoietic Stem Cells in the Vascular Niche. Immunity.

King, C.C., Gardiner, E.M.M., Zenke, F.T., Bohl, B.P., Newton, A.C., Hemmings, B.A., and Bokoch, G.M. (2000). p21-activated kinase (PAK1) is phosphorylated and activated by 3-phosphoinositide-dependent kinase-1 (PDK1). J. Biol. Chem.

Kioon, M.D.A., Tripodo, C., Fernandez, D., Kirou, K.A., Spiera, R.F., Crow, M.K., Gordon, J.K., and Barrat, F.J. (2018). Plasmacytoid dendritic cells promote systemic sclerosis with a key role for TLR8. Sci. Transl. Med.

Klages, B., Brandt, U., Simon, M.I., Schultz, G., and Offermanns, S. (1999). Activation of G12/G13 results in shape change and Rho/Rho-kinase- mediated myosin light chain phosphorylation in mouse platelets. J. Cell Biol.

Königs, V., Jennings, R., Vogl, T., Horsthemke, M., Bachg, A.C., Xu, Y., Grobe, K., Brakebusch, C., Schwab, A., Bähler, M., et al. (2014). Mouse Macrophages completely lacking Rho subfamily GTPases (RhoA, RhoB, and RhoC) have severe lamellipodial retraction defects, but robust chemotactic navigation and altered motility. J. Biol. Chem.

Kosoff, R.E., Aslan, J.E., Kostyak, J.C., Dulaimi, E., Chow, H.Y., Prudnikova, T.Y., Radu, M., Kunapuli, S.P., McCarty, O.J.T., and Chernoff, J. (2015). Pak2 restrains endomitosis during megakaryopoiesis and alters cytoskeleton organization. Blood.

Kowata, S., Isogai, S., Murai, K., Ito, S., Tohyama, K., Ema, M., Hitomi, J., and Ishida, Y. (2014). Platelet demand modulates the type of intravascular protrusion of megakaryocytes in bone marrow. Thromb. Haemost.

De La Cruz, E.M., Mandinova, A., Steinmetz, M.O., Stoffler, D., Aebi, U., and Pollard, T.D. (2000). Polymerization and structure of nucleotide-free actin filaments. J. Mol. Biol.

Lai, A.A., and Korn, E.D. (1986). Effect of Muscle Tropomyosin on the Kinetics of Polymerization of Muscle Actin. Biochemistry.

Lane, W.J., Dias, S., Hattori, K., Heissig, B., Choy, M., Rabbany, S.Y., Wood, J., Moore, M.A.S.,

and Rafii, S. (2000). Stromal-derived factor 1-induced megakaryocyte migration and platelet production is dependent on matrix metalloproteinases. Blood.

Lapchak, P.H., Ioannou, A., Rani, P., Lieberman, L.A., Yoshiya, K., Kannan, L., Dalle Lucca, J.J., Kowalska, M.A., and Tsokos, G.C. (2012). The role of platelet factor 4 in local and remote tissue damage in a mouse model of mesenteric ischemia/reperfusion injury. PLoS One.

Larocca, L.M., Heller, P.G., Podda, G., Pujol-Moix, N., Glembotsky, A.C., Pecci, A., Alberelli, M.A., Balduini, C.L., Landolfi, R., Cattaneo, M., et al. (2015). Megakaryocytic emperipolesis and platelet function abnormalities in five patients with gray platelet syndrome. Platelets.

Larsen, T.E. (1970). Emperipolesis of granular leukocytes within megakaryocytes in human hemopoietic bone marrow. Am. J. Clin. Pathol.

Lasagni, L., Grepin, R., Mazzinghi, B., Lazzeri, E., Meini, C., Sagrinati, C., Liotta, F., Frosali, F., Ronconi, E., Alain-Courtois, N., et al. (2007). PF-4/CXCL4 and CXCL4L1 exhibit distinct subcellular localization and a differentially regulated mechanism of secretion. Blood.

Lawlor, M.A., Mora, A., Ashby, P.R., Williams, M.R., Murray-Tait, V., Malone, L., Prescott, A.R., Lucocq, J.M., and Alessi, D.R. (2002). Essential role of PDK1 in regulating cell size and development in mice. EMBO J.

Lawson, C.D., and Ridley, A.J. (2018). Rho GTPase signaling complexes in cell migration and invasion. J. Cell Biol.

Lefrançais, E., Ortiz-Muñoz, G., Caudrillier, A., Mallavia, B., Liu, F., Sayah, D.M., Thornton, E.E., Headley, M.B., David, T., Coughlin, S.R., et al. (2017). The lung is a site of platelet biogenesis and a reservoir for haematopoietic progenitors. Nature.

Levin, C., Koren, A., Pretorius, E., Rosenberg, N., Shenkman, B., Hauschner, H., Zalman, L., Khayat, M., Salama, I., Elpeleg, O., et al. (2015). Deleterious mutation in the FYB gene is associated with congenital autosomal recessive small-platelet thrombocytopenia. J. Thromb. Haemost.

Liu, A.-X., Rane, N., Liu, J.-P., and Prendergast, G.C. (2001). RhoB Is Dispensable for Mouse Development, but It Modifies Susceptibility to Tumor Formation as Well as Cell Adhesion and Growth Factor Signaling in Transformed Cells. Mol. Cell. Biol.

Lorenz, M., Poole, K.J.V., Popp, D., Rosenbaum, G., and Holmes, K.C. (1995). An atomic model of the unregulated thin filament obtained by X-ray fiber diffraction on oriented actin-tropomyosin gels. J. Mol. Biol.

Lowery, J., Kuczmarski, E.R., Herrmann, H., and Goldma, R.D. (2015). Intermediate filaments play a pivotal role in regulating cell architecture and function. J. Biol. Chem.

Lu, D.H., Hsu, C.C., Huang, S.W., Tu, H.J., Huang, T.F., Liou, H.C., Liao, H.M., Chen, C.H., Fu, W.M., and Gau, S.S.F. (2017). ARHGEF10 knockout inhibits platelet aggregation and protects mice from thrombus formation. J. Thromb. Haemost.

Machlus, K.R., and Italiano, J.E. (2013). The incredible journey: From megakaryocyte development to platelet formation. J. Cell Biol.

Machlus, K.R., Johnson, K.E., Kulenthirarajan, R., Forward, J.A., Tippy, M.D., Soussou, T.S., El-Husayni, S.H., Wu, S.K., Wang, S., Watnick, R.S., et al. (2016). CCL5 derived from platelets increases megakaryocyte proplatelet formation. Blood.

Mammadova-Bach, E., Nagy, M., Heemskerk, J.W.M., Nieswandt, B., and Braun, A. (2019).

Store-operated calcium entry in thrombosis and thrombo-inflammation. Cell Calcium.

Manne, B.K., Münzer, P., Badolia, R., Walker-Allgaier, B., Campbell, R.A., Middleton, E., Weyrich, A.S., Kunapuli, S.P., Borst, O., and Rondina, M.T. (2018). PDK1 governs thromboxane generation and thrombosis in platelets by regulating activation of Raf1 in the MAPK pathway. J. Thromb. Haemost.

Marcos-Ramiro, B., García-Weber, D., Barroso, S., Feito, J., Ortega, M.C., Cernuda-Morollón, E., Reglero-Real, N., Fernández-Martín, L., Durán, M.C., Alonso, M.A., et al. (2016). RhoB controls endothelial barrier recovery by inhibiting Rac1 trafficking to the cell border. J. Cell Biol.

Mashukova, A., Forteza, R., Wald, F.A., and Salas, P.J. (2012). PDK1 in apical signaling endosomes participates in the rescue of the polarity complex atypical PKC by intermediate filaments in intestinal epithelia. Mol. Biol. Cell.

Massaad, M.J., Ramesh, N., and Geha, R.S. (2013). Wiskott-Aldrich syndrome: A comprehensive review. Ann. N. Y. Acad. Sci.

Massberg, S., Gawaz, M., Grüner, S., Schulte, V., Konrad, I., Zohlnhöfer, D., Heinzmann, U., and Nieswandt, B. (2003). A crucial role of glycoprotein VI for platelet recruitment to the injured arterial wall in vivo. J. Exp. Med.

Maurer, M., Su, T., Saal, L.H., Koujak, S., Hopkins, B.D., Barkley, C.R., Wu, J., Nandula, S., Dutta, B., Xie, Y., et al. (2009). 3-Phosphoinositide-dependent kinase 1 potentiates upstream lesions on the phosphatidylinositol 3-kinase pathway in breast carcinoma. Cancer Res.

May, F., Hagedorn, I., Pleines, I., Bender, M., Vögtle, T., Eble, J., Elvers, M., and Nieswandt, B. (2009). CLEC-2 is an essential platelet-activating receptor in hemostasis and thrombosis. Blood.

McCarty, O.J.T., Larson, M.K., Auger, J.M., Kalia, N., Atkinson, B.T., Pearce, A.C., Ruf, S., Henderson, R.B., Tybulewicz, V.L.J., Machesky, L.M., et al. (2005). Rac1 is essential for platelet lamellipodia formation and aggregate stability under flow. J. Biol. Chem.

Messaoudi, K., Ali, A., Ishaq, R., Palazzo, A., Sliwa, D., Bluteau, O., Souquère, S., Muller, D., Diop, K.M., Rameau, P., et al. (2017). Critical role of the HDAC6-cortactin axis in human megakaryocyte maturation leading to a proplatelet-formation defect. Nat. Commun.

Mezger, M., Nording, H., Sauter, R., Graf, T., Heim, C., von Bubnoff, N., Ensminger, S.M., and Langer, H.F. (2019). Platelets and Immune Responses During Thromboinflammation. Front. Immunol.

Moers, A., Nieswandt, B., Massberg, S., Wettschureck, N., Grüner, S., Konrad, I., Schulte, V., Aktas, B., Gratacap, M.P., Simon, M.I., et al. (2003). G13 is an essential mediator of platelet activation in hemostasis and thrombosis. Nat. Med.

Morodomi, Y., Kanaji, S., Won, E., Kawamoto, T., and Kanaji, T. (2020). Modified application of Kawamoto's film method for super-resolution imaging of megakaryocytes in undecalcified bone marrow. Res. Pract. Thromb. Haemost.

Münzer, P., Walker-Allgaier, B., Geue, S., Geuss, E., Hron, G., Rath, D., Eißler, D., Winter, S., Schaeffeler, E., Meinert, M., et al. (2016). PDK1 Determines Collagen-Dependent Platelet Ca 2+ Signaling and Is Critical to Development of Ischemic Stroke in Vivo. Arterioscler. Thromb. Vasc. Biol.

Nagy, Z., Vögtle, T., Geer, M.J., Mori, J., Heising, S., Di Nunzio, G., Gareus, R., Tarakhovsky, A., Weiss, A., Neel, B.G., et al. (2019). The Gp1ba-Cre transgenic mouse: A new model to

delineate platelet and leukocyte functions. Blood.

Ngo, A.T.P., Thierheimer, M.L.D., Babur, Ö., Rocheleau, A.D., Huang, T., Pang, J., Rigg, R.A., Mitrugno, A., Theodorescu, D., Burchard, J., et al. (2017). Assessment of roles for the rho-specific guanine nucleotide dissociation inhibitor Ly-GDI in platelet function: A spatial systems approach. Am. J. Physiol. - Cell Physiol.

Nieswandt, B., Bergmeier, W., Rackebrandt, K., Engelbert Gessner, J., and Zirngibl, H. (2000a). Identification of critical antigen-specific mechanisms in the development of immune thrombocytopenic purpura in mice. Blood.

Nieswandt, B., Bergmeier, W., Schulte, V., Rackebrandt, K., Gessner, J.E., and Zirngibl, H. (2000b). Expression and function of the mouse collagen receptor glycoprotein VI is strictly dependent on its association with the FcRγ chain. J. Biol. Chem.

Nieswandt, B., Schulte, V., Bergmeier, W., Mokhtari-Nejad, R., Rackebrandt, K., Cazenave, J.P., Ohlmann, P., Gachet, C., and Zirngibl, H. (2001). Long-term antithrombotic protection by in vivo depletion of platelet glycoprotein VI in mice. J. Exp. Med.

Nieswandt, B., Pleines, I., and Bender, M. (2011). Platelet adhesion and activation mechanisms in arterial thrombosis and ischaemic stroke. J. Thromb. Haemost.

Nieuwenhuis, J., Adamopoulos, A., Bleijerveld, O.B., Mazouzi, A., Stickel, E., Celie, P., Altelaar, M., Knipscheer, P., Perrakis, A., Blomen, V.A., et al. (2017). Vasohibins encode Tubulin detyrosinating activity. Science (80-.).

Noetzli, L.J., French, S.L., and Machlus, K.R. (2019). New Insights Into the Differentiation of Megakaryocytes From Hematopoietic Progenitors. Arterioscler. Thromb. Vasc. Biol.

Patel-Hett, S., Richardson, J.L., Schulze, H., Drabek, K., Isaac, N.A., Hoffmeister, K., Shivdasani, R.A., Bulinski, J.C., Galjart, N., Hartwig, J.H., et al. (2008). Visualization of microtubule growth in living platelets reveals a dynamic marginal band with multiple microtubules. Blood.

Patel-Hett, S., Wang, H., Begonja, A.J., Thon, J.N., Alden, E.C., Wandersee, N.J., An, X., Mohandas, N., Hartwig, J.H., and Italiano, J.E. (2011). The spectrin-based membrane skeleton stabilizes mouse megakaryocyte membrane systems and is essential for proplatelet and platelet formation. Blood.

Patel, S.R., Hartwig, J.H., and Italiano, J.E. (2005). The biogenesis of platelets from megakaryocyte proplatelets. J. Clin. Invest.

Paul, D.S., Casari, C., Wu, C., Piatt, R., Pasala, S., Campbell, R.A., Poe, K.O., Ghalloussi, D., Lee, R.H., Rotty, J.D., et al. (2017). Deletion of the Arp2/3 complex in megakaryocytes leads to microthrombocytopenia in mice. Blood Adv.

Perry, S. V. (2001). Vertebrate tropomyosin: Distribution, properties and function. J. Muscle Res. Cell Motil.

Pleines, I., Elvers, M., Strehl, A., Pozgajova, M., Varga-Szabo, D., May, F., Chrostek-Grashoff, A., Brakebusch, C., and Nieswandt, B. (2009). Rac1 is essential for phospholipase C-γ2 activation in platelets. Pflugers Arch. Eur. J. Physiol.

Pleines, I., Eckly, A., Elvers, M., Hagedorn, I., Eliautou, S., Bender, M., Wu, X., Lanza, F., Gachet, C., Brakebusch, C., et al. (2010). Multiple alterations of platelet functions dominated by increased secretion in mice lacking Cdc42 in platelets. Blood.

Pleines, I., Hagedorn, I., Gupta, S., May, F., Chakarova, L., Van Hengel, J., Offermanns, S., Krohne, G., Kleinschnitz, C., Brakebusch, C., et al. (2012). Megakaryocyte-specific RhoA deficiency causes macrothrombocytopenia and defective platelet activation in hemostasis and thrombosis. Blood.

Pleines, I., Dütting, S., Cherpokova, D., Eckly, A., Meyer, I., Morowski, M., Krohne, G., Schulze, H., Gachet, C., Debili, N., et al. (2013). Defective Tubulin organization and proplatelet formation in murine megakaryocytes lacking Rac1 and Cdc42. Blood.

Pleines, I., Woods, J., Chappaz, S., Kew, V., Foad, N., Ballester-Beltrán, J., Aurbach, K., Lincetto, C., Lane, R.M., Schevzov, G., et al. (2017). Mutations in tropomyosin 4 underlie a rare form of human macrothrombocytopenia. J. Clin. Invest.

Pleines, I., Cherpokova, D., and Bender, M. (2019). Rho GTPases and their downstream effectors in megakaryocyte biology. Platelets.

Pollard, T.D. (2016). Actin and actin-binding proteins. Cold Spring Harb. Perspect. Biol.

Potts, K.S., Farley, A., Dawson, C.A., Rimes, J., Biben, C., de Graaf, C., Potts, M.A., Stonehouse, O.J., Carmagnac, A., Gangatirkar, P., et al. (2020). Membrane budding is a major mechanism of in vivo platelet biogenesis. J. Exp. Med.

Poulter, N.S., Pollitt, A.Y., Davies, A., Malinova, D., Nash, G.B., Hannon, M.J., Pikramenou, Z., Rappoport, J.Z., Hartwig, J.H., Owen, D.M., et al. (2015). Platelet actin nodules are podosome-like structures dependent on Wiskott-Aldrich syndrome protein and ARP2/3 complex. Nat. Commun.

Primo, L., Di Blasio, L., Roca, C., Droetto, S., Piva, R., Schaffhausen, B., and Bussolino, F. (2007). Essential role of PDK1 in regulating endothelial cell migration. J. Cell Biol.

Pronk, M.C.A., van Bezu, J.S.M., van Nieuw Amerongen, G.P., van Hinsbergh, V.W.M., and Hordijk, P.L. (2019). RhoA, RhoB and RhoC differentially regulate endothelial barrier function. Small GTPases.

Pula, G., and Poole, A.W. (2008). Critical roles for the actin cytoskeleton and cdc42 in regulating platelet integrin α2β1. Platelets.

Raimondi, C., and Falasca, M. (2011). Targeting PDK1 in Cancer. Curr. Med. Chem.

Reymond, N., Riou, P., and Ridley, A.J. (2012). Rho GTPases and cancer cell transendothelial migration. Methods Mol. Biol.

Rohn, J.L., and Baum, B. (2010). Actin and cellular architecture at a glance. J. Cell Sci.

Roostalu, J., and Surrey, T. (2017). microtubule nucleation: Beyond the template. Nat. Rev. Mol. Cell Biol.

Rouiller, I., Xu, X.P., Amann, K.J., Egile, C., Nickell, S., Nicastro, D., Li, R., Pollard, T.D., Volkmann, N., and Hanein, D. (2008). The structural basis of actin filament branching by the Arp2/3 complex. J. Cell Biol.

Roweth, H.G., Malloy, M., Goreczny, G., Johnson, K.E., McAllister, S.S., Italiano, J.E., and Battinelli, E. (2019). Megakaryocyte Reprogramming in Breast Cancer. Blood.

Sabatel, C., Malvaux, L., Bovy, N., Deroanne, C., Lambert, V., Gonzalez, M.L.A., Colige, A., Rakic, J.M., Noël, A., Martial, J.A., et al. (2011). MicroRNA-21 exhibits antiangiogenic function by targeting RhoB expression in endothelial cells. PLoS One.

Sabri, S., Foudi, A., Boukour, S., Franc, B., Charrier, S., Jandrot-Perrus, M., Farndale, R.W., Jalil, A., Blundell, M.P., Cramer, E.M., et al. (2006). Deficiency in the Wiskott-Aldrich protein induces premature proplatelet formation and platelet production in the bone marrow compartment. Blood.

Sadoul, K., Wang, J., Diagouraga, B., Vitte, A.L., Buchou, T., Rossini, T., Polack, B., Xi, X., Matthias, P., and Khochbin, S. (2012). HDAC6 controls the kinetics of platelet activation. Blood.

Sahai, E., and Marshall, C.J. (2002). RHO - GTPases and cancer. Nat. Rev. Cancer.

Sahebekhtiari, H.A., and Tavassoli, M. (1976). Marrow Cell Uptake by Megakaryocytes in Routine Bone Marrow Smears during Blood Loss. Scand. J. Haematol.

De Sauvage, F.J., Hass, P.E., Spencer, S.D., Malloy, B.E., Gurney, A.L., Spencer, S.A., Darbonne, W.C., Henzel, W.J., Wong, S.C., Kuang, W.J., et al. (1994). Stimulation of megakaryocytopoiesis and thrombopoiesis by the c-Mpl ligand. Nature.

Schachtner, H., Calaminus, S.D.J., Sinclair, A., Monypenny, J., Blundell, M.P., Leon, C., Holyoake, T.L., Thrasher, A.J., Michie, A.M., Vukovic, M., et al. (2013). Megakaryocytes assemble podosomes that degrade matrix and protrude through basement membrane. Blood.

Schaffner, A. (2005). Regulated expression of platelet factor 4 in human monocytes--role of PARs as a quantitatively important monocyte activation pathway. J. Leukoc. Biol.

Scheller, I., Stritt, S., Beck, S., Peng, B., Pleines, I., Heinze, K.G., Braun, A., Otto, O., Ahrends, R., Sickmann, A., et al. (2020). Coactosin-like 1 integrates signaling critical for shear-dependent thrombus formation in mouse platelets. Haematologica.

Schmitt, A., Guichard, J., Massé, J.M., Debili, N., and Cramer, E.M. (2001). Of mice and men: Comparison of the ultrastructure of megakaryocytes and platelets. Exp. Hematol.

Schulte, V., Rabie, T., Prostredna, M., Aktas, B., Grüner, S., and Nieswandt, B. (2003). Targeting of the collagen-binding site on glycoprotein VI is not essential for in vivo depletion of the receptor. Blood.

Schulze, H., Korpal, M., Hurov, J., Kim, S.W., Zhang, J., Cantley, L.C., Graf, T., and Shivdasani, R.A. (2006). Characterization of the megakaryocyte demarcation membrane system and its role in thrombopoiesis. Blood.

Schurr, Y., Sperr, A., Volz, J., Beck, S., Reil, L., Kusch, C., Eiring, P., Bryson, S., Sauer, M., Nieswandt, B., et al. (2019). Platelet lamellipodium formation is not required for thrombus formation and stability. Blood.

Schwer, H.D., Lecine, P., Tiwari, S., Italiano, J.E., Hartwig, J.H., and Shivdasani, R.A. (2001). A lineage-restricted and divergent β-Tubulin isoform is essential for the biogenesis, structure and function of blood platelets. Curr. Biol.

Shi, D.S., Smith, M.C.P., Campbell, R.A., Zimmerman, P.W., Franks, Z.B., Kraemer, B.F., Machlus, K.R., Ling, J., Kamba, P., Schwertz, H., et al. (2014a). Proteasome function is required for platelet production. J. Clin. Invest.

Shi, G., Field, D.J., Ko, K.A., Ture, S., Srivastava, K., Levy, S., Kowalska, M.A., Poncz, M., Fowell, D.J., and Morrell, C.N. (2014b). Platelet factor 4 limits Th17 differentiation and cardiac allograft rejection. J. Clin. Invest.

Sohma, Y., Akahori, H., Seki, N., Hori, T. aki, Ogami, K., Kato, T., Shimada, Y., Kawamura, K., and Miyazaki, H. (1994). Molecular cloning and chromosomal localization of the human

thrombopoietin gene. FEBS Lett.

Song, Y., and Brady, S.T. (2015). Post-translational modifications of Tubulin: Pathways to functional diversity of microtubules. Trends Cell Biol.

Spangrude, G.J., Lewandowski, D., Martelli, F., Marra, M., Zingariello, M., Sancillo, L., Alba Rana, R., and Rita Migliaccio, A. (2016). P-Selectin Sustains Extramedullary Hematopoiesis in the Gata1low Model of Myelofibrosis. Stem Cells.

Spindler, M., van Eeuwijk, J.M.M., Schurr, Y., Nurden, P., Nieswandt, B., Stegner, D., Reinhold, A., and Bender, M. (2018). ADAP deficiency impairs megakaryocyte polarization with ectopic proplatelet release and causes microthrombocytopenia. Blood.

Stegner, D., Vaneeuwijk, J.M.M., Angay, O., Gorelashvili, M.G., Semeniak, D., Pinnecker, J., Schmithausen, P., Meyer, I., Friedrich, M., Dütting, S., et al. (2017). Thrombopoiesis is spatially regulated by the bone marrow vasculature. Nat. Commun.

Strassel, C., Eckly, A., Léon, C., Moog, S., Cazenave, J.P., Gachet, C., and Lanza, F. (2012). Hirudin and heparin enable efficient megakaryocyte differentiation of mouse bone marrow progenitors. Exp. Cell Res.

Strassel, C., Moog, S., Mallo, L., Eckly, A., Freund, M., Gachet, C., and Lanza, F. (2018). microtubule plus-end tracking Adenopolyposis Coli negatively regulates proplatelet formation. Sci. Rep.

Strassel, C., Magiera, M.M., Dupuis, A., Batzenschlager, M., Hovasse, A., Pleines, I., Guéguen, P., Eckly, A., Moog, S., Mallo, L., et al. (2019). An essential role for α4A-Tubulin in platelet biogenesis. Life Sci. Alliance.

Stritt, S., Nurden, P., Turro, E., Greene, D., Jansen, S.B., Westbury, S.K., Petersen, R., Astle, W.J., Marlin, S., Bariana, T.K., et al. (2016). A gain-of-function variant in DIAPH1 causes dominant macrothrombocytopenia and hearing loss. Blood.

Stritt, S., Beck, S., Becker, I.C., Vögtle, T., Hakala, M., Heinze, K.G., Du, X., Bender, M., Braun, A., Lappalainen, P., et al. (2017). Twinfilin 2a regulates platelet reactivity and turnover in mice. Blood.

Stritt, S., Birkholz, I., Beck, S., Sorrentino, S., Sapra, K.T., Viaud, J., Heck, J., Gaits-Iacovoni, F., Schulze, H., Du, X., et al. (2018). Profilin 1-mediated cytoskeletal rearrangements regulate integrin function in mouse platelets. Blood Adv.

Taha, A.A., Taha, M., Seebach, J., and Schnittler, H.J. (2014). ARP2/3-mediated junction-associated lamellipodia control VE-cadherin-based cell junction dynamics and maintain monolayer integrity. Mol. Biol. Cell.

Thomas, S.G., Poulter, N.S., Bem, D., Finney, B., Machesky, L.M., and Watson, S.P. (2017). The actin binding proteins cortactin and HS1 are dispensable for platelet actin nodule and megakaryocyte podosome formation. Platelets.

Thon, J.N., Montalvo, A., Patel-Hett, S., Devine, M.T., Richardson, J.L., Ehrlicher, A., Larson, M.K., Hoffmeister, K., Hartwig, J.H., and Italiano, J.E. (2010). Cytoskeletal mechanics of proplatelet maturation and platelet release. J. Cell Biol.

Truebestein, L., Elsner, D.J., and Leonard, T.A. (2016). Made to measure – keeping Rho kinase at a distance. Small GTPases.

Vale, R.D., and Fletterick, R.J. (1997). The design plan of kinesin motors. Annu. Rev. Cell Dev.

Biol.

Varga-Szabo, D., Braun, A., and Nieswandt, B. (2009). Calcium signaling in platelets. J. Thromb. Haemost.

Vega, F.M., and Ridley, A.J. (2008). Rho GTPases in cancer cell biology. FEBS Lett.

Vega, F.M., and Ridley, A.J. (2018). The RhoB small GTPase in physiology and disease. Small GTPases.

Vega, F.M., Fruhwirth, G., Ng, T., and Ridley, A.J. (2011). RhoA and RhoC have distinct roles in migration and invasion by acting through different targets. J. Cell Biol.

Vega, F.M., Colomba, A., Reymond, N., Thomas, M., and Ridley, A.J. (2012). RhoB regulates cell migration through altered focal adhesion dynamics. Open Biol.

Volz, J., Mammadova-Bach, E., Gil-Pulido, J., Nandigama, R., Remer, K., Sorokin, L., Zernecke, A., Abrams, S.I., Ergün, S., Henke, E., et al. (2019). Inhibition of platelet GPVI induces intratumor hemorrhage and increases efficacy of chemotherapy in mice. Blood.

Wallar, B.J., DeWard, A.D., Resau, J.H., and Alberts, A.S. (2007). RhoB and the mammalian Diaphanous-related formin mDia2 in endosome trafficking. Exp. Cell Res.

Weber, D.S., Taniyama, Y., Rocic, P., Seshiah, P.N., Dechert, M.A., Gerthoffer, W.T., and Griendling, K.K. (2004). Phosphoinositide-dependent kinase 1 and p21-activated protein kinase mediate reactive oxygen species-dependent regulation of platelet-derived growth factor-induced smooth muscle cell migration. Circ. Res.

Webster, D.R., and Borisy, G.G. (1989). microtubules are acetylated in domains that turn over slowly. J. Cell Sci.

Weisberg, E., Banerji, L., Wright, R.D., Barrett, R., Ray, A., Moreno, D., Catley, L., Jiang, J., Hall-Meyers, E., Sauveur-Michel, M., et al. (2008). Potentiation of antileukemic therapies by the dual PI3K PDK-1 inhibitor, BAG956: Effects on BCR-ABL and mutant FLT3-expressing cells. Blood.

Wheeler, A.P., and Ridley, A.J. (2004). Why three Rho proteins? RhoA, RhoB, RhoC, and cell motility. Exp. Cell Res.

Wheeler, A.P., and Ridley, A.J. (2007). RhoB affects macrophage adhesion, integrin expression and migration. Exp. Cell Res.

Wherlock, M., Gampel, A., Futter, C., and Mellor, H. (2004). Farnesyltransferase inhibitors disrupt EGF receptor traffic through modulation of the RhoB GTPase. J. Cell Sci.

Whyte, J., Thornton, L., McNally, S., McCarthy, S., Lanigan, F., Gallagher, W.M., Stein, T., and Martin, F. (2010). PKCζ regulates cell polarisation and proliferation restriction during mammary acinus formation. J. Cell Sci.

Williams, C.M., Harper, M.T., Goggs, R., Walsh, T.G., Offermanns, S., and Poole, A.W. (2015). Leukemia-associated Rho guanine-nucleotide exchange factor is not critical for RhoA regulation, yet is important for platelet activation and thrombosis in mice. J. Thromb. Haemost.

Wloga, D., Joachimiak, E., and Fabczak, H. (2017). Tubulin post-translational modifications and microtubule dynamics. Int. J. Mol. Sci.

Wolter, S., Löschberger, A., Holm, T., Aufmkolk, S., Dabauvalle, M.C., Van De Linde, S., and

Sauer, M. (2012). RapidSTORM: Accurate, fast open-source software for localization microscopy. Nat. Methods.

Yoneda, M., Hirokawa, Y.S., Ohashi, A., Uchida, K., Kami, D., Watanabe, M., Yokoi, T., Shiraishi, T., and Wakusawa, S. (2010). RhoB enhances migration and MMP1 expression of prostate cancer DU145. Exp. Mol. Pathol.

Zabkiewicz, J., Pearn, L., Hills, R.K., Morgan, R.G., Tonks, A., Burnett, A.K., and Darley, R.L. (2014). The PDK1 master kinase is over-expressed in acute myeloid leukemia and promotes PKC-mediated survival of leukemic blasts. Haematologica.

Zalcman, G., Closson, V., Linares-Cruz, G., Lerebours, F., Honore, N., Tavitian, A., and Olofsson, B. (1995). Regulation of Ras-related RhoB protein expression during the cell cycle. Oncogene.

Zaoui, K., Rajadurai, C. V., Duhamel, S., and Park, M. (2019). Arf6 regulates RhoB subcellular localization to control cancer cell invasion. J. Cell Biol.

Zaru, R., Mollahan, P., and Watts, C. (2008). 3-Phosphoinositide-dependent kinase 1 deficiency perturbs toll-like receptor signaling events and actin cytoskeleton dynamics in dendritic cells. J. Biol. Chem.

Zhao, M., Perry, J.M., Marshall, H., Venkatraman, A., Qian, P., He, X.C., Ahamed, J., and Li, L. (2014). Megakaryocytes maintain homeostatic quiescence and promote post-injury regeneration of hematopoietic stem cells. Nat. Med.

Zimmet, J., and Ravid, K. (2000). Polyploidy: Occurrence in nature, mechanisms, and significance for the megakaryocyte-platelet system. Exp. Hematol.

Zuidscherwoude, M., Green, H.L.H., and Thomas, S.G. (2019). Formin proteins in megakaryocytes and platelets: regulation of actin and microtubule dynamics. Platelets.

7. Appendix

7.1. Abbreviations

ACD	Acid-Citrate-Dextrose
ADAP	Adhesion and degranulation-promoting adaptor protein
ADF	Actin depolymerizing factor
ADF-H	ADF-homology domain
ADP	Adenosine diphosphate
Akt	Protein kinase B
ALS	Amyotrophic lateral sclerosis
APC	Adenomatous polyposis coli
APS	Ammonium persulfate
Arf6	ADP-ribosylation factor 6
Arp2/3	Actin-related proteins 2/3
ATP	Adenosine triphosphate
AU	Arbitrary unit
BCA	Bicinchoninic acid assay
BF	Brightfield
BM	Bone marrow
BSA	Bovine serum albumin
Ca2+	Calcium cation
cAMP	Cyclic adenosine monophosphate
CCL	C-C motif chemokine ligand 5
CD	Cluster of differentiation
Cdc42	Cell division control protein 42 homolog
CLEC-2	C-type lectin-like receptor 2
c-Mpl	Myeloproliferative leukemia protein
Cof1	Cofilin1
Col	Collagen
CRP	Collagen-related peptide
CP	Capping protein
CT	Computed tomography
CVX	Convulxin
DAPI	4'-6-Diamidino-2-phenylindole
°C	Degree Celsius
Diaph1	Mammalian Diaphanous
DIC	Differential interference contrast

DNA	Deoxyribonucleic acid
dNTP	Deoxynucleotide triphosphates
DMEM	Dulbecco's modified eagle medium
DMS	Demarcation membrane system
DMSO	Dimethylsulfoxide
DPBS	Dulbecco's phosphate buffered saline
EB	End binding protein
EC	Endothelial cell
ECL	Enhanced chemiluminescence
ECL	Erythrina cristagalli lectin
ECM	Extracellular matrix
EDTA	Ethylenediaminetetraacetic acid
e.g.	Exempli gratia
EGTA	Ethylene glycol tetraacetic acid
ELISA	Enzyme-linked immunosorbent assay
EPI	Epifluorescence
ERK	Extracellular-signal Regulated Kinase
et al.	Et alii
F(ab)	Fragment antigen-binding
F-actin	Filamentous actin
FCS	Fetal calf serum
FH2	Formin homolog 2
FITC	Fluorescein-isothiocyanate
FTI	Farnesyltransferase inhibitors
FOG	Friend of GATA
FSC	Forward scatter
G-actin	Globular actin
GAP	GTPase activating protein
GAPDH	Glycerinaldehyd-3-phosphate-dehydrogenase
GATA	GATA-binding factor
gDNA	Genomic DNA
GEF	Guanine nucleotide exchange factor
GGTI	Geranylgeranyl transferase inhibitors
GP	Glycoprotein
GPCR	G-protein-coupled receptor
GTP	Guanine triphosphate
h	Hour
HCl	Hydrogen chloride
H&E	Hematoxylin and eosin

HEPES	N-2-Hydroxyethylpiperazine-N'-2-ethanesulfonic acid
HPC	Hematopoietic progenitor cells
HRP	Horseradish peroxidase
HSC	Hematopoietic stem cell
HSPC	Hematopoietic stem and progenitor cells
HUVEC	Human umbilical vein endothelial cells
Ig	Immunoglobulin
IL	Interleukin
i.p.	Intraperitoneally
ITAM	Immunoreceptor tyrosine-based activation motif
i.v.	Intravenously
IVM	Intravital microscopy
kb	Kilo base pairs
kDa	Kilo Dalton
LIMK	LIM kinase
MAPK	Mitogen-activated protein kinase
mDia	Mammalian Diaphanous
MFI	Mean fluorescence intensity
MGL	Macrophage galactose lectin
min	Minute
MK	Megakaryocyte
MLC	Myosin light chain
MMP	Matrix metalloproteinase
mRNA	Messenger RNA
MYH	Non-muscle myosin heavy chain
N	Number of chromosome sets
NaCl	Sodium chloride
NaOH	Sodium hydroxide
NBEAL2	Neurobeachin-like 2
NFE	Neurofibromin
NIH	National Institute for Health Research
NMIIa	Non-muscle myosin IIa
NMIIb	Non-muscle myosin IIb
NP-40	Nonidet P-40
n.s.	Non-significant
PAGE	Polyacrylamide gel electrophoresis
PAK	p21-activated kinase
PCR	Polymerase chain reaction
PDK1	Phosphoinositide-dependent kinase-1

PE	Phycoerythrin
Pf4	Platelet factor 4
PFA	Paraformaldehyde
Pfn	Profilin
PGI_2	Prostacyclin
PI	Propidium iodide
PI3K	Phosphoinositide 3-kinase
PIPES	Piperazine-N, N'-bis (2-ethanesulfonic acid)
PK	Protein kinase
PLC	Phospholipase C
PLP	Platelet like particle
PPF	Proplatelet formation
PRP	Platelet-rich plasma
PVDF	Polyvinylidene difluoride
PS	Phosphatidylserine
Rac1	Ras-related C3 botulinum toxin substrate 1
RBC	Red blood cell
RC	Rhodocytin
Rest	Resting
Rhc	Rhodocytin
RhoA	Ras homologue family member A
RhoGDIα	Rho GDP-dissociation inhibitor 1 alpha
RNA	Ribonucleic acid
ROCK	Rho kinase
ROP	Retinopathy of prematurity
rpm	Rotation per minute
RT	Room temperature
RUNX	Runt-related transcription factor
s	Soluble
S1P	Sphingosine-1-phosphate
Sca1	Stem cell antigen 1
SCF	Stem cell factor
SD	Standard deviation
SDS	Sodium dodecyl sulfate
SDF	Stromal cell derived factor
SFK	Src family kinase
SIRT2	NAD-dependent deacetylase sirtuin-2
Src	Sarcoma
SSC	Side scatter

TEM	Transmission electron microscopy
TEMED	Tetramethyl ethylenediamine
TF	Transcription factor
TGF	Transforming growth factor
Thr	Thrombin
TIRF	Total internal reflection fluorescence
TLR	Toll-like receptor
TO	Thiazol Orange
TPO	Thrombopoietin
TRIS	Tris(hydroxymethyl)aminomethane
Twf	Twinfilin
TxA$_2$	Thromboxane A2
U46	U46619
VE-Cadherin	Vascular endothelial cadherin
VEGF	Vascular endothelial growth factor
VWD	Von Willebrand disease
vWF	Von Willebrand factor
WAS	Wiskott-Aldrich syndrome
WBC	White blood cell
wt	Wildtype
°C	Degree Celsius

7.2. Acknowledgements

Dr. Sebastian Dütting, for the support at the very start of my PhD and for his help in the RhoB project.

Sylvia, Birgit, Juliana, Steffi and Ewa for their valuable support, stimulating talks and their efforts to keep the lab running.

The MK seminar for the valuable discussions, the scientific input that helped me improving my data and the pleasant atmosphere during the seminars.

The graduate school of life sciences for giving me the opportunity to doing my thesis under the PhD program and for allowing me to attend and participate in scientific conferences and excellent transferable skills courses. Especially thank you for your great support at the end of this thesis.

The Bioimaging Centre (Rudolf Virchow Center) for providing technical infrastructure and support.

The members of the former ´Office 3´ in D15. Isi, Charly, Stefano, Julia, Tobi, Kiran, Bodo, Maxi. Thank you for the great atmosphere in our office, the fruitful discussions about science, life and everything else.

A special thank you goes to the one and only Isi. We were always there for each other, during all the ups and downs (many, many of them) and I can't imagine finishing my PhD without you. Thank you for being my friend and accepting me for who I am, even though the two of us are just two woodpeckers fond of tippling. ;)

Marki, thank you for the lab support, all the evenings in the cinema and for proofreading this thesis.

Stefano, thank you for making my last years in the lab so, so funny and special.

All present and former members of the Nieswandt lab, who have not been mentioned here by name. Thank you for your support and the pleasant atmosphere during my time in the AG Nieswandt. Thank you for the great talks and all the fun moments during work.

The members of the AG Sumara next to our office: Thank you for all the great moments together. Especially a big thank you to my gossip-partner Alex.

A big 'I love you' to the Kapuhood. You made my years in Würzburg so special. Thank you for supporting me in all times, for the deep-talks, the fun talks, the crazy talks, just for everything. Matze, Basti, Katrin, Sandra, Max, and Christoph.

Hanaa, thank you for your strong female support, the discussions, your deep understanding and all the great lebanese food you and Rabih prepared. Love you granny.

Friedi and Nadine, it's finally my turn. Thank you two for being there the last 11 years!

Svenja, Alex and Philipp: Without you and our tours around Würzburg, everything would be only half as fun. Especially Sveni you are my favorite witch. ;)

And to all the others bringing joy and happiness throughout my thesis: Julia, Maria, Tin, Adrian, Hanna and Louisa.

Denis, without you and your constant encouragement I wouldn't have finished this thesis. I always felt supported and knowing that you had my back no matter what, gave and gives me so much strength. I am so happy that you are in my life.

Lastly, I want to thank my family: My mum, who is so so supportive and just the loveliest mum anyone can image. My dad, who is super proud of me and always wants the best for me. I miss to go out on concerts with you! My sister Lena, her husband Christian, my little nephew Leo and the little soon to be born Knödel. Thank you for being there and for your love.

7.3. Publications

7.3.1. Articles

Becker IC*, Scheller I*, Wackerbarth LM, Beck S, Heib T, **Aurbach K**, Manukjan G, Gross C, Spindler M, Nagy Z, Stritt S, Witke W, Lappalainen P, Bender M, Schulze H, Pleines I, Nieswandt B. Actin/microtubule crosstalk during platelet biogenesis in mice is critically regulated by Twinfilin1 and Cofilin1. Blood Adv. 2020 May 26;4(10):2124-2134. doi: 10.1182/bloodadvances.2019001303.

Geue S*, **Aurbach K***, Manke M, Manukjan G, Münzer P, Stegner D, Brähler C, Walker-Allgaier B, Märklin M, Borst C, Quintanilla-Fend L, Rath D, Geisler T, Salih H, Seizer P, Lang F, Nieswandt B, Gawaz M, Schulze H, Pleines I, Borst O. Pivotal role of PDK1 in megakaryocyte cytoskeletal dynamics and polarization during platelet biogenesis. Blood 2019. 134(21) 1847-1858. doi: 10.1182/blood.2019000185.

Aurbach K*, Spindler M*, Haining EJ, Bender M, Pleines I. Blood collection, platelet isolation and measurement of platelet count and size in mice-a practical guide. Platelets. 2019;30(6):698-707. doi: 10.1080/09537104.2018.1528345. Epub 2018 Oct 22.

Münzer P, Walker-Allgaier B, Geue S, Langhauser F, Geuss E, Stegner D, **Aurbach K**, Semeniak D, Chatterjee M, Gonzalez Menendez I, Märklin M, Quintanilla-Martinez L, Salih HR, Litchfield DW, Buchou T, Kleinschnitz C, Lang F, Nieswandt B, Pleines I, Schulze H, Gawaz M, Borst O. CK2β regulates thrombopoiesis and Ca2+-triggered platelet activation in arterial thrombosis. Blood. 2017 Dec 21;130(25):2774-2785. doi: 10.1182/blood-2017-05-784413. Epub 2017 Sep 19.

Dütting S, Gaits-Iacovoni F, Stegner D, Popp M, Antkowiak A, van Eeuwijk JMM, Nurden P, Stritt S, Heib T, **Aurbach K**, Angay O, Cherpokova D, Heinz N, Baig AA, Gorelashvili MG, Gerner F, Heinze KG, Ware J, Krohne G, Ruggeri ZM, Nurden AT, Schulze H, Modlich U, Pleines I, Brakebusch C, Nieswandt B. A Cdc42/RhoA regulatory circuit downstream of glycoprotein Ib guides transendothelial platelet biogenesis. Nat Commun. 2017 Jun 15; 8:15838. doi: 10.1038/ncomms15838.

Pleines I, Woods J, Chappaz S, Kew V, Foad N, Ballester-Beltrán J, **Aurbach K**, Lincetto C, Lane RM, Schevzov G, Alexander WS, Hilton DJ, Astle WJ, Downes K, Nurden P, Westbury SK, Mumford AD, Obaji SG, Collins PW, Delerue F, Ittner LM, Bryce NS, Holliday M, Lucas CA, Hardeman EC, Ouwehand WH, Gunning PW, Turro E, Tijssen MR, Kile BT. Mutations in

tropomyosin 4 underlie a rare form of human macrothrombocytopenia. J Clin Invest. 2017 Mar 1;127(3):814-829. doi: 10.1172/JCI86154. Epub 2017 Jan 30.

7.3.2. Oral presentations

I0th International Platelet meeting, Ramat Gan, Israel. April 2018. The role of the small GTPase RhoB in platelet function.

XXVIIth Congress of the International Society on Thrombosis and Haemostasis, Melbourne, Australia. July 2019. The role of the small GTPase RhoB in platelet function.
(ISTH 2019 Early Career Award).

7.3.3. Poster presentations

International Symposium of the Graduate School of Life Science: EUREKA! Würzburg, Germany, October 2016. The role of the Rho Kinase ROCK2 in platelet biogenesis.

Joint Symposium of the Collaborative Research Center 688 and the Comprehensive Heart Failure Center Würzburg, Germany, October 2017. The role of the small GTPase RhoB in platelet function. (Awarded with the 1st Poster Price)

XXVIth Congress of the International Society on Thrombosis and Haemostasis, Berlin, Germany, July 2017. The role of the small GTPase RhoB in platelet and MK function.

International Symposium of the Graduate School of Life Science: EUREKA! Würzburg, Germany, October 2017. ´The role of the small GTPase RhoB in platelet function´.

International Symposium of the Graduate School of Life Science: EUREKA! Würzburg, Germany, October 2018. The role of the small GTPase RhoB in MK function.

7.4. Curriculum vitae

Name   Katja Aurbach

Date of Birth   14.07.1990

Place of Birth   Neumarkt i.d. OPf., Germany

Nationality   German

Education

2015 - now   PhD student in the group of Prof. Bernhard Nieswandt,

                  Institute of Experimental Biomedicine, University Hospital and Rudolf-

                  Virchow-Center, Julius-Maximilians University Würzburg, Germany

2012 - 2015   Master of Science (M.Sc.): Biology

                  Justus-Liebig-University of Gießen, Germany

2009 - 2012   Bachelor of Science (B.Sc.): Biology

                  Justus-Liebig-University of Gießen, Germany

2009   German high school diploma (Neumarkt i.d.OPf.)

Würzburg, January 2021   _____

                              Katja Aurbach

7.5. Affidavit

I hereby confirm that my thesis entitled ´Studies on the role of the cytoskeleton in platelet production´ is the result of my own work. I did not receive any help or support from commercial consultants. All sources and/or materials applied are listed and specified in the thesis.

Furthermore, I confirm that this thesis has not yet been submitted as part of another examination process neither in identical nor in similar form.

Würzburg, January 2021 _____

Katja Aurbach

7.6. Eidesstattliche Erklärung

Hiermit erkläre ich an Eides statt, die Dissertation „Studien über die Rolle des Zytoskeletts in der Produktion von Thrombozyten" eigenständig, d.h. insbesondere selbstständig und ohne Hilfe eines kommerziellen Promotionsberaters, angefertigt und keine anderen als die von mir angegebenen Quellen und Hilfsmittel verwendet zu haben.

Ich erkläre außerdem, dass die Dissertation weder in gleicher noch in ähnlicher Form bereits in einem anderen Prüfungsverfahren vorgelegen hat.

Würzburg, Januar 2021 _____

Katja Aurbach